SCIENCE • TECHNOLOGY • RESEARCH HIGHLIGHTS • VISIONS •

Dissertation
162

Flexible pigment-cellulose nanofibril composites for printed electronics applications

Katariina Torvinen

VTT

VTT SCIENCE 162

Flexible pigment-cellulose nanofibril composites for printed electronics applications

Katariina Torvinen

VTT Technical Research Centre of Finland Ltd

Doctoral dissertation
Laboratory of Paper Coating and Converting
Center for Functional Materials
Faculty of Science and Engineering
Åbo Akademi University
Åbo, Finland, 2017

Thesis for the degree of Doctor of Science (Technology) to be presented with due permission for public examination and criticism in Turku at Åbo Akademi on the 27th of October 2017 at 12.00

ISBN 978-951-38-8571-7 (Soft back ed.)
ISBN 978-951-38-8570-0 (URL: http://www.vttresearch.com/impact/publications)

VTT Science 162

ISSN-L 2242-119X
ISSN 2242-119X (Print)
ISSN 2242-1203 (Online)
http://urn.fi/URN:ISBN:978-951-38-8570-0

JULKAISIJA – UTGIVARE – PUBLISHER

Teknologian tutkimuskeskus VTT Oy
PL 1000 (Tekniikantie 4 A, Espoo)
02044 VTT
Puh. 020 722 111, faksi 020 722 7001

Teknologiska forskningscentralen VTT Ab
PB 1000 (Teknikvägen 4 A, Esbo)
FI-02044 VTT
Tfn +358 20 722 111, telefax +358 20 722 7001

VTT Technical Research Centre of Finland Ltd
P.O. Box 1000 (Tekniikantie 4 A, Espoo)
FI-02044 VTT, Finland
Tel. +358 20 722 111, fax +358 20 722 7001

Juvenes Print, Tampere 2017

Abstract

The aim of this work was to expand the possibilities of novel use of cellulose micro- and nanofibrils (CMNF) for bio-based composites. The new approach in this work was to combine inorganic pigments and CMNF in a relatively wide range of component combinations for the generation of pigment-cellulose micro- and nanofibril (PCMNF) composites. The amount of CMNF in these studies varied between 20 and 50 wt-% in the studied composites. The main focus of the work was on clarifying the relationship between the raw materials used and the composite structural properties of the final product, such as smoothness and porosity. The influence of manufacturing process steps on the composite properties was studied experimentally in both laboratory and semi-pilot scale. The composites were manufactured by vacuum filtration in laboratory scale and by film casting in semi-pilot scale, in both cases followed by wet pressing, drying, and calendering. Based on feasibility studies including techno-economic and life-cycle assessment, new product opportunities and markets can be captured with PCMNF composites for printed electronics applications.

There is nowadays a growing need for the production of flexible, cost-effective, and environmentally friendly substrates for printed electronics applications. CMNF as a raw material has attracted significant interest in this field. In this work, different functional devices were manufactured as proof-of-concept structures to demonstrate the usability of the developed composites for printed electronics applications. The studied proof-of-concepts were: 1) ink-jet printing with a silver-nanoparticle ink, 2) double-functional separator substrate for printed supercapacitors, 3) an ion-modulated transistor deposited on the substrate, and 4) screen printed antennas using silver ink and a commercial radio frequency identification (RFID) chip attached using a silver epoxy resin as a functional near field communication RFID tag on the substrate.

The developed PCMNF composites have a nanoporous pigment-CMNF network structure that allows controlled ink absorption properties. The required substrate porosity and smoothness strongly depend on the used printing method, ink, solvent, and device design. The PCMNF composites offer a sustainable substrate for printed electronics applications to be used at high temperatures that only very special plastic films can currently withstand.

Keywords: cellulose nanofibrils, cellulose microfibrils, nanocellulose, composite films, printed electronics, mineral pigment, casting method, substrate

Abstrakt

Arbetet strävar att utvidga användningsmöjligheterna för cellulosa mikro- och nanofibriller (CMNF) inom biobaserade kompositer. Det nya sättet att närma sig detta är att kombinera inorganiskt pigment med CMNF i relativt höga komponentproportioner för att generera pigment-cellulosa mikro- och nanofibrill (PCMNF) kompositer. Halten av CMNF i dessa studier varierade mellan 20 och 50 v-% i kompositerna. Den huvudsakliga fokusen i arbetet var att utvärdera sambandet mellan råmaterial och strukturella egenskaper, såsom släthet och porositet, i den producerade kompositen. Påverkan av produktions-processsteg på kompositernas egenskaper studerades experimentellt både i laboratorie- såsom i semi-pilot skala. Kompositerna producerades genom vakuumfiltrering i laboratorieskala och via filmgjutning i semi-pilot skala, följt av våtpressning, torkning och kalandrering. På basis av genomförbarhetsstudier, som inkluderar tekno-ekonomiska och livscykel-utvärderingar, kan man nå nya produktmöjligheter och -marknader med PCMNF-kompositer inom tryckta elektronikapplikationer.

I denna dag finns ett växande behov för flexibla, kostnadseffektiva samt miljövänliga substrat för tryckta elektronikapplikationer. Intresset för CMNF som råmaterial i detta område har ökat märkbart. I detta arbete har olika funktionella apparater tillverkats för att konceptvalideras och demonstrera kompositernas användbarhet inom tryckt elektronik. De rannsakade konceptvalideringarna var: 1) utskrift av silver-nanopartikel bläck med bläckstråle 2) ett dubbel-funktionellt separator-substrat för tryckta superkondesatorer 3) en jon-modulerad transistor deponerad på substratet 4) en funktionell närfältskommunikationstagg på substratet genom serigrafi-tryckta antenner med silverbläck samt ett kommersiellt radiofrekvens identifikationschipp (RFID) fäst med silver-epoxi.

De utvecklade PCMNF-kompositerna har en nanoporös pigment-CMNF nätverksstruktur som tillåter kontrollerad bläckabsorption. Substratets porositets- och släthetskrav beror starkt på tillämpad tryckmetod, bläck, lösningsmedel samt apparatdesign. PCMNF-kompositerna erbjuder ett hållbart substrat för tryckta elektronikapplikationer för höga temperaturförhållanden, vilka enbart ett fåtal specialplaster klarar av i denna dag.

Nyckelord: cellulosa nanofibrill, cellulosa mikrofibrill, nanocellulosa, kompositfilm, tryckt elektronik, mineralpigment, gjutningsmetod, substrat

Supervisors

Adjunct Professor Jarkko J. Saarinen
Åbo Akademi University, Turku, Finland

Professor Martti Toivakka
Åbo Akademi University, Turku, Finland

Pre-examiners

Professor Thaddeus Maloney
Bio-based Material Technology, Department of Bioproducts and Biosystems
Aalto University, Espoo, Finland

and

Professor Lokendra Pal
Pulp & Paper Labs, Department of Forest Biomaterials
North Carolina State University, Raleigh, North Carolina, United States

Opponent for the public defense

Professor Thaddeus Maloney
Bio-based Material Technology, Department of Bioproducts and Biosystems
Aalto University, Espoo, Finland

Preface

The work was carried out in the Laboratory of Paper Coating and Converting of Åbo Akademi. A significant part of work was performed during the EffNet (Efficient Networking towards Novel Products and Processes) program funded by FIBIC (nowadays CLIC) during the years 2010–2013. After that, the work was funded by VTT Technical Research Centre of Finland in 2014–2017. I express my thanks to CLIC, Tekes, Stora Enso, and VTT for providing financial support. The support from Imerys and Specialty Minerals in providing raw materials for the work is highly appreciated.

I am extremely grateful to my supervisor, docent Jarkko J. Saarinen for giving me a vitally important boost and for supporting the finalization of my work. I also thank my other supervisor, Professor Martti Toivakka for his valuable guidance and advice while writing the thesis.

Special thanks go to Jenni Sievänen, Jukka Ketoja, and Erkki Hellén for fruitful co-operation during the EffNet-program. Your support in the preparation of my article manuscripts for publication was crucial. The support from the technical personnel of VTT was of the highest quality and I particularly thank Merja Selenius and Joni Myyryläinen. I appreciate the cooperation carried out with Antti Penttilä from University of Helsinki, Sampo Tuukkanen and Suvi Lehtimäki from Tampere University of Technology, and Kai Arstila from University of Jyväskylä. I thank all my colleagues and other co-authors from VTT: Tuomo Hjelt, Kimmo Ojanperä, Oleg Timofeev, Timo Kaljunen, Jarmo Kouko, Janne T. Keränen, Jari Vartiainen and Panu Lahtinen, for helping me with experiments and manuscripts. Furthermore, I also thank my co-authors from Åbo Akademi, Fredrik Pettersson, Vinay Kumar and Professor Ronald Österbacka. I am grateful for support from the management of VTT, especially Kristian Salminen, Pia Qvintus, Anna Suurnäkki, Tomi Erho and Jani Lehto, that gave me the opportunity to finalize my thesis work. In addition to professional support, I thank my colleagues from the VTT Biomass processing and products area for an excellent working atmosphere and fruitful discussions.

This work is dedicated to my three extraordinary and precious daughters, Kaisla, Vilja and Malva. They are my treasures and hopefully this work will encourage them to reach their own dreams and work with passion in future. Finally, and most of all, I express my gratitude to my husband Aki who has always believed in me and supported me whenever necessary. The writing of this work required long working days from me and much patience and extra homecare actions from him.

Jyväskylä 14.05.2017, Katariina Torvinen

List of abbreviations

AR	Aspect ratio
CBH	Cellobiohydrolase
CF	Cellulose fibril
CMF	Cellulose microfibril
CMNF	Cellulose micro-and nanofibril
CNC	Cellulose nanocrystals
CNF	Cellulose nanofibril
CNT	Carbon nanotubes
CV	Current-voltage
DP	Degree of polymerization
FE-SEM	Field emission scanning electronic microscope
FET	Field-effect transistor
FOM	Figure of merit
FOV	Field of view
HIM	Helium ion microscope
IoT	Internet of things
IR	Infrared
ITO	Indium tin oxide
NC	Nanocellulose
NFC	Near field communication
NP	Nanoparticles
OFET	Organic light-emitting diodes
Opex	Operational expenditure
PCC	Precipitated calcium carbonate
PCMNF	Pigment-cellulose micro-and nanofibril
PE	Printed electronics
PEDOT-PPS	Poly (ethylene-dioxythiophene):poly(styrene sulfonate)
PET	Polyethylene terephthalate
PLA	Particle layer analysis

PVA	Polyvinyl alcohol
RFID	Radio frequency identification
RH	Relative humidity
SEC	Specific energy consumption
SEM	Scanning electron microscope
SWCNT	Single-wall carbon nanotubes
TEMPO	2,2,6,6-tetramethylpiperidine-1-oxyl radical
UV	Ultraviolet
ÅAGWR	Modified Åbo Akademi gravimetric water retention method

List of publications

This thesis is based on results published in five articles listed below. The papers are referred to with Roman numerals in the text.

Paper I "Smooth and flexible filler-nanocellulose composite structure for printed electronics applications" Katariina Torvinen, Jenni Sievänen, Tuomo Hjelt, and Erkki Hellén, *Cellulose* 19, Issue 3, 821–829 (2012).

Paper II "Filler-nanocellulose substrate for printed electronics: experiments and model approach to structure and conductivity" Antti Penttilä, Jenni Sievänen, Katariina Torvinen, Kimmo Ojanperä, and Jukka A. Ketoja *Cellulose* 20, Issue 3, 1413–1424 (2013).

Paper III "Drying of Pigment-Cellulose Nanofibril Substrates" Oleg Timofeev, Katariina Torvinen, Jenni Sievänen, Timo Kaljunen, Jarmo Kouko, and Jukka A. Ketoja, *Materials* 7, 6893–6907 (2014).

Paper IV "Pigment-cellulose nanofibril composite and its application as a separator-substrate in printed supercapacitors" Katariina Torvinen, Suvi Lehtimäki, Janne T. Keränen, Jenni Sievänen, Jari Vartiainen, Erkki Hellén, Donald Lupo, and Sampo Tuukkanen, *Electronic Materials Letters* 11, 1040–1047 (2015).

Paper V "Nanoporous kaolin – cellulose nanofibril composites for printed electronics" Katariina Torvinen, Fredrik Pettersson, Panu Lahtinen, Kai Arstila, Vinay Kumar, Ronald Österbacka, Martti Toivakka, and Jarkko J. Saarinen, *Flexible and Printed Electronics* Volume 2, Number 2, Focus on Paper Electronics, 11 p. (2017).

Author's contribution

Paper I. The author planned the experimental work together with the co-authors. The author was responsible for the surface and structural analyses of the composite and conducted all the experiments related to the surface characterization and performed the data analysis. The author prepared samples in the laboratory scale and interpreted the results. The article was mainly written by the author.

Paper II. The author took part in planning the experimental work together with the co-authors. The author was responsible for the surface and structural analyses of the composite, prepared the samples and conducted all the experiments for the composite characterization together with the co-authors and analysed the results. The author wrote most of the experimental part of the article and interpreted the results.

Paper III. The author took part in planning the experimental work together with the co-authors. The author was responsible for surface and structural analyses of the composite. The author conducted the experiments related to the surface characterization and performed the data analysis. The author produced the composite materials and prepared the pilot scale webs together with the co-authors. The author wrote the article together with the co-authors.

Paper IV. The author planned the experimental work together with the co-authors. The author was responsible for the surface and structural analyses of the composite. The author produced materials and prepared the samples in pilot scale webs together with the co-authors. The author conducted many of the measurements (thermal tolerance, roughness) of composites and performed the data analysis. The author interpreted the results. The article was mainly written by the author.

Paper V. The author planned the experimental work and was responsible for the raw material combinations. The author was responsible for manufacturing of composite films. The author conducted the analysis of measured data and composite characterization. The author interpreted the results. The article was mainly written by the author.

Table of contents

1 Introduction

Cellulose is the most abundant organic polymer and shares fascinating structure and properties with other renewable polymeric materials such as starch, chitosan, and soy protein. The total annual biomass growth of cellulosic material is about 1.5 trillion tons (Klemm *et al*., 2005), which is currently facing an increasing demand as a raw material source for bio-based, environmentally friendly products of the future. Renewable materials such as cellulose are extremely important for sustainability, carbon capture, and prevention of climate change.

Raw material costs and energy efficiency are the key drivers of profitability for the forest products industry. The future paper and board machine concepts need a renewal of current technologies (T. Xu, Sathaye, & Kramer, 2013), (Hong *et al*., 2011). There is also an increasing demand for novel bio-based products that are resource- and capital efficient. There has been growing interest in the area of cellulose micro- and nanofibril (CMNF) research during the past decade, especially in composites (J. H. Kim *et al*., 2015), (Klemm *et al*., 2011), (Zhang *et al*., 2013), (Hubbe, Rojas, Lucia, & Sain, 2008), (Abdul Khalil, Bhat, & Ireana Yusra, 2012).

In this work, novel applications of printed electronics were developed utilizing new materials, particularly cellulose nanofibrils (CNF) and mineral pigments as composite films. The aim of this work was to improve resource efficiency and create a wider application range for future bio-based products. Next generation technologies are needed to expand traditional paper and board production and their properties for new fiber-based products outside the conventional value chains. Cellulose nanomaterials, both in nano- and microscales, present new opportunities for future manufacturing processes as a part of material mixtures together with inorganic pigments.

Printed electronics (PE) and printed intelligence are developing at a fast pace due to their high estimated market potential (Kantola *et al*., 2009) (Rogers, 2010). Conventionally, most applications are printed on plastic, ceramics, or silicon substrates. However, there is a need for new flexible, smooth and low-cost substrates. Printed electronics is not a substitute which will replace conventional silicon-based electronics, but it opens new avenues for low-cost printed circuits based on conductive, semiconductive, and dielectric printed materials in high-volume market segments in which the high performance of conventional electronics is not required (Molesa, 2006). The main challenge for developing a suitable substrate material for printed electronics is that various conditions of the printing process need to be satisfied. The internet of things (IoT) is an emerging megatrend that connects physical devices, vehicles, and homes to the internet, allowing transmission, collection, and exchange of data between them (Bai, 2016) (Madakam, Ramaswamy, & Tripathi, 2015), (S. Li, Xu, & Zhao, 2015). IoT combines sensors, actuators, and electronics with network connectivity. IoT with

interconnected devices enables significant improvements in logistics, with considerable consequent economic benefits. The integration of sensors into individual packages requires only a very low cost for a single unit device (less than 0.01 USD/device), which gives them significant potential for reducing food waste (Fao, 2013), (Njie, 2012). Functional printing is expected to play a key role in such cost-efficient production, as it allows for a large number of devices to be manufactured in a roll-to-roll (R2R) process flow resulting in a significant unit cost reduction.

There has also been an increasing interest in developing new types of supercapacitors to meet the requirements of various energy storage applications (Halper & Ellenbogen, 2006), (Shi *et al*., 2013). Supercapacitors are rechargeable electrochemical energy storage devices that offer advantages such as high power capability, high rates of charge and discharge, long cycle life, flexible packaging, and low weight compared to other energy storage devices. Future developments are moving towards thin, low-cost, lightweight, and flexible solutions that can be utilized in wearable and disposable electronics applications (Yoo *et al*., 2011), (Kaempgen, Chan, Ma, Cui, & Gruner, 2009). The use of flexible substrates such as paper or plastic is significantly more cost-effective compared to silicon in electronic applications (Tobjörk, 2012). Other advantages include high volume production, scalable processes and easy integration, reduced use of toxic substances, thinner end-use products and customized design possibilities.

The reasons to use paper as a flexible substrate for PE applications instead of plastics on the one hand are related to its sustainability, disposability, resilience, easy availability, controlled transparency, recyclability, and foldability. However, modifications of paper properties are needed in order to obtain working electronic devices. The key factors affecting paper properties are the raw materials used and the manufacturing technologies. On the other hand, this gives an advantage of using paper or novel composite films as substrates for printed electronics instead of plastics: the important surface and structural properties can be adjusted by optimizing raw materials and manufacturing processes.

The use of cellulose nanofibrils (CNF) in printed electronics applications has been growing recently (Hoeng, Denneulin, Bras, *et al*., 2016). However, there are still only a limited number of publications and patents available in the field of PE compared to the other application areas of CNF (Figure 1). In these publications, CNF has been used both as a substrate and also as a blend with conductive particles in printing or coating inks. In this work, the use of CNF was focused on composite films as a substrate for printed electronics. In addition, literature related to the use of paper as a substrate for printed electronics is reviewed.

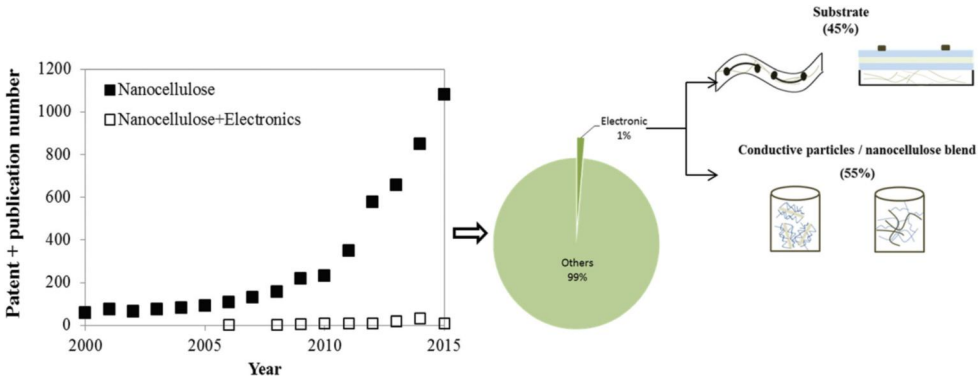

Figure 1. *Annual number of publications and patents on cellulose nanofibrils and CN in electronics. Source: SciFinder & Espacenet – descriptors. (Hoeng, Denneulin, & Bras, 2016)*

The most important advantages of novel composites are their flexibility and recyclability in addition to low cost that will provide opportunities for new end-use application areas such as wearable electronics, throw-away/one-time use-electronics, and consumer packages. The metallic nanoparticles used in printing and coating inks and polymers will affect the obtained conductivity of lines and features in functional devices. Therefore, solutions of dispersions and substrate properties must be designed to match the requirements of the used printing or coating process.

The main objective of this work is to understand the influence of the raw materials and manufacturing phases in novel composite films so that critical properties, such as porosity, surface roughness and dimensional stability, for printed electronics can be identified. Manufacturing of inorganic pigment-CMNF composite films are demonstrated in a semi-pilot scale by the film casting method. Paper manufacturing for printing applications has a long history, whereas CMNF with a high pigment loading as composite films for printed electronics is a new research area. Modification and optimization of composite raw materials and relevant process parameters are required for obtaining working electronic devices. Understanding the interactions between raw materials and printing processes plays a key role in this work. The properties of developed new composites for printed electronics are investigated. Compatibility between achieved properties and functional inks and printing methods is also studied. Finally, several functional proof-of-concept devices including supercapacitors, transistors, and antennas are demonstrated and analyzed.

2 Review of the literature

2.1 Pigment-cellulose micro-and nanofibril composites (PCMNFs)

2.1.1 Background and manufacturing of CMNF

The global markets of cellulose fibrils (CF) comprise cellulose micro- and nanofibrils (CMF and CNF, combined CMNF), cellulose nanocrystals (CNC), and bacterial cellulose (BC). The major market share is represented by CMNF. In cellulose, the amorphous and crystalline parts are sequentially located in a row along the fiber direction. Strong hydrogen bonding between hydroxyl groups of the composite glucose molecules makes it almost impossible to break the crystalline parts of cellulose. However, the amorphous parts are relatively easy to break using mechanical refining, homogenization, crushing, or chemical and enzymatic treatments (Hubbe *et al*., 2008), and these extraction methods can also be combined. In the following sections the main characteristics and production methods of both CMNF and CNC are presented.

Cellulose micro- and nanofibrils (CMNF) are generally manufactured from wood pulps (see Figure 2), but annual plants, bacteria, and algae can offer alternative sources. They are manufactured by mechanical treatments such as grinding (Iwamoto, Nakagaito, & Yano, 2007), (Wang *et al*., 2012), high-pressure homogenization (Nakagaito & Yano, 2004), (Liimatainen *et al*., 2013), and microfluidization (Zimmermann, Pöhler, & Geiger, 2004). The microfibrils forming the fiber cell wall are separated from each other during the mechanical treatment. As a result, a viscous gel is formed, consisting of individual nanoscale fibrils (Figure 3).

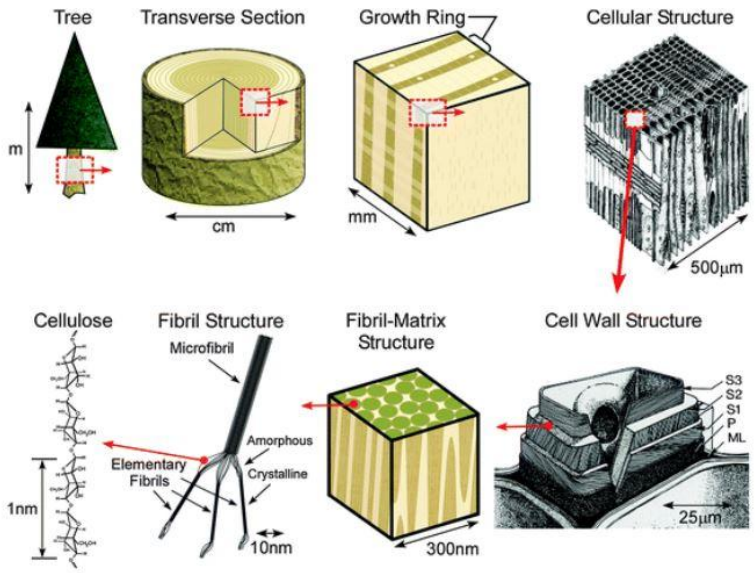

Figure 2. *Schematic of the tree hierarchical structure. (Moon, Martini, Nairn, Simonsen, & Youngblood, 2011a).*

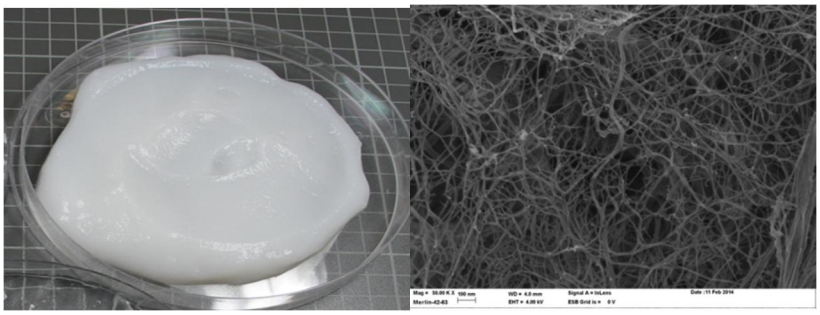

Figure 3. *Left: CNF gel produced by Masuko grinding. Right: Scanning Electron microscope (SEM) image of CNFs. Scale: 100 nm (Image source: VTT).*

Chemical (*e.g.* TEMPO oxidation) (Tsuguyuki Saito, Nishiyama, Putaux, Vignon, & Isogai, 2006),(Wågberg *et al*., 2008) and enzymatic pretreatments (Pääkko *et al*., 2007), (Zhu *et al*., 2016), (M. Henriksson, Henriksson, Berglund, & Lindström, 2007) can be combined with mechanical shearing and high-pressure homogenization for decreased energy consumption during the fibrillation. The goal for both enzymatic and chemical treatments is to loosen the tight hydrogen-bonded structure in the fiber wall. As a result of TEMPO oxidation, C6 hydroxyl groups of native cellulose are converted to carboxyl groups without any changes to the original crystallinity (~74%) or crystal width of wood celluloses (T. Saito, Okita, Nge, Sugiyama, & Isogai, 2006). This leads to highly anionically-charged cellulose microfibrils, of which the zeta-potential values in water are approximately -75 mV (Isogai, Saito, & Fukuzumi,

2011). The modification of the fiber structure is followed by an easier liberation of fibrils from fibers, which decreases the energy consumption and results in more cost-efficient processes. This has generated a basis for industrialization of CMNF since 2010. Cationic, anionic, or amphiphilic groups can also be introduced to the CMNF structure by chemical modification.

The fibrils manufactured by a mechanical treatment are flexible and highly branched and have a high aspect factor (length/width). Typically, wood-based CMNFs have 20-100 nm cross-sectional size and 1-5 µm fiber length (J. H. Kim *et al*., 2015), (Siro & Plackett, 2010), (Klemm *et al*., 2011) and are generally manufactured in aqueous suspensions. The CMNF-materials usually also contain micro-scale fibrils and their aggregates, fibers with variable degree of fibrillation, and even unfibrillated fibers. The aggregates are due to the free hydroxyl groups on the surface of cellulose fibrils, and the agglomeration takes place especially during drying of the CNFs.

On the other hand, *cellulose nanocrystals (CNC*) are rigid, rod-like nanoparticles containing the crystalline parts of cellulose fibers (Rånby, 1951), (Boluk, Lahiji, Zhao, & McDermott, 2011), (Moon *et al*., 2011a). CNC can be isolated by a mild acid hydrolysis chemical treatment of cellulose. Various acids have been used for the CNC isolation, in which the amorphous regions are dissolved due to infiltration of the acid into the accessible amorphous regions. The structure of CNC is very different to that of CMNF. Its diameter is in most cases smaller, from 10 to 50 nm, and the length is also generally shorter to that of CMNF, from 100 to 500 nm depending on the raw material used (Bras, Viet, Bruzzese, & Dufresne, 2011). CNC has a high surface area and excellent mechanical properties. The films produced by CNC are usually more brittle than those of CMNF, due to their crystalline nature. This work focuses on studying different CMNF grades, with particular emphasis on their nanoporous web-like structure and ability to produce smooth and less porous films. (Fukuzumi, Saito, Iwata, Kumamoto, & Isogai, 2009).

Commercial production of CF materials

According to Frost & Sullivan (see Figure 4), the nanocellulose (NC) market generated a revenue of around $73 MUSD in 2015 that is expected to reach $268 MUSD by 2020. There is already an impressive amount of commercial production of cellulose nanomaterials around the world. Based on press-releases, the following companies produce cellulose nanomaterials: Blue Goose Biorefineries (CAN), American Process Inc. (USA), and Cellulose Lab (USA) in North America, FiberLean (GB), Cellucomp (GB), Rettenmaiyer (GER), InoFib (FR), Betulium (FI), Stora Enso (FI), and Borregaard (NO) in Europe, and Asahi Kasei, Chuetsu Pulp & Paper, Daicel, Dai-ichi Kogyo, and Sugino Machine in Japan. There are also many more entrepreneurs currently in the phase of pre-commercial, pilot, or in preparation stages.

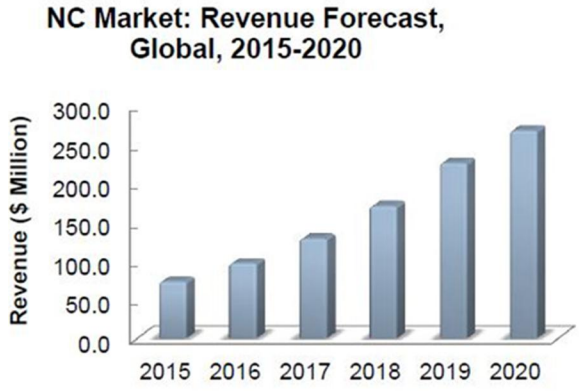

Figure 4. *Source: Frost & Sullivan. Emerging applications of nanocellulose technology (TechVision). D6DF-TV. May 2016*

2.1.2 CMNF applications in films and composites

The specific characteristics of CMNF material, such as its high aspect ratio, large specific surface area, and high strength together with its biocompatibility, biodegradable and non-petroleum basis are key motivators for development of a wide range of new applications (J. H. Kim *et al*., 2015). The end-use applications of CMNF material include use as a rheology modifier in films (K. Dimic-Misic, Gane, & Paltakari, 2013), (K. Dimic-Misic *et al*., 2013), and as reinforcement material in biocomposites (Berglund, 2005), (Nakagaito & Yano, 2005), (K. Y. Lee, Aitomäki, Berglund, Oksman, & Bismarck, 2014), as well as use as hydrogel for 3D-printing (Markstedt *et al*., 2015), (Rees *et al*., 2015), (Kopeček, 2007) and wound healing applications (Liu *et al*., 2016), (Chinga-Carrasco & Syverud, 2014). CMNF material has already been widely used in paper and board applications as a strength additive (Taipale, Österberg, Nykänen, Ruokolainen, & Laine, 2010), (Brodin, Gregersen, & Syverud, 2014), (Kajanto & Kosonen, 2012), (Lahtinen *et al*., 2014).

Furthermore, a fast-growing potential application area of CMNFs is their use as a renewable and sustainable substrate for printed electronics (PE) applications to replace plastic films. However, many studies have concentrated on producing films from pure CMNF material (Nogi, Iwamoto, Nakagaito, & Yano, 2009), (Kristin Syverud & Stenius, 2009), (Fujisawa, Okita, Fukuzumi, Saito, & Isogai, 2011), (Kumar *et al*., 2014). The hydrophilic nature of CMNF films is the most challenging property, which impairs the moisture barrier properties. Recently, a considerable amount of effort has been put into modification of CMNF films to be hydrophobic for PE applications and also for reinforcement effects in other polymer interactions (K. Y. Lee *et al*., 2014), (Nair, Zhu, Deng, & Ragauskas, 2014), (Shimizu, Saito, Fukuzumi, & Isogai, 2014).

The reinforcing effect of CMNF material in polymer composites has been widely studied mostly in connection with polylactid acid (PLA) as a biodegradable polymer (Oksman, Skrifvars, & Selin, 2003), (Pracella, Haque, Puglia, & Alvarez, 2012), (Aitomäki & Oksman, 2014), (Graupner, Herrmann, & Müssig, 2009), (Trifol *et al*., 2016), (K. Y. Lee *et al*., 2014). The mechanical strength of the composites can be improved with a small addition of CMNF. The increase of tensile modulus can be as much as 100% and for tensile strength up to 60%. Several studies have also been made with starch (Abdul Khalil *et al*., 2012), (Subramaniyan & Sun, 2006), (F. Xie, Pollet, Halley, & Av??rous, 2013), synthetic biodegradable poly(vinyl) alcohol (PVA) (Ching, Rahman, Ching, Sukiman, & Chuah, 2015), (S. Y. Lee *et al*., 2009), and chitosan (Azeredo *et al*., 2010) together with CMNF in a matrix of composites. These biomaterial combinations open up new possibilities for renewable, biodegradable solutions for future applications.

Manufacturing of neat CMNF films

Neat CMNF films consist of an interconnected CMNF network structure held together by extensive hydrogen bonding. Neat films have remnant porosity in the gaps between particle networks. Neat CN films have typically been produced using solution casting techniques from suspensions made of CMF, CNF or CNC both in laboratory and pilot scale (Moon, Martini, Nairn, Simonsen, & Youngblood, 2011b), (K. Syverud, Xhanari, Chinga-Carrasco, Yu, & Stenius, 2011), (Nakagaito & Yano, 2005), (Zimmermann *et al*., 2004). CMNF material is dispersed with a solids content of 0.05–5 wt%, typically containing water but other organic media are also used. The casting substrate can be either a solid surface or a filter membrane. The remaining dispersing medium is removed either by evaporation, vacuum filtration, pressing or by a combination of these methods. The neat films are typically 25–100 µm thick and film density varies from 0.8 to 1.5 g/cm³. Additional mechanical pressing up to 160 MPa has been applied to further densify CMNF films (Nogi e*t al*., 2009). The CMNFs are isotropically oriented in the plane of the film, resulting in isotropic in-plane film properties. To manufacture CNF films for roll-to-roll production, the production is based on the precise control of adhesion, and spreading and drying of the CNF on a plastic substrate (Mäkelä, Kainlauri, Willberg-Keyriläinen, Tammelin, & Forsström, 2016). After drying (evaporation of water), the film is then separated from the plastic substrate and reeled. Recently, roll-to-roll produced micro pillars have been fabricated on CMNF neat films using a nano-imprinting method (Mäkelä *et al.*, 2016).

Drying of CMNF material has been studied earlier using different methods such as air drying, freeze drying, spray drying, and supercritical drying (Qing, Sabo, Wu, Zhu, & Cai, 2015), (Y. Peng, Gardner, & Han, 2012), (Y. Peng, Gardner, Han, Cai, & Tshabalala, 2013). The aim has been to preserve the morphology of the CNMF materials. The air drying of CMNF suspensions forms a dense material network, and thus other drying methods could be more effective in film applications. In this

work, several available drying methods and their combinations, which are typically used in paper and board technology, were studied for the PCNMF composites. The studied drying methods were drying on a hot metal surface, air impingement drying, and hot pressing. In the paper and board industry, water from the web after the forming section is first removed in the press section and then subsequently in the drying section. The typical solids content of wet paper web is 45–55% after wet pressing. The amount of water removed by pressing is a function of the applied pressure, nip width (dwell time), and water viscosity (Walker *et al.*, 1990). Mechanical dewatering is a more cost-efficient way to remove water than drying based on evaporation. The most common drying methods for paper, board, and cellulose are cylinder (contact) drying, and air float and air impingement drying. Usually a low steam pressure is used in cylinder dryers, and the drying rates are not very high, in the range of 10–25 kg/m^2/h (Asensio *et al*., 2007).

2.1.3 CMNF and pigments in composites

Inorganic pigments and fillers are widely used in the paper and board industry. The most common ones are calcium carbonate, kaolin clay, talc, and titanium dioxide. In the printing industry, the profitability depends on raw material costs, operating methods, logistics, and efficiency. The renewable raw material is cellulosic fibers, with a relatively high price, whereas the inorganic mineral pigments are less expensive than fibers, with typically approximately 80% lower costs. These pigments are also used to improve the dewatering and optical and printing properties of papers and boards.

From the economical point of view the advantage of replacing fibers with pigments is evident. Hence, pigments are an important component in practically all printing and writing papers (R. Subramanian, Fordsmand, & Paulapuro, 2007). Recently, there has been growing interest in increasing the pigment content of papers utilizing CNF as a binding component (Brodin *et al.*, 2014), (Torvinen, Kouko, Passoja, Keränen, & Hellén, 2014), (Macdonald, 2015), (M. He, Cho, & Won, 2016).

The challenge of increasing the pigment content of papers is the decrease in mechanical strength properties. The replacement of fibers by mineral particles substantially decreases the bonding between cellulose fibers inside the sheet, thus reducing the dry strength of papers (De Oliveira, Tejado, & Van De Ven, 2009). The pigments are not able to produce strong bonds with cellulosic fibers. The typically used pigment amount is below 40 wt-% in industrial papers due to this reduced bonding ability.

An increased pigment amount will improve the dewatering of pulp furnish. This is also a significant advantage of using pigments together with CNFs, which in contrast have a disadvantage of a high ability to bind water, resulting in poor dewatering properties. The combination of pigments and CNF can therefore lead to improved drainage, better efficiency of wet pressing, and increased drying rates

compared to the manufacturing of pure CNF films. The use of pigments will also have an effect on absorption, optical and porosity properties of the papers and composites.

The production and study of hybrid materials consisting of CMNF combined with pigments is therefore an attractive field due to the tendency of CMNF to form strong and porous network structures in which inorganic particles can be homogeneously embedded (Sehaqui, Zhou, Ikkala, & Berglund, 2011). Such flexible hybrid materials can be used for packaging applications, coatings, and film composites as in this thesis work (Aulin, Salazar-Alvarez, & Lindström, 2012). Moreover, flexible printed electronics and separation membranes can be obtained with further modification of hybrid composite structures (Wei, Rodriguez, Renneckar, & Vikesland, 2014). However, in this thesis work the focus was on the PE application area.

CMNF has been studied for use in packaging applications together with clay pigments to improve barrier properties (C. N. Wu, Saito, Fujisawa, Fukuzumi, & Isogai, 2012), (Liimatainen *et al*., 2013), (Österberg *et al*., 2013). Understanding the structural properties of PCMNF composite films will also help to predict their performance as a coating layer for packaging applications. A rapid production method for combination of CNF and inorganic nanoparticles in laboratory scale was published by Sehaqui *et al*. (Sehaqui *et al*., 2011). The procedure allowed montmorillonite to be used up to 50 wt-%. However, only a very limited amount of data was available about the formed composite properties.

High strength and high gas-barrier CNF/clay-layered composite films were prepared by mimicking natural nacre, having high transparency and oxygen-barrier properties despite having low densities (C. N. Wu *et al*., 2012). Blends of TEMPO-oxidized CNF and inorganic montmorillonite up to 50 wt-% in the matrix had a high mechanical strength and toughness. The produced films were also transparent and flexible. Similarly, high-strength CNF-talc hybrid barrier films manufactured by a nano-layered biomimetic technique were studied by Liimatainen *et al*. (Liimatainen *et al*., 2013). The inorganic talc content in these studies was also up to 50 wt-%. Talc platelets resulted in a decrease in the moisture absorption in high pigment-loaded experiments, and a low average pore size of the films was obtained. Moreover, transparent CMNF-pigment composite films were manufactured by Honorato *et al*. (Honorato *et al*., 2015). The effect of raw materials on composite film mechanical, barrier, and optical properties was studied using both clay and calcium carbonate ($CaCO_3$) combined with softwood and hardwood as a raw material for TCNF. The maximum pigment load in these studies was 25 wt-%. The use of clay as a filler material showed more potential to produce better barrier and mechanical properties compared to $CaCO_3$. The agglomeration of $CaCO_3$ particles resulted in highly brittle films with uneven formation. Aulin *et al.* also studied high strength and flexible CMNF-nanoclay hydrid composite films for improved oxygen

and water vapor permeability (Aulin *et al*., 2012). The nanoclay (vermiculite nano platelets) portion in experiments was up to 20 wt-%. The obtained films were thin, strong, and transparent, with good barrier properties. Thus, they are promising candidates for packaging applications.

The manufacturing of CMNF composite films including a high amount of inorganic pigment and pulp fibres was studied by Rantanen *et al*. (Rantanen & Maloney, 2013), (Rantanen, Dimic-Misic, Kuusisto, & Maloney, 2015). The properties of CMNF composite papers were studied using different compositions of pigment (up to 70 wt-%), CMNF (in various portions), and pulp fibers (mainly at 10 wt-%). The optical properties of the composite papers were excellent, as both a micro- and nanoporous network structure of the paper was obtained. The manufacturing of composite papers was demonstrated in high consistency giving rise to conditions that resulted in 33% dry solids content of the web after the wet pressing section. The main outcome of the pilot trials was that pressing requires long pulses to remove water efficiently, and under these circumstances the dewatering can be even better compared to that of Kraft pulp furnish. Moreover, CMNF composite papers can be formed using a feasible and economical process in pilot scale.

The FiberLean® Technologies, as a joint venture of Imerys and Omya, has production and a patent for a composite which includes inorganic pigment particles and CMF material. The process is based on co-grinding of mineral particles and pulp fibers. This composite material can be used as a part of paper and board making in the wet end addition. The mineral plays an essential role in the transfer of mechanical energy from regular pulp into CMF. This also allows the use of robust and reliable industrial equipment. A wide range of pulp furnishes can be fed into the process without any pretreatment. A number of different pigment particles such as calcium carbonate, kaolin, graphite, and talc can be used. In future applications, FiberLean composite product may also be used as a film material and substrate for printed electronics.

2.2 Printed electronics on paper and composites

Nowadays there is a growing interest in using flexible composite films as substrates for printed electronics (PE) applications instead of conventional materials such as glass, silicon and plastic films. The interest in flexible and wearable electronics has increased exponentially within the past decade. PE is a combination of traditional printing processes of paper and board industry and novel ink chemistry for production of electronic components. Moreover, traditional paper coating technologies can be used in a novel way. The goal of PE is to produce flexible, low-cost, and environmentally friendly electronic products. The most common flexible substrates used in PE applications are polymer plastic films.

The motivation for using paper and novel CMNF material films as a substrate for PE applications to replace plastic films is obvious. Paper is a biocompatible,

biodegradable, cost-effective, thin, lightweight, and flexible material that is commonly available (Tobjörk & Österbacka, 2011), (Chang, Ge, & Sanchez-Sinencio, 2012), (Hodgson, 2011). As a porous material, paper also provides a high surface area for active components to be embedded and stored on its surface or inside the structure depending on the application (Dogome, Enomae, & Isogai, 2013), (Öhlund, Örtegren, Forsberg, & Nilsson, 2012), (Ihalainen *et al*., 2012), (Kattumenu, Rebros, Joyce, Fleming, & Neelgund, 2009), (Hyun *et al*., 2015), (Choi, Yoo, Lee, & Lee, 2016).

Interest in the use of CMNF films as a substrate for PE applications has recently been growing. The main reason for this is the possibility to manufacture transparent and flexible films for devices such as solar cells, screens, and sensors (B. Peng & Chan, 2014), (Y. H. Jung *et al*., 2015), (Yan *et al*., 2014), (Grau, Kitsomboonloha, Swisher, Kang, & Subramanian, 2014), (Yan *et al.*, 2014). There are numerous studies indicating that CMNF films provide a higher smoothness and lower porosity of structure compared to traditional paper. The properties of CMNF films are approaching those of polymer plastic films (González *et al*., 2014), (Kristin Syverud & Stenius, 2009).

Processes and applications in PE applications are briefly presented in the following sections. An overview of using paper and CMNF material in composite films as a substrate for PE is given. This work concentrates mainly on the use of CMNF material in substrates.

2.2.1 Materials, processes and applications in printed electronics

Printed electronics is a combined technology field with a predicted $73 billion global market size by 2025 (Das & Harrop, 2012). A major advantage of using flexible substrates compared to traditional ones is higher productivity and a lower amount of waste in production. An overview of the PE materials, processes, and applications is summarized in the following sections.

Materials

Conductive materials for electrical conductive inks are typically conductive polymers, metallic particles, and carbon-based particles such as graphene and carbon nanotubes (CNT). Metal nanoparticle inks are traditionally made of gold or silver with high bulk metal conductivity (even 50% of bulk conductivity) (Setti *et al*., 2004). However, costs represent a challenge for the widespread use of gold particles, and therefore silver is the most common choice, offering high conductivity, high resistance to oxidation, and low enough reactivity to be used in ambient conditions (Hsieh, Kim, Nogi, & Suganuma, 2013), (Nge, Nogi, & Suganuma, 2013), (L. Xie *et al*., 2012). The most common conductive silver inks are based on spherical nanoparticles (NP) or flakes. In recent years, copper has also been studied due to its high bulk conductivity and low cost. The challenge with

copper inks is their instability under ambient conditions. Some studies have focused on improving the oxidation stability of copper particles (Y. Lee, Choi, Lee, Stott, & Kim, 2008), (Magdassi, Grouchko, & Kamyshny, 2010). The conductive particles are generally selected for specific printing processes due to physico-chemical ink characteristics, particle dimensions and the required performance of the end-use application (Figure 5).

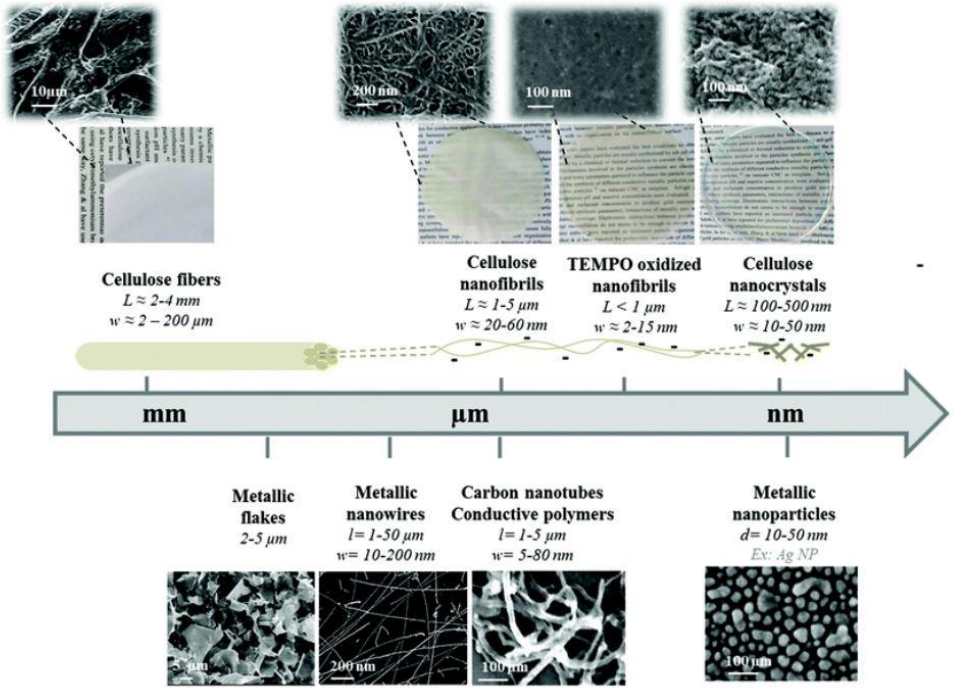

Figure 5. *Schematic length-scale representation of networks obtained with different cellulosic materials (up) compared to specific dimensions of different conductive particles (down) (Hoeng, Denneulin, Bras, et al., 2016).*

Thermal annealing (>150 °C) is typically required in order to achieve highly conducive structures by removing the organic protecting agents and sintering the nanoparticles to some extent. The advantage of paper and novel CMNF neat films is that they do not deform as much as plastic substrates during heating processes, with the exception of special high-cost thermal resistive plastics such as Kapton® film. Conventional heating in an oven or on a hot plate are typical sintering methods. The most common, however, is the tradeoff between sintering time and temperature. This electrical sintering, i.e. compatibility with a fast manufacturing process and a flexible substrate, has been used by Allen *et al.* and Magdassi *et al.* (Allen *et al*., 2008), (Magdassi, Grouchko, Berezin, & Kamyshny, 2010). In their studies designed to identify suitable photopapers and plastics, sintering occurred spontaneously at room temperature after desorption of the organic stabilizing

agents. Other sintering techniques for metal NPs are the argon plasma treatment, microwaves, and various light sources such as IR and UV (Layani, Cooperstein, & Magdassi, 2013), (Tobjörk *et al.*, 2012), (Gaspar, Passoja, Olkkonen, & Smolander, 2016), (S. Jung & Kim, 2010), (Wünscher *et al*., 2012).

The conductivity of conductive polymers and carbon particle inks is about one 100th of that of silver inks. The advantage of conductive polymers is that they can exhibit conductivity with transparency and flexibility at same time. These polymers also tolerate higher processing temperatures compared to metal inks. The most common conductive polymer used is poly (ethylene-dioxythiophene):poly(styrene sulfonate) (PEDOT-PSS), which is stable in water. The lowest reported surface resistivity on paper was 2.6 Ω sq^{-1}, which is twice as high as that on a PET substrate (Trnovec *et al.*, 2009). Graphite has been widely used in flexible batteries. Carbon nanotubes and graphene are common materials used to produce conductive layers in low cost energy storage applications (Hu, Wu, & Cui, 2010), (Lehtimäki, Li, *et al*., 2014), (Tuukkanen *et al*., 2014), (Lehtimäki, Tuukkanen, *et al*., 2014). A specific capacity of 33 F/g at a high specific power of 250 000 W/kg was achieved with an organic electrolyte for CNT films by Hu *et al*. (Hu *et al*., 2010). Conductivity of thin films of CNTs is up to 10^3-10^4 S cm^{-1} and the surface resistivity of 50 nm thick films made of single-wall CNTs (SWCNTs) prepared by vacuum filtration was reported to be 30 Ω sq^{-1} (Z. Wu *et al.*, 2004).

Metal nanowires and nanofibers are attractive mainly due to their high aspect ratio. The elongated particles can form a percolated network at very low concentrations, which makes it possible to produce flexible transparent conductive layer sheets for wearable applications (Kamyshny & Magdassi, 2014), (Yao & Zhu, 2014), (Persano, Camposeo, & Pisignano, 2015) and indium tin oxide (ITO) thin films on glass and polymer substrates (Guillén & Herrero, 2005), (Nisha, Anusha, Antony, Manoj, & Jayaraj, 2005).

Printing processes

The most common printing processes for printed electronics are inkjet printing (Jang, Lee, Lee, & Oh, 2013), (Dogome *et al*., 2013), screen-printing (Chang *et al*., 2012), (B. Peng & Chan, 2014), flexography (Kattumenu *et al.*, 2009), (Hübler *et al*., 2011), gravure printing (Zhu *et al*., 2014), (Hübler *et al.,* 2011), and offset printing (Reuter, Kempa, Brandt, Bartzsch, & Huebler, 2007). The printing technologies have several advantages compared to laboratory scale processes such as photolithography and vacuum processes: the printing processes are fast and use widely available low-cost technology. Magazines, books, and newspaper are printed in trillions of pages annually at a very high speed. New business opportunities are being surveyed for high volume printing machines, due to decreased graphic paper product consumption. However, the requirements for PE applications are different compared to those for graphic papers (Tobjörk & Österbacka, 2011), (R Bollström, Tobjörk, & Dolietis, 2012), (Chang *et al.*, 2012). For

PE applications, a continuous and homogeneous track is needed for functionality, compared to a good visual impression needed in graphic papers. Therefore, layer thickness, smoothness, and print resolution play crucial roles in PE applications.

Inkjet printing is a non-contact, additive process in which the ink is ejected through micrometric nozzles onto the printing substrate. It has high flexibility to use different geometries and applications (Jang *et al.*, 2013), *(Sanchez-Romaguera et al.*, 2015), (Choi *et al.*, 2016). The deposition of thin layers (approximately 0.3-20 µm) is possible at a high speed and resolution using low viscosity inks. Therefore, substrate properties are important in terms of controlling ink spreading and to achieve the required print performance and functionality. The limitations of inkjet technology are in droplet ejection and restriction of particle size for avoiding nozzle blocking. In screen printing, the ink is squeezed through a screen mask using an applied pressure. The non-printed areas in the screen are blocked by a polymer emulsion which allows the ink to pass through the remaining openings into the printed area. The ink properties and wire density of the mesh have an effect on the obtained print resolution and thickness. The used ink in screen-printing usually has a high viscosity and a printed wet layer thickness can be up to 100 µm. Relatively thick layers allow the formation of low resistance structures using conductive polymers.

In flexography, the applications are mostly related to the fabrication of conducting structures, transistors, and organic light-emitting diodes (OFETs) (Hübler *et al*., 2011), (J. Huang *et al.*, 2013), (B. Kang, Lee, & Cho, 2013). A low cost flexible plate is attached to the cylinder and the printed objects are transferred onto the plate. The viscosity of flexography inks is less than that of the screen printing inks. It is possible to form continuous lines by modifying ink properties (higher viscosity and surface tension), although the anilox roll itself consists of discrete cells. A limited solvent compatibility, swelling and ink squeezing at high print pressure, and low viscosities cause problems in flexographic printing processes. Gravure printing has previously been widely used in high volume printing processes for producing conductive structures such as antennas (Zhu *et al*., 2014) and organic solar cells (Hübler *et al*., 2011). The printed structures are engraved into a metallic cylinder by laser, chemical etching, or electromechanically, and a high print resolution can be obtained by gravure printing. The gravure rolls are expensive to manufacture but useful for large volume printing applications. The offset (lithography) printing technology requires high viscosity inks with suitable surface tension for printed patterns. The offset printing is based on wetting differences, with the offset printing roll having different surface energy areas. The non-printing areas are usually wetted with fountain water before transferring the ink onto the image areas. The printing process is indirect: the ink is first transferred to an intermediate cylinder and then to the image areas on substrate. The offset method is rather limited for PE applications due to the presence of water and the viscoelastic properties of the ink.

Coating technologies including spray technology (Zheng, Li, Shi, & Yu, 2014), (Azarova *et al*., 2010), slot die (Krebs, 2009), (H. Kang, Park, & Shin, 2014), and bar and blade coating (Pierre *et al*., 2014), (Lehtimäki, Pörhönen, *et al*., 2014) can also be used to produce conductive layers. These coating technologies can provide large scale, fast, and easy processes to scale up the roll-to-roll production. The limitations of coating methods are the impossibility to produce detailed patterns and a high level of waste production. However, for energy storage applications, rapid production of conductive layers of graphene and CNT inks can be achieved using coating technologies (Lehtimaki *et al.,* 2014).

Applications

Applications for printed electronics include, for example, energy storages (Hu *et al*., 2010), (X. He, 2015), transistors (Fredrik Pettersson, Remonen, *et al*., 2015) *(Grau et al*., 2014), (Eda & Chhowalla, 2009), displays (Berggren, Nilsson, & Robinson, 2007), (X. Xu *et al*., 2016), antennas (Zhu *et al*., 2014), (Rida, Yang, Vyas, & Tentzeris, 2009), and solar cells (Krebs, 2009), (Kamyshny & Magdassi, 2014). Electronic components can be divided into two groups: passive and active. The antennas, inductors, capacitors, conducting wires, and fibers are classified as passive components, whereas transistors, diodes, memories, solar cells, and energy storages such as batteries and supercapacitors are considered as active ones. Basically, all PE applications need some kind of power source such as a battery, capacitor or solar cell. The transistors are probably the most fundamental components needed, but at the same time are the most challenging ones to be fabricated. The functional devices *e.g.* sensors can also work without electricity, for example based on colorimetric indicators. In the following sections the most common PE components for flexible substrates are summarized.

Energy storages consist of capacitors, batteries, and solar cells. A capacitor is fabricated with two electrodes separated by an electrolyte. Thin, even papers have been used as separators. The capacitor structure is filled with a non-aqueous or aqueous electrolyte. The electrostatic charge is stored in the form of an electric double layer at the interface of the electrolyte and electrodes. Therefore, energy is stored by the mechanism of charge polarization. The structure of a battery is similar to that of a capacitor, but the electric charge is stored as chemical energy via the electrochemical redox reaction in the electrode materials. There are already some commercial thin-film batteries fabricated in paper on the market, produced *e.g.* by Enfucell Oy, Power Paper, and Blue Spark Technologies utilizing screen printing and lamination. Recycling of these novel batteries is still a challenge due to the metals used in the batteries. Therefore, development of the recycling process and eco-design were recently investigated (Georgi-Maschler, Friedrich, Weyhe, Heegn, & Rutz, 2012), (Larcher & Tarascon, 2015). Solar (photovoltaic) cells are an alternative energy source to batteries or capacitors (Eom *et al*., 2009), *(*Galagan *et al*., 2013). The most potential use of solar cells is considered to be in large area and

flexible applications on the roofs of buildings. The working principle of bulk heterojunction solar cells is that the donor and acceptor materials represent the key semi-conductive materials, enabling release of electrons when exposed to light. Glass, polymer plastics, and also recently CNF films have been used as substrates for organic solar cells (Costa, Pingel, Janietz, & Nogueira, 2016).

There has been increasing interest in developing new types of *supercapacitors,* also called ultracapacitors, to meet the requirements of energy storage applications (Halper & Ellenbogen, 2006), (Kaempgen *et al*., 2009), (F. Pettersson *et al.*, 2014), (Shi *et al*., 2013). Supercapacitors are rechargeable electrochemical energy storage devices that offer the advantages of high power capability, high rates of charge and discharge, long cycle life, flexible packaging, and low weight compared to other energy storage devices. Future developments are moving towards thin, low-cost, lightweight, and flexible solutions that can be utilized in wearable and disposable electronics applications. An emerging field of energy harvesting applications, for example, from light, RF fields, or vibrations lacks complementary energy storage solutions (Radousky & Liang, 2012), (H. S. Kim, Kim, & Kim, 2011). Low-cost, flexible, metal-free, non-toxic, and disposable supercapacitors produced by efficient processes are needed for applications in PE systems. Nanostructured carbon materials such as CNT and graphene are promising future materials for supercapacitors due to their excellent electrical conductivity and high surface area (An *et al*., 2001), (Z. Chen *et al*., 2011), (T. Chen & Dai, 2013), (Y. Huang, Liang, & Chen, 2012)

Transistors are used as electronic components in displays and logic gates in digital circuits. A logic inverter can be made by simply connecting a transistor to a resistor or a second transistor. The field-effect transistor (FET) is a transistor that uses an electric field to control the electrical behavior of the device. The structure of FET consists of at least four layers: source and drain electrodes, semiconductor, gate dielectric (insulator), and gate electrode. In organic FETs (OFETs) the semiconductor film includes organic polymers. The high operation voltages (10–100 V) are the main challenge of traditional OFETs for portable solutions. Therefore, a low operation voltage is required if batteries, solar cells, or other forms of electromagnetic induction are used together with OFETs. Humidity also increases the risk of electric shocks or irreversible electrochemical reactions at high voltages. The deposition methods and substrate characteristics will also have an effect on the transistor performance, in addition to the transistor type, the raw materials used, and the dimensions.

There is growing interest in electronic memory devices, actuators, displays, and *RFID tags* to be used in future PE applications. RFID tags can be used as a replacement for optical barcodes for keeping track of products. There is a large market potential if these tags can be manufactured at a low cost onto flexible, environmentally friendly substrates. The active RFID tags are powered by batteries

for long reading distances (up to 30 m), whereas passive tags are powered by the reader device (up to 3 m). In addition to the antenna, RFID tags usually need a capacitor, a rectifier, and a transponder that consists of transistor circuits and memory. The identification data is read from the memory and sent to the modulator. The modulator (*e.g.* a transistor) modulates the energy, which is absorbed by the antenna. The reader will then sense and decode the energy. Reading of the data requires the presence of an electric field, where the passive RFID tag and antenna will be exposed (V. Subramanian *et al*., 2006), (Chan, Kung, & Pei, 2005), (Tobjörk & Österbacka, 2011).

2.2.2 Papers and novel composites for printed electronics

The interest in using paper and novel CMNF material films and composites has increased due to the needs of bio-based material, low cost, recyclable, and flexible substrates for PE applications. There have been many recent advances in the field of paper electronics. The obtained conductivity or resistivity of electronic devices depends strongly on the used printing or coating processes and conductive materials. Overall, the critical parameters cannot be established due to the individual main characteristics of each electronic device. However, the sections below summarize the main findings in the field of paper and CMNF as a substrate for PE applications.

The main requirements for substrate properties are smoothness, moisture and thermal resistivity, low porosity, durability, flexibility, dimensional stability, stiffness, and optical transparency depending on the target application. The barrier properties of paper also play an important role in some end-use applications (Grau *et al*., 2014). Moisture and gas vapor barrier properties can be enhanced using different coatings and special surface treatments (Brodin *et al*., 2014). The porosity of paper will also affect transmission rates, *i.e.* the transmission rate will be reduced by increasing the tortuosity. The low porosity and small pore sizes will also reduce the transmission rates of gases and their penetration into the substrate. The smoothness of traditional papers can be improved using pigments and CMNF material (Brodin *et al*., 2014), (Bundy & Ishley, 1991). Paper can also be coated by multiple layers in order to achieve accurate print quality. In many cases, for example, calendering is needed to obtain sufficient characteristics. Another approach to produce smooth and non-absorbing substrates for PE components is to use functional coatings or polymer lamination with for example polyethylene (PE), polypropylene (PP), polyethylene terephthalate (PET), wax, or aluminium. The recyclability and sustainability might also present challenges in these applications.

A multi-layer coated special paper was developed by Bollström *et al*. (Roger Bollström *et al*., 2009). It was demonstrated that sufficiently high smoothness was achieved and that transistors could be fabricated onto it. The authors also demonstrated that a multi-layer coated paper can be used as a substrate for roll-

to-roll processes (R Bollström *et al*., 2012). Trnovec *et al*. used special coatings of mineral pigments, kaolin and $CaCO_3$ and binders, polyvinyl alcohol (PVA), starch and latex for paper in order to achieve high smoothness for PE applications (Trnovec *et al*., 2009). The mechanical and electronic properties of the actuators were studied on hybrid composite and cellulose-based films by Kim *et al (J. Kim et al*., 2010). In many studies the RFID tag was assembled on paper together with an inkjet printed antenna and wires (Rida *et al*., 2009), (Sanchez-Romaguera *et al*., 2015). Paper-based capacitive touch-pads and direct writing on paper with silver nanowire inks were demonstrated by Li *et al.* (R. Z. Li, Hu, Zhang, & Oakes, 2014) and Mazzeo *et al.* (Mazzeo *et al*., 2012).

Paper and paper-like batteries and energy storages have attracted widespread attention. A simpler production of PE applications can be achieved if the power source can be integrated directly to the paper (Hu *et al*., 2010), (Tuukkanen *et al*., 2014), (Andersson, 2012), (Choi *et al*., 2016). Moreover, in these applications the rougher surface of paper and a porous structure can be beneficial. The ion transport across the entire structure is possible and high-power performance can be achieved.

New paper-based products are already on the market. The Arjowiggins "PowerCoat" is a pure, cellulose-based coated paper with a high smoothness polymer-like coating. The resolution of printed features is up to 5 µm. The paper is recyclable and can easily be bended, folded, and torn. Felix Schoeller has also introduced a special paper for PE markets, called "p_e:smart" and having an extremely smooth surface and excellent dimensional stability even at high temperatures. RR Donnelley's RFID Tag Solutions produce a printed electronics platform in which antennas printed directly onto a paper will eliminate the need of using additional PET substrates. This may also lead to thinner labels, lower material costs, and faster production cycles. It also eliminates the need for a chemical etching process.

The novel CMNF materials provide possibilities for cellulose-based substrates in the PE field. Highly transparent, flexible, and recyclable films can be produced with CMNF materials. Several recent publications have studied PE applications in pure CMNF films (Hu e*t al*., 2009), (Koga *et al*., 2014), (Hsieh *et al*., 2013), (Zhu *et al*., 2014), (Yan *et al*., 2014), (J. Huang *et al*., 2013), (Hoeng, Denneulin, & Bras, 2016). Composite CMNF and polymer films were studied by Martin *et al*. (Martin & Jean, 2014). They showed that physical properties of a thin film, including mechanical properties, can be tuned using layer-by-layer assembly techniques. Koga *et al.* compared vacuum filtration, coating, and spin coating methods on CMNF nanopaper (Koga *et al*., 2014). Vacuum filtration provided the best results in terms of conductivity of silver nanowires and CNF, as compared to the coating methods. A major advantage of using 100% cellulose films is their sustainability. The possibility of recycling a transparent and smooth CMNF film used as a solar cell

device was studied by Zhou *et al.* (Zhou *et al*., 2013). Simple immersion of the solar cell in water was used, followed by swelling and dissolution of the CNC substrate. The solar cell components were separated by washing and filtration. The demonstrated recycling procedure was environmentally friendly and straightforward. The other way of recycling was to combust the solar cells, whereupon the CNC material goes with the ashes, and the metal components can be recovered. In addition, Jung *et al.* demonstrated a new method by biological degradation of the CNF substrates (Y. H. Jung *et al*., 2015). Fungal degradation was found to be successful for both 100% CNF films and also for CNF-coated epoxy films. After a certain encapsulation time (84 days), the electronic components were recovered.

The grand challenge for using neat PCMNF films for future consumer products is due to the water sorption. Approaches need to be developed to investigate new effective mechanisms to alter he hygroscopic nature of CMNF materials. Solutions for this purpose will improve barrier properties of CMNF-based films and thus provide better prevention properties for gases in PE applications. This will require more detailed knowledge of interface characterization and mechanisms of CMNF within the matrix of polymers and pigments. More work is needed to develop characterization tools and then to analyze interfaces, e.g. their geometry, thickness, and physical properties which can be used as input values for various models. The variation in properties according to various length scales of CMNF material and its influences on the macroscopic properties of neat composites films need to be further clarified, although some answers were found in this thesis work. The cost challenge of pure neat CMNF films can be tackled by using low-cost pigments, and this thesis work provided some new solutions in this area.

This work demonstrates the fabrication of nanoporous composite films containing CMNFs and mineral pigment in the form of kaolin clay or PCC particles. After an extensive literature survey of pure CMNF films and also several inorganic and CMNF material mixtures for composite films, a few relevant publications were found that combine pigment-CMNF films in PE applications (Hoeng, Denneulin, & Bras, 2016). The developed PCMNF composites have a nanoporous pigment-fiber network structure allowing control of the ink absorption properties. Therefore, high quality functional printing is possible on these smooth, low cost, and nanoporous surfaces. Currently, considering the price of CMNF material, it is believed that their use should be emphasized in PE applications with the use of a lower amount of additive. However, it is noteworthy that the electrical performance of PE applications cannot compete with conventional electronics, and will therefore find alternative end-uses where other aspects than the electrical performance are important.

3 Materials and methods

3.1 Composite raw materials

3.1.1 Mineral pigments

Precipitated calcium carbonate (PCC)

Precipitated calcium carbonate (PCC) pigment was produced synthetically by a reaction between slaked lime and carbon dioxide. In this work, two different commercial types of PCC were used in laboratory scale: Rosette shaped Albacar (Specialty Minerals Inc.) in *Papers I, II and IV,* and rhombohedral OptiCal CP (Imerys) in *Paper I*. Aragonite-shaped Opacarb A40 PCC (Specialty Minerals Inc.) was used in semi-pilot scale in *Paper IV*.

Kaolin

Kaolin consists of hydrated aluminosilicate in which kaolinite is the dominant material. Kaolinite has a layered structure with a particle shape and size depending on the pigment origin. In this work, plate-shaped Intramax 60 (Imerys) was used as kaolin filler in laboratory and pilot scale in *Papers I-IV*. In addition, two platy kaolin grades, Capim SP (Imerys) and a coating grade Capim DG (Imerys) were used in the pilot-scale trials in *Paper IV*. The pigments used in the laboratory scale studies included platy kaolin Capim SP (Imerys) and ultra-platy crystal kaolin HX spray dried Barrisurf™ (Imerys) in *Paper V*.

Table 1. *Information of pigments provided by manufacturers (Imerys and Specialty Minerals). Properties may vary depending on the production location.*

Pigment type	Chemical composition and morphology	Shape factor (if known)	Average pigment size [wt-% <2μm]	D50 [μm] / Specific surface area (SSA)
Intramax 60 (Imerys)	Platy filler kaolin	30	60	
Capim DG (Imerys)	Platy coating kaolin	15	92	D50 = 0.56
Capim SP (Imerys)	Platy coating kaolin	30	90	
Barrisurf HX (Imerys)	Barrier coating kaolin	Hyper-platy	64	
Albacar (Specialty Minerals)	PCC filler grade; scalenohedral (exhibit clusters (rosettes) of triangular-shaped crystals			D50= 1.9 μm SSA = 6 to 12 m^2/g
Optical (Imerys)	Coating PCC with fine narrow particle size distribution			D50=0.4
Opacarb A40 (Specialty Minerals)	PCC coating grade; aragonitic individual needle-shaped (acicular) crystals that are long and narrow			D50 = 0.5

3.1.2 Cellulose micro- and nanofibrils (CNF and CMF)

Cellulose microfibrils (CMF) used in *Papers I–II* was a commercial product Celish KY 100G from Daicel Chemicals ltd., Japan. The cellulose nanofibrils (CNF) in *Papers II–III* were made from a once-dried bleached hardwood (birch, *Betula* L.) The CNF was obtained after eight passes through a super mass colloider grinder (Masuko Sangyo type MKZA10-15J, Masuko Sangyo Ltd., Kawaguchi, Saitama, Japan) by using a decreasing gap width and an increasing operating power. The rotation speed was set to 1500 rpm.

TEMPO-oxidized cellulose nanofibrils (TCNF) were produced from never-dried bleached softwood Kraft pulp in *Paper V*. The pulp fibers were fibrillated by a two-pass treatment using a Microfluidizer M7115-30 after oxidation. Never-dried bleached softwood Kraft pulp was the source of native (CNF) and enzymatic (ECMF) grades. The same source material was used as an unbleached grade for lignocellulosic grade (LCNF). The fibril cellulose gels (CNF and LCNF grades) were obtained after six passes through a Masuko grinder with a rotation speed of 1500 rpm. Enzymatic grade (ECMF) was processed at a high consistency (20–30% dry solids content) using cellobiohydrolase (CBH) enzymes and low energy mixing.

3.1.3 Characterization of cellulose micro- and nanofibrils (CMNF)

Optical microscopy was used to characterize the CMNF materials, using Congo Red (0.5%) and Toluidine Blue (0.1%) as marker colors. Rheological properties, including storage modulus, loss modulus and shear viscosity, for the studied CNF grades (CNF, LCNF, ECMF and Daicel) were measured using a rotational rheometer at a consistency of 0.5% (Anton Paar MCR301, ST22.4V vane spindle method). VTT fine grade (*Papers II–III*) rheological properties were measured using a Brookfield rheometer model RVDV-III Ultra at 1.5% consistency using vane type spindles.

Water retention of the CMNF grades (CNF, ECMF, TCNF and LCNF) in *Paper V* was measured using a modified SCAN-C 62:00 (ÅAGWR method). The capacity of the fibrillated material to hold water under centrifugal force and pressure filtration was measured. The method illustrates the level of fibrillation and the network structure of material. The charge of cellulosic gels was measured according to the standard SCAN-CM 65:02. The amount of residual fibers was measured using a Kajaani Fiberlab analyzer. The estimation for non-fibrillated fraction was made using the starting initial material and produced CNF material, which were analyzed based on the amount of detected fibers and the concentration of the suspension.

Table 2. *Summary of used CNF / CMF grades.*

CNMF code	Origin of material	Production method
Celish KY 100G (Daicel) *(Papers I-II)*	Commercial	-
CNF *(Papers II-III)*	Once-dried bleached hardwood (birch)	Super mass colloider grinder (Masuko) after 8 times
TCNF (Paper V)	Never-dried bleached softwood kraft pulp	TEMPO-oxidized and after that two-pass treatment by Microfluidizer
CNF *(Paper V)*	Never-dried bleached softwood kraft pulp	Super mass colloider grinder (Masuko) after 6 times
LCNF *(Paper V)*	Never-dried softwood kraft pulp	Super mass colloider grinder (Masuko) after 6 times
ECMF *(Paper V)*	Never-dried bleached softwood kraft pulp	Enzymatic treatment by cellobiohydrolase enzymes

3.1.4 Additives and references

The additive used in *Paper V* was a plasticizer, D-Sorbitol (S1876, Sigma Aldrich). In *Paper I* and in unpublished data, different plastic films were used as reference materials: polyethylene terephthalate (PET) film Mylar A 50 and 190 µm from Dupont Teijin Films, Lumirror 40.01 PET from Toray Plastics Europe and polyimide film Kapton from DuPont. HP Everyday Photo paper, PEL Nano P60 (specialty paper for printed electronics) from Printed Electronics Ltd. (Cambridge, UK) and handsheets produced from chemical hardwood Kraft pulp were used as paper-based references. In *Paper V* a multi-layer coated paper (Roger Bollström *et al.*, 2009) was used as a reference material.

In the pilot scale tests poly(ethylene terephthalate) (PET) film was used as a plastic carrier material in *Papers III–IV*. The plasma activation was made for the carrier film with an argon and nitrogen blend at an intensity of 50 W/m²/min using a Vetaphone Corona-Plus (Type TF-415, CP1C MKI1 2.0 kW) device. The objective of the plasma treatment was to increase the surface energy of the carrier film.

The reference sheets for drying tests in *Paper III* were cut from the never-dried pulp made on a Valmet pilot machine with a grammage of 106 g/m² and an initial dry solids content of approximately 50%.

3.2 Manufacturing of composites

3.2.1 Forming

The composites were manufactured by vacuum filtration in laboratory scale and by film casting in semi-pilot scale. The forming methods are described in this section. In this work, pressing and drying processes were studied extensively, and the methods were developed during the work. All the studied pressing, drying, and calendering methods are outlined here.

Vacuum filtration in laboratory scale (Papers I, II and V)

The composites including mineral pigment and CMNF were produced by vacuum filtration in laboratory scale in *Papers I, II and V*. The CMNF material was activated in a 0.2–0.5% dry solids content using a high shear mechanical mixing. The mixing was done using, for example, IKA or NETZSCH Shearmaster for approximately 15 minutes at room temperature, and deionized water was used as a diluter. The mineral pigments were dispersed to 18–20% dry solids content using a mixer. The pigments were then diluted together with CMNF material to a forming consistency of 0.2%. Pigment-CMNF suspension was filtered through a sintered glass funnel device with a pressure of 0.8 bar. A blue stripe Whatman filter paper with a porosity of 10–16 µm was used in the glass funnel to retain both micro- and nanoscale fibrils and pigments.

Film casting in semi-pilot scale (Papers III and IV)

The semi-pilot scale composites were manufactured using a solvent casting method at a coating pilot line (Coatema® Coating Machinery GmbH, Dormagen, Germany). The suspension included 80 wt-% of pigment and 20 wt-% of CNF. The components were dispersed using high shear forces in a dissolver Diaf 100WH for 50 minutes at 400 rpm. The pigment-CMNF suspension at 7% dry solids content was formed by the applicator with a speed of 2 m/min on plastic film. The web width was 300 mm with a length of 6–8 m. The grammage of the slightly wet pressed composites varied between 150 and 220 g/m², and there was a similar variation in the initial solids content in the range of 20–35%. (*Paper III* and *IV*)

3.2.2 Wet pressing

A gentle wet pressing of filtered composites was performed directly after forming. The composites were pressed according to the procedure described in Figure 6. The initial pressing was performed by passing a metal roller ten times over the composites. The composites were sandwiched between the filter and board papers. Glass or metal plates were used as rigid supporting materials. The smooth filter paper was used together with board samples to absorb the excess water.

After the pressing phase in *Papers I* and *II* the samples were directly extracted from the filter paper and dried in an oven under a weight to prevent drying shrinkage. In *Paper V* the samples were pre-dried with a contact dryer at a temperature of 62°C for approximately three minutes and then extracted. The required pre-heating and pressing times were dependent on the CMNF material used.

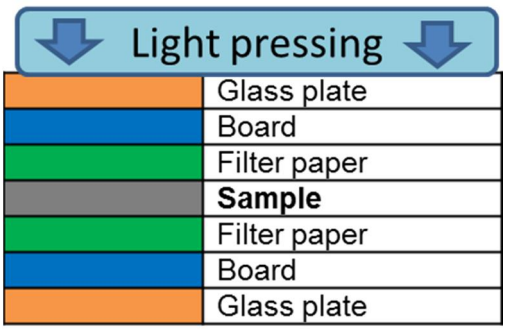

Figure 6. *A schematic diagram of the pressing procedure of composite samples.*

The composites manufactured on the semi-pilot line (*Papers III–IV*) were cut to A4 size together with the supporting PET film and sandwiched between filter papers, boards and metal plates. The gentle pressing was performed similarly to the laboratory scale studies in order to remove excess water. The composites were sealed in plastic bags at room temperature for further pressing and drying studies carried out in *Paper III.*

3.2.3 Drying

In *Papers I–IV* the vacuum filtered composites were dried in an oven at 55 °C at 5.6 kPa pressure for 48 hours in order to prevent drying shrinkage, with the samples sandwiched in between the glass plates. Furthermore, the semi-pilot scale composites were dried under the same conditions. In addition, other drying possibilities were studied in *Papers III* and *IV*. Three different drying methods and their combinations were investigated in *Paper III* based on paper and board technology: contact drying, impingement drying and press drying (Figure 7).

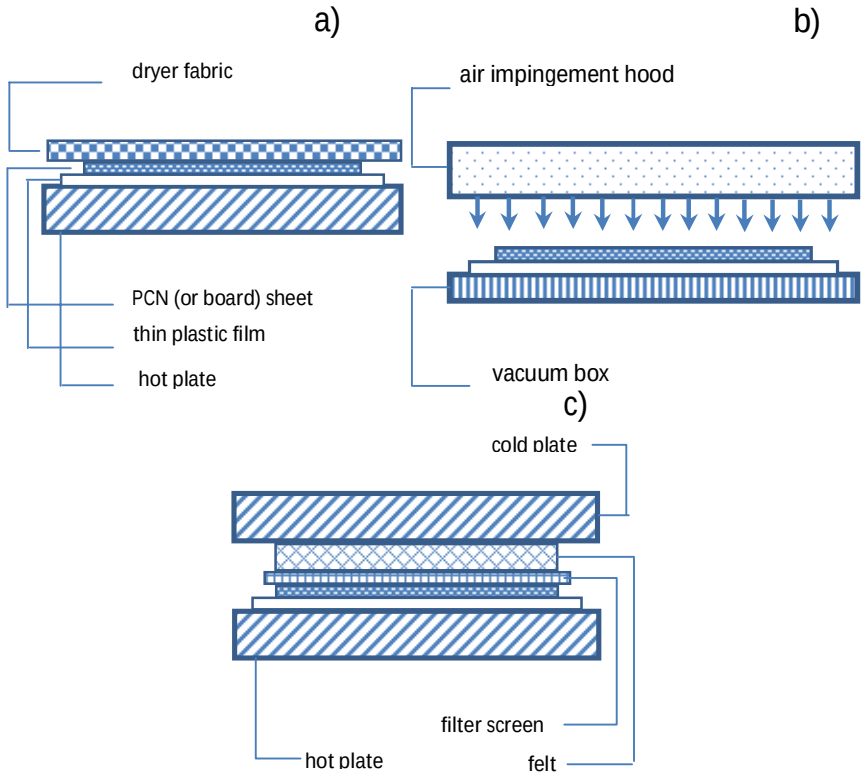

Figure 7. *Three different drying methods used: a) contact drying b) impingement drying and c) press drying. PCN means the studied PCMNF composite.*

The contact dryer, as outlined schematically in Figure 7a, includes a curved metal plate, heated by electrical coils on the bottom side, and a tensioned dryer fabric. The drying experiments were carried out at temperatures varying from 50 °C to 80 °C in *Paper III* and at a temperature of 60–62 °C in *Papers IV and V* for approximately 15–20 minutes. The commercial fabric tension was set to 2 kg/cm with a permeability of 1600 $m^3/m^2/h$ in all the studied trial points. The studied composite surface was set on top against the hot plate.

The impingement dryer consisted of an air impingement hood, a vacuum box, and an air heating system (Figure 7b). The geometry of the air impingement hood had an open area, nozzle distances, nozzle diameter and a distance to the studied material that corresponded with commercial dryers. The samples were moving together with a vacuum box under the hood for a certain time.

The hot press drying was carried out using a hydraulic laboratory sheet press device with an additional hot plate in the bottom (Figure 7c). In *Paper III* the experiments were carried out with two different pressures, 60 and 420 kPa. The temperature of

the pre-heated plate was either 80 or 110 °C and the size of the sample was 160 × 160 mm² with a thickness of 25 mm.

In *Paper IV,* semi-pilot scale composites were dried either in an oven or using a contact dryer with varying parameters. In *Paper V,* the contact dryer was the only drying method used.

Throughout the drying experiments performed in *Paper III*, the moisture ratio MR_i was obtained from

$$MR_{\mathrm{i}} = \frac{m_{\mathrm{i}} - m_{\mathrm{d}}}{m_{\mathrm{d}}} \left[\mathrm{kg/kg}\right] \quad (1)$$

where m_i is the initial mass of sample before drying and m_d the final mass of sample after keeping it in an oven for 2 hours at a temperature of 105 °C after the drying experiments.

3.2.4 Calendering

The composites were conditioned for at least 24 h in standard climate conditions (temperature 23 °C and 50% relative humidity, RH) after the drying and before calendering and physical testing. The composites were single pass calendered using a laboratory scale calender with a hard roll nip. The applied pressure was approximately 20 MPa, with a surface temperature of the lower roll of 150–170°C (*Papers I–V*).

3.3 Printing

3.3.1 Inkjet-printed conductive lines (Papers I and II)

Inkjet printing was studied using a silver nanoparticle ink in *Papers I* and *II*. Conductive patterns were printed using a Dimatix DMP-2800 inkjet printer on composites using AGP Silverjet DGP (30LT) ink from ANP Co. Ltd., Seoul, Korea in *Paper I*. The silver ink was sintered in an oven at 125 °C for 60 minutes. Ink layers were printed for composites and for the reference PET film (Mylar A). The layout for the test platform included 20 mm long lines with contacting pads at both line ends. A multimeter Fluke 175 was used to measure the resistance of the silver lines, given by

$$R = l / (\sigma \times w \times h) \quad (2)$$

where l is length, w is width, and h is thickness of conductive lines, and σ is conductivity of the material. The sheet resistance R_s can be calculated from

$$R_s = 1 / (\sigma \times h) = R \times w / l, \quad (3)$$

where R_s is the resistance of a square shaped conductor (l=w) with uniform thickness.

AGP Silverjet DGP (30LT) silver nanoparticle ink was used in *Paper II* for printing conductive patterns. The inkjet printing was carried out using Autodrop System (Microdrop Technologies) with an MD-K-130 dispenser head (50 ml size of the nozzle). Four-point resistance measurement was performed using an Abilent 34970 data acquisition unit for 10 mm effective sample lengths. The composites were sintered on an Instec hot plate at 220 °C for 300 or 600 seconds. In addition, the height and width of conductive lines were measured using a surface profiler (Wyko NT9100, Veeco Instruments Inc. Arizona USA) in vertical scanning interferometry mode from an area of approximately 1.2 mm².

3.3.2 Screen-printed and spray-coated supercapacitors (Paper IV)

Screen-printing was used for electrodes with a conductive commercial graphene ink (Vor-ink X103, Vorbeck). The electrodes were printed on both sides of the composite. The samples were dried in an oven at 120 °C for two minutes after printing. Further drying for ten minutes was performed after all layers had been deposited in order to ensure proper ink drying. In addition, a spray-coating method was used for producing carbon nanotube (CNT) electrodes on both sides of the composite. The used CNT-xylan nanocomposite ink was produced by Nemcel (Lehtimäki, Tuukkanen, *et al*., 2014). The structure of a supercapacitor was obtained on both of these manufactured electrodes. The ink contained 3.0 wt-% CNT with 1.5 wt-% xylan in a water suspension. A PET mask was used to define the electrode area during the spray-coating.

The length of the graphene electrodes was 3.2 cm, with a width of 1.4 cm having an overlap of 1.4 cm that produced an active device area of 2 cm² (Figure 8). The active area of the supercapacitor was soaked in aqueous NaCl (1 M) suspension during the measurements.

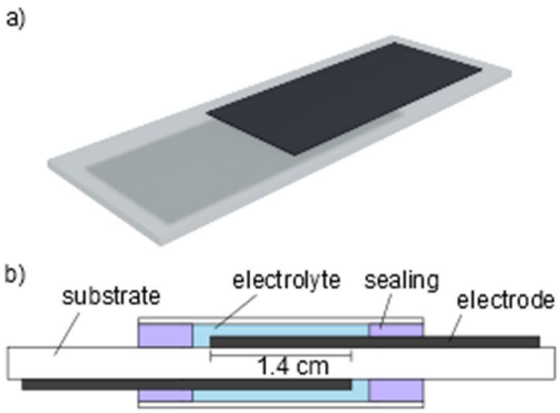

Figure 8. *A schematic overview of the produced supercapacitor structure: (a) a cross-sectional view and (b) the device configuration and assembly.*

The produced graphene and CNT supercapacitors were characterized using a 2-electrode configuration in a Zahner Zennium potentiostat / galvanostat. A cyclic voltammetry (CV) was recorded from 0 to 0.9 V at voltage sweep rates of 5, 10, 50, and 100 mV/s. The supercapacitor properties were determined from a galvanostatic (constant-current) experiment according to an industrial standard (IEC 62391–1 (2006)). The devices were charged to 0.9 V for one minute and then held at 0.9 V for 30 minutes. After charging, the samples were discharged with a constant current. The capacitance was calculated from the slope of the discharge curve. The equivalent series resistance (ESR) was defined from the initial IR drop at the beginning of discharge.

3.3.3 Screen-printed antennas

One proof-of-concept demonstration was made using screen printing to produce antennas for kaolin-based composites. The silver ink (DuPont 5029) was used in printing and a commercial RFID chip (strap) was attached using silver epoxy. Thickness of the printed lines was 5–10 µm, measured using a DeKTak stylys profilometer. The readout demonstration by near field communication (NFC) technology was made using a Samsung-Google Nexus S NFC phone.

3.3.4 Manufacturing and electrical performance of transistors (Paper V)

Transistor device structure consisted of a blend of poly(3-hexyl thiophene) with an environmentally friendly and biodegradable insulating polymer poly(L-lactid acid) (P3HT:PLLA) as a semiconductor layer. The weight ratio of the used blend P3HT:PLLA was 1:4. The solid electrolyte in the transistor structure was a mixture of D-sorbitol, Choline Chloride (ChoCl) and a polyolefin binder. The electrolyte was dispersed in a water dispersed binder (HYPODTM 8501). Sorbitol and ChoCl were mixed at a molar ratio of 1:1 until the mixture turned into a liquid gel. This gel was

then mixed with the water-dispersed binder. The electrolyte was finally spin casted at 3 000 RPM for 30 s. Water evaporated during the casting process, resulting in a solid film containing approximately 50% sorbitol/ChoCl and 50% binder. The source-, drain-, and gate electrodes were all thermally evaporated at approximately 10 mbar pressure. All transistor devices were fabricated and measured in a nitrogen atmosphere. (Roger Bollström *et al*., 2009), (Fredrik Pettersson *et al*., 2014), (Fredrik Pettersson, Remonen, *et al*., 2015), (Fredrik Pettersson, Adekanye, & Österbacka, 2015).

The transistors were characterized by measuring transfer curves in a saturation mode, where the drain voltage (V_D) was kept at -1 V and the gate voltage (V_G) was swept from 0 V to -1.2 V and back to 0 V. The figures of merit (FOMs) were extracted from the measured transfer curves. These include the drain current (I_D) measured at V_G = -1.2 V (ON-current), I_D measured at the point where V_G starts to increase logarithmically (OFF-current), the ratio between the ON- and OFF-current (ON/OFF-ratio), the gate current at V_G = -1.2 V (leakage) and the ratio between the leakage current and the ON-current (leakage/ON-current).

3.4 Characterization of composites

Morphological, mechanical, and optical properties of the sheets were characterized with standard methods commonly used in paper testing and in regular testing conditions (23 °C and 50% RH).

3.4.1 Surface roughness

The composite surface roughness was measured using an Altisurf 500 optical profilometer in *Papers I-III* and *V*, and reported as an average deviation of surface height, *i.e.* the roughness values R_a given by

$$Ra = \frac{1}{NM}\sum_{x=0}^{N-1}\sum_{y=0}^{M-1}\left|z_{x,y}\right|, \qquad (4)$$

where z_i is the normalized height of surface at a measurement point i. A sampling interval of 1 µm was used in all measurements. 10-20 lines with a length of 30 mm were measured with a Gaussian filter used to remove variations over 5 mm in *Paper I*. The upper side of the composite was measured with an area of 1 × 1 mm^2, and variations in excess of 0.25 mm were removed with various (5–18) replicate measurements in *Papers II, II* and *V*. Heights z_i were further treated by removing 0.5% of the smallest and largest values of data after Gaussian filtration of all the measured samples. In *Paper V* the sampling resolution was 1 µm and the total measured area was 0.5 × 0.5 mm². The results were filtered with a 0.1 mm

Gaussian screen. The measurement was repeated six times for each measured sample.

In *Paper IV* surface roughness was measured using a Dektak 150 Surface profiler (Veeco) with a 2.5 µm probe at 1 mg pressure. The reported values included the arithmetic mean roughness R_a, the root mean squared roughness R_q, and the peak-to-valley value as the height difference between the minimum and maximum points in the measured data.

3.4.2 Porosity

Porosity was calculated using the measured grammage with the thickness values of the composites with estimated mass densities of the pigment and CNF. The use of a porosimeter is challenging for several reasons. Firstly, the porosimeter might not be able to detect small pores between the pigments and CNF, and thus produce valid values for these. The second reason is related to the simulation performed in *Paper II*: only the packing of the pigment particles was simulated without CNF and thus the porosity without CNF would be needed to compare simulated and experimental structures. Finally, in vacuum filtration the upper side of the composite was pigment-rich, whereas the bottom side was CNF-rich. This means that measuring the structure with a porosimeter results in values which are not reliable for the upper side used in the composite testing and characterization. In the porosity calculation, mass densities of 1.5 g/cm^3 were used for cellulose, 2.6 g/cm^3 for kaolin, and 2.71 g/cm^3 for PCC. The porosity ∅ in an n-component composite was calculated according to the equation

$$\emptyset = 1\left(\sum_i^n \frac{c_i \rho_b}{\rho_i}\right), \quad (5)$$

where c_i is the weight fraction of material i, ρ_i is the mass density, and ρ_b is the bulk density of the sheet calculated from the grammage g and sheet thickness h as $\rho_b = g/h$.

3.4.3 Mechanical properties (*Papers I, III* and *V*)

Mechanical properties of the composites, including tensile strength, tensile stiffness, stretch, tensile absorption energy, tear strength and modulus of elasticity were measured using a Zwick tensile tester, EN ISO 1924-2:1994 in *Paper I*. Mechanical strengths were also measured using a so-called C-Impact tensile tester with a sample length of 50 mm and a width of 15 mm in *Paper III*. The elongation speed was set to 10 mm/s with a strain rate of 20%/s. Data recording frequency was 2 kHz. The strength and breaking strain were obtained based on the measured stress-strain curve as the values corresponding to the maximal stress. The experiments were repeated five times for each trial point. Instron 8872 equipped with a 10 kN load cell was used in *Paper V* to characterize the mechanical

properties. Stress-strain data were produced using a strain rate of 1 mm/min for ten replicate measurements.

3.4.4 Structural analysis (SEM and HIM)

Scanning electron microscopy (SEM) images were used to characterize the effects of various parameters on the composite structures and morphology (*Papers I–IV*).

Additionally, scanning helium ion microscopy (HIM) was utilized in *Paper V,* providing high-resolution images with a large depth of field on a wide range of materials. HIM can be used directly for high-resolution imaging of various non-conductive organic samples such as cellulose fibers, without the need for a conductive carbon or metal coating. HIM can be used for imaging the composites from macro to nanoscale that complement X-ray and optical coherence tomography. The composites were imaged using HIM with a beam current of 0.2–0.3 pA at 30 keV energy in *Paper V*. Three samples were prepared for each studied composite: top, bottom, and cross-section. The top and bottom sides were imaged with a 950 µm (the smallest possible magnification), 100 µm, 20 µm, and 4 µm field of view (FOV) at the same region on the sample. Sample charging was neutralized with an electron flood gun in all images with approximately 10 min of total collection time for each image. The original image resolution was 2048x2048 pixels. In this study, the images have been compressed to half of the pixel resolution and image contrast has been enhanced.

3.4.5 Dimensional stability (Paper I)

The dimensional stability of composites was measured using different RH change loops to which samples were subjected. The first RH change was from 50% to 10%, followed by an RH increase to 66% and 90%. Finally, the samples were tested again in 10% RH. The dimensional change percentages in sample size were detected in every HM step. The samples were scanned with a Umax 3000 device in grey scale with a resolution of 300 dpi.

3.4.6 Grammage, thickness, density, bulk and air permeability

The composite testing was performed according to the following standards: Grammage (EN ISO 536:1995); Density, Bulk, sheet thickness (ISO 534:1988) in *Papers I, III* and *IV*. The grammage was measured using SCAN-P 6:75, for thickness SCAN-P 7:75 was used and for air permeability SCAN-P 19:78 with a measuring head of 10 cm^2 in *Paper II*. Density and bulk values were calculated based on these measurements. The composite grammage was analyzed by scanning the composite surface area using an Epson Perfection 3200 PHOTO scanner, whereas the thickness and density were determined with a Lorenzen & Wettre micrometer (SCAN-P 7:75) in *Paper V*. The air permeability was measured using a Lorentzen & Wettre SE 166 device utilizing the SCAN P-26:78 standard.

3.4.7 Formation (Paper V)

The evenness of composites was measured using a β-ray method with a storage phosphor screen (SPS). The samples were exposed to beta radiation using carbon C_{14} as a source of the radiation. The screen was scanned with a Fuji BAS-1800 II SPS reader with a resolution of 0.1 mm to determine the radiation absorption map, which was then converted into a grammage map. The standard deviation of grammage, *i.e.* formation was then calculated using the measured area of 100 × 100 mm². The formation values were reported as specific formation numbers (unit √g/m) in which the deviation of the basis weight was taken into account.

3.4.8 Thermal resistivity (Paper IV)

Thermogravimetric analysis (TGA) was conducted using a Mettler TGA 851e thermogravimetric analyzer (Mettler Toledo) for composites. The measurements were performed in normal atmosphere and using an air flow of 50 ml/min. The heating rate was 100 °C/min up to a temperature of 230 or 270 °C.

3.4.9 Stain length (Paper V)

An IGT printability tester was used to determine the stain length of samples according to the AIC2-5T2000 standard and the Global Standard Tester instructions. The printing disc and a paper strip were placed on the sector of the IGT-printability tester and a drop of oil with a volume of 5.8 ± 0.3 mg was spread to a stain in the printing nip. The length of the stain was measured. The test measures the porosity of a surface if the surface smoothness of samples is the same.

3.4.10 Numerical modeling (Paper II)

The numerical model describes the skeleton structure formed by pigment particles with various shape and size distributions. CNF material is assumed to fill the voids of the pigment structure. The collection of computer codes (called Particle Layer Analysis, PLA) was developed for complete generation and analysis of sheet-like structures consisting of pigments. The model includes five separate programs: particle creation (PC), particle packing (PP), format conversion (FC), profilometer simulation (PS), and structure visualization (SV). All codes except the SV were developed using Fortran 95 programming language, that can be used in any standard computing platform.

4 Results and discussion

In this work the effect of raw materials, including pigment types and content as well as CMNF grades, on the composite properties was studied. The influence of manufacturing parameters on the composite properties was also examined. Furthermore, the main findings of using PCMNF composites as substrates for printed electronics are presented and discussed here. This section presents the main results of the published articles. Table 3 summarizes the studied composite raw materials, variables and used references.

Table 3. *Studied composite raw materials, composition variables, forming type and references identified to the attached publications.*

Composite raw materials	Composition and variable of it	Forming	References	Paper
Kaolin, PCC and Daicel CMF	Pigment content of 50, 80 and 90 wt-% CMF content of 50, 20 and 10 wt-% Different kaolin and PCC types	Vacuum filtration in laboratory scale	Different plastic films, HP Everyday Photo paper, PEL Nano P60 Electronic grade paper and handsheets	*Paper I*
Kaolin, PCC, Daicel CMF, CNF	Pigment content of 80 wt-% CMNF content of 20 wt-% Different kaolin and pigment types	Vacuum filtration in laboratory scale		*Paper II*
Kaolin, CNF	Pigment content of 80 wt-% CNF content of 20 wt-%	Film casting in semi-pilot scale	Reference board in drying tests	*Paper III*

Kaolin, PCC, CNF	Pigment content 80 wt-% CNF content of 20 wt-% Different pigment and CNF types	Vacuum filtration in laboratory scale and film casting in semi-pilot scale		*Paper IV*
Native CNF, LCNF, ECMF and TCNF Kaolin pigment	Cellulose nanofibrils composition of 20 and 43 wt-% Pigment content of 80 to 43 wt-%. Different CMNF types (see Table 4) In addition plasticizer (15 wt-%) in some trial points (see Table 5)	Vacuum filtration in laboratory scale	ÅA multi-layer coated paper	*Paper V*

4.1 The effect of raw materials on composite properties

Novel composites consisting of combinations of inorganic pigments, such as kaolin and precipitated calcium carbonate (PCC), and cellulose micro-and nanofibrils were developed in this work. The impact of raw materials on composite properties was studied, with the results presented in this section.

4.1.1 Pigment type and content (Papers I and II)

The effect of pigment type on composite properties was studied using different grades of PCC and kaolin. It was observed that pigment type has a significant effect on surface smoothness, porosity, and thermal resistivity of composites. Furthermore, based on the differences in composite properties, conductivity and other functionalities were influenced by the pigment used.

Cross-sectional images of composites containing PCC filler amounts from 50 wt-% (A and B) to 90 wt-% (C and D) are shown in Figure 9. High resolution SEM images

show that CMF formed layer-like film structures in the composites containing 50 wt-% filler, which has also been reported for pure CMF films (Marielle Henriksson, Berglund, Isaksson, Lindström, & Nishino, 2008). The pigment agglomerates settled between CMF layers. When the filler amount was increased from 50 to 80 wt-% and simultaneously the CMF amount decreased from 50 to 20 wt-%, there was not enough CMF surface area to produce a layered structure and highly packed microfibril individuals were located around the filler agglomerates, thus gluing them together.

Moreover, in *Paper V* it was shown that platy kaolin pigments (Barrisurf, Imerys) created a tortuous path with a long migration path through the composite. The long migration path suggests better barrier properties.

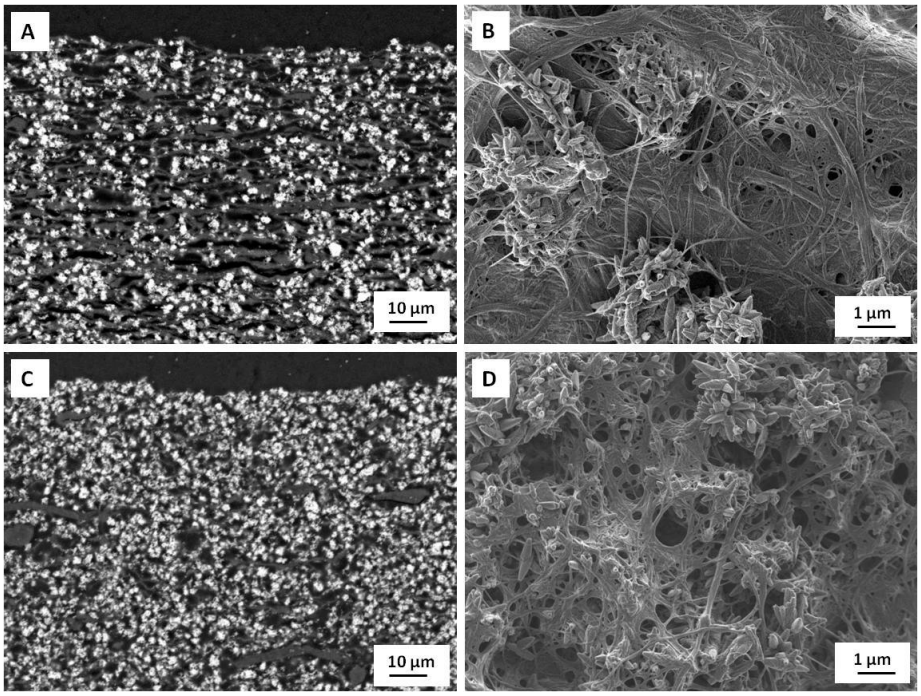

Figure 9. *SEM images of cross-sections (A and C) and surfaces (B and D) of composites containing 50 wt-% (A and B) and 80 wt-% PCC Albacar filler (C and D). The used CMF was commercial Daicel KY-100G in this study.*

Mechanical properties

Figure 10 presents tensile and tear strengths of PCC-based composites with different filler contents. Naturally, when the amount of filler content increased, both strength properties were significantly decreased. Nevertheless, the strength properties of composites containing 80 wt-% of pigment were sufficient for further handling of the films *e.g.* in roll-to-roll printing processes. The composites had a

flexible and plastic-like surface after calendering. The 20 wt-% CMF amount was sufficient to bring elasticity to the structure.

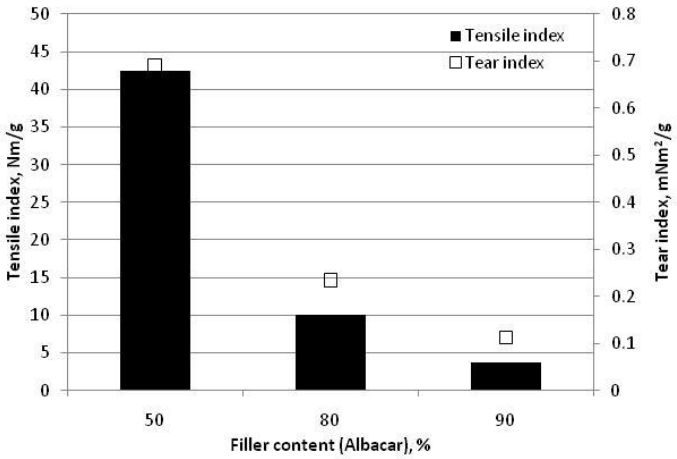

Figure 10. Tensile (bars) and tear (squares) index of composites at different PCC filler loading levels. *The used CMF was commercial Daicel KY-100G in this study.*

Surface roughness

Low surface roughness is one of the most important requirements for substrates that are used for printed electronics in terms of achieving continuous conductive lines. In this study, roughness values were investigated using an optical profilometer. In Figure 11 the effects of filler type and also of calendering on the surface roughness of vacuum filtered composites containing 80 wt-% of filler were studied. The calendering was essential for composites to produce smooth surfaces. After calendering, PCC (Albacar) produced a smoother surface compared to the kaolin and PCC (Optical) substrates. Daicel KY-100G was used as CMF material in all these trial points. The smoothness of the composites was at a similar level compared to the reference materials measured in this study. PCC (Albacar) based substrates were smoother than commercial photopaper. The measurement of PET-film (Mylar A) encountered some difficulties due to transparency, which should be taken into account when comparing the results. In conclusion, calendered composites can be expected to have a sufficient smoothness level for printed electronic applications.

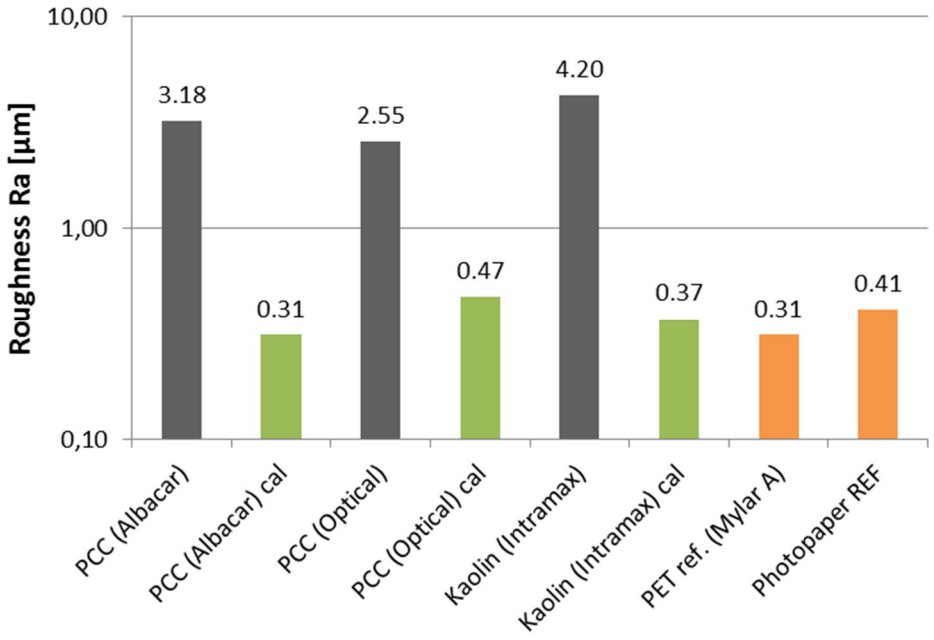

Figure 11. *The effect of pigment type and calendering on surface roughness. The right hand side shows the corresponding values of reference materials. The amounts of filler and CMF were 80 wt-% and 20 wt-%, respectively. The used CMF was commercial Daicel KY-100G in this study.*

Porosity

The relative area fractions of CMF, fillers, and pores were calculated from the SEM cross-sectional images. The results show that the composite porosity decreases when the filler content increases (Figure 12). Furthermore, a higher filler loading decreased composite porosity. The calendering affected the porosity as expected, resulting in dense composite structures with a relative porosity area close to zero. The filler component dominated the structure after the calendering and the CMF content was as low as 11% in this study. The calculation of porosity had some uncertainty due to the small measured SEM image area.

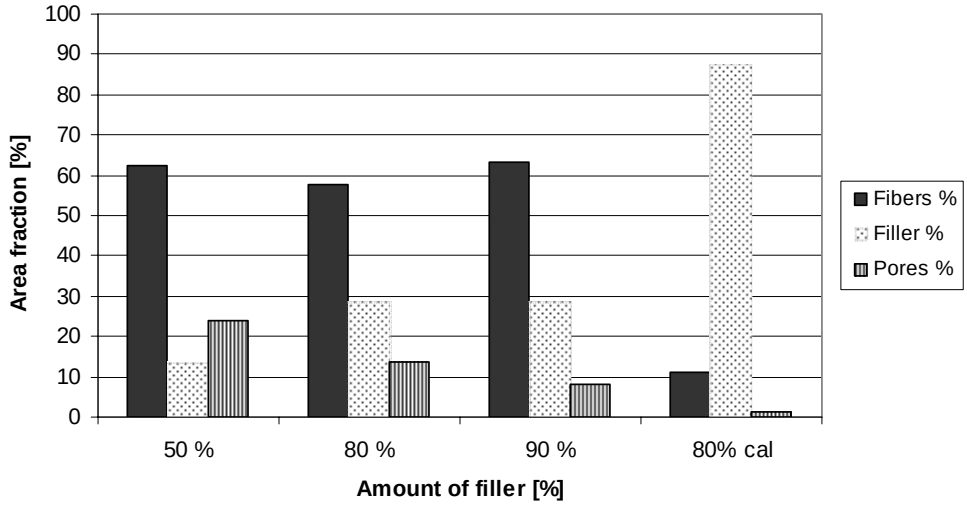

Figure 12. *Relative area fractions of CMF, fillers, and pores calculated from the composite SEM cross-sectional images. The used filler and CMF were PCC (Albacar) and Daicel KY-100G, respectively. The cross-section surfaces were examined under a scanning electron microscope (SEM) in back-scattered (BS) mode. BS-mode gives a contrast between a filler, a fiber structure and an embedding resin that makes it possible to segment different regions according to their grey level with an image analysis program. After removing the background, a semi-interactive segmentation was performed in the region of interest, i.e. the cross-section of the paper. The amounts of fibers, fillers and pores were calculated as an area fraction %.*

The composite porosity was further studied with a modeling tool, which describes the skeleton structure of the formed pigment particle structure. Figure 13 shows examples of pigment structures in composites simulated in Particle layer analysis (PLA). The differences between PCC- and kaolin-based sheets can clearly be observed from the simulated structures. Using simulation as a tool, it was shown that a PCC-based surface with low roughness still had an open and porous structure. This leads to ink penetration into the structure (Figure 14) and low conductivity values for test patterns. The kaolin-based structure had a higher surface roughness but a lower porosity compared to the PCC-based structures due to the layered clay structure simulated by the numerical modeling tool. The experimental data supported these observations. A layered structure of clay particles produced a closed and dense surface, which was more optimal for printed electronics. It can be concluded that kaolin-based substrates had a more suitable structure for printed electronics compared to the PCC.

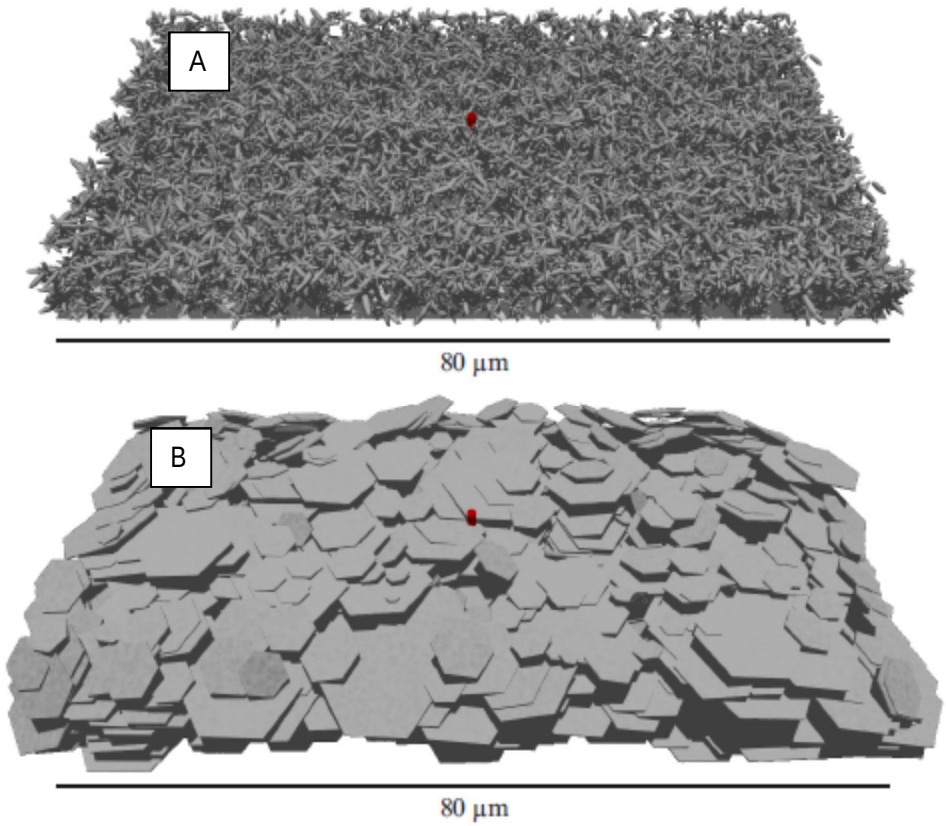

Figure 13. *Examples of PLA-simulated filler structures. Image A) shows a PCC filler, whereas kaolin is shown in image B). The small red cylinder in the center of both the sheets illustrates the 1 µm spot size of the optical profilometer, which is typically used in roughness measurements.*

In Figure 14, different absorption and penetration of conductive ink into the structure for kaolin- and PCC-based substrates can be detected. Despite the smooth PCC composite surfaces, remarkably better conductivity was obtained on kaolin substrates due to the dense structure. Furthermore, printed conductors on PCC–CMF (course grade) composites did not work at all in these studies. The PCC surfaces enabled the silver ink to absorb into the structure more easily due to the open and porous structure. On the basis of simulations, PCC-based structures also had a large number of open channels leading into the structure. This observation is due both to the tendency of PCC particles to form a star-like shape and to the porous structure of individual PCC particles.

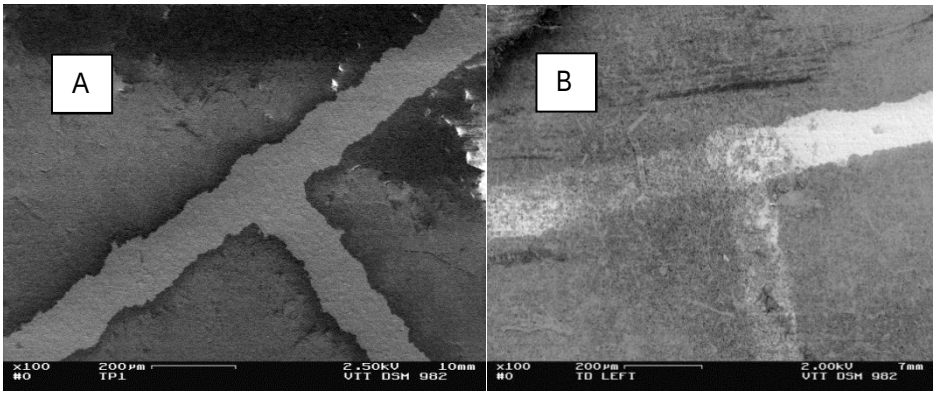

Figure 14. *Two SEM examples of printed conductor test lines on PCMNF composite with A) kaolin-based composite (80 wt-%) and B) PCC-based composite (80 wt-%). The used CMF was Daicel KY-100G. The ink penetrated inside the PCC-based composite, with a consequent negative effect on the conductivity.*

Figure 15 presents the calculated total composite porosity with the measured surface roughness. The smoothness values of produced composites were either lower or at the same level compared to the other commercial paper reference samples (photopaper, PEL) for printed electronics. However, commercial Mylar A and kapton plastic films had smoother surfaces. The calendering significantly decreased the roughness values. In general, PCC-based composites had a lower roughness compared to the kaolin-based composites. Composites with a finer VTT CNF grade had smoother surfaces before calendering. In that scale the effect cannot be seen any more after calendaring, but in rougher kaolin-based composites the finer CNF produced smoother surfaces. PCC-based composites were smoother than kaolin-based structures after calendaring. In this roughness level the used CMNF grade had no effect. One explanation may be that on this particular roughness scale, the size and shape of the filler begins to dominate. Similar results were also obtained in *Paper V*.

The calculated porosity (*Paper II*) clearly shows the effect of pigment type. Firstly, the total porosity was lower in both uncalendered and calendered state in kaolin-based composites compared to PCC-based composites. Secondly, it can be concluded that the pigment type had a higher and a more systematic impact than surface roughness on the achieved composite porosity level.

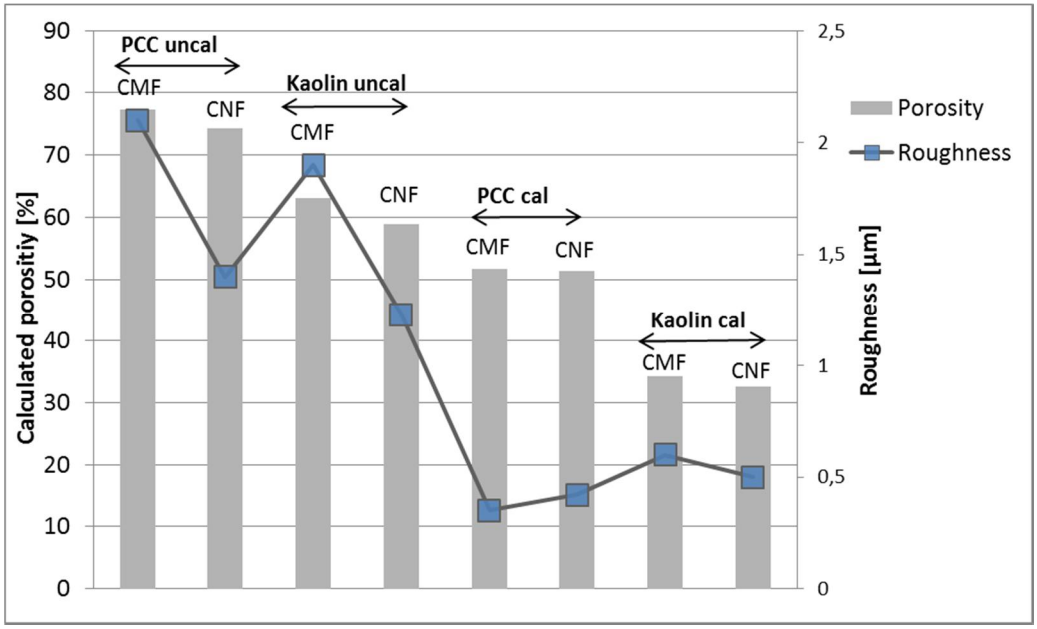

Figure 15. *Measured roughness and calculated total porosity of uncalendered and calendered composites including PCC / Kaolin and CMF (Daicel) or VTT CNF. The pigment amount was 80 wt-% and CMNF was 20 wt-%.*

Dimensional stability

The high amount of inorganic pigments increased the dimensional stability of the composites. Dimensional stability of vacuum filtered composites was studied by measuring dimensional changes when the relative humidity (RH) was changed in a loop from 50% to 10%, then to 66% and 90% and back to 10%. In paper-based materials, dimensional changes are reversible in low relative humidity conditions. Most of the irreversible changes occur in the RH range from 65% to 80%, depending on the hysteresis of humidity cycling [Mark E. Richard "Handbook of Physical and Mechanical testing of Paper and Paperboard"]. The dimensional changes of all studied pigment-CMNF substrates were lower compared to the paper hand sheet reference made from chemical pulp (Figure 16). The kaolin pigments had slightly lower values in RH 90% and 10% levels compared to PCC grades. The values were also close to those of the reference plastic film (Lumirror, PET).

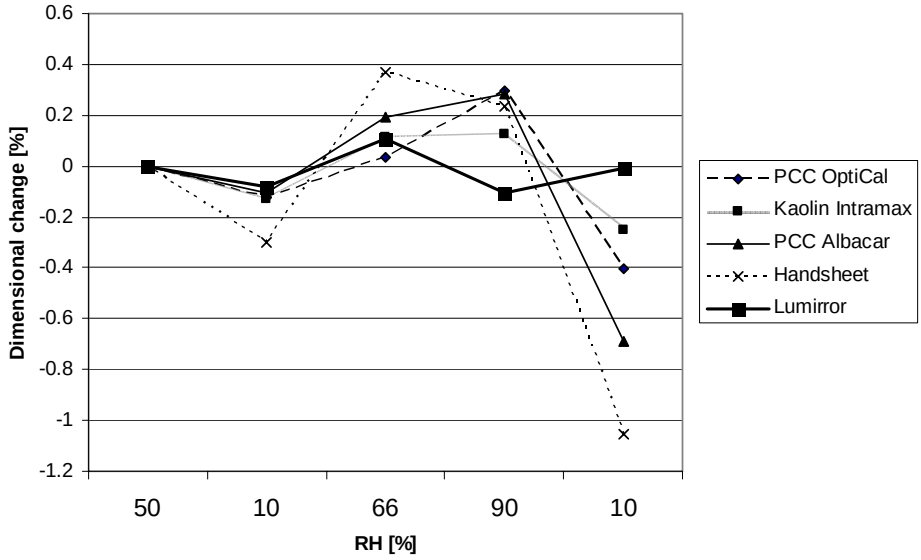

Figure 16. *Dimensional changes of various substrates when relative humidity (RH) was changed from 50% → 10% → 66% → 90% → 10%. The CMF was commercial Daicel KY-100G in this study and amount of pigment 80 wt-%.*

Thermal resistivity

The developed composites have a low thermal expansion because of their high amount of stable inorganic pigments and nanoscale fibrils. Thermogravimetric analysis (TGA) showed that the composites can tolerate brief exposure to temperatures up to 270 °C and over 12 h exposure to 230 °C as shown in Figure 17. These temperatures are significantly higher than current substrates for printed electronics can tolerate, enabling e.g. high sintering temperatures and increase in the production speed of printing machines. Additionally, in oven tests it was also observed that the PCC-based composites can withstand temperatures over 200 °C better than the kaolin-based composites. The kaolin pigment had a tendency to become brittle and dark due to the ingredients involved in the kaolin production process. Similar effects were not observed with the PCC-based composites.

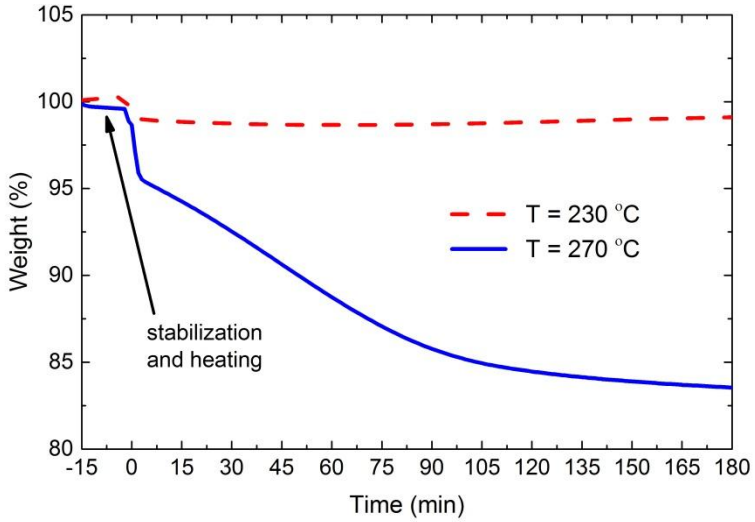

Figure 17. *Thermogravimetric analysis of pigment-CNF composites shows that the substrate can withstand temperatures as high as 230 °C (red) for hours. The used pigment was PCC and Daicel was used as a CMF material in the analysis.*

4.1.2 CMNF grade and content

Cellulose micro- and nanofibril grades (CMNF) vary significantly based on the used raw materials and process treatments. In this work, six different CMNF grades were used in the composites as raw materials. In *Papers II* and *IV*, Daicel CMF and VTT CNF grades were used in experiments. In *Paper V*, a more precise study was performed for benchmarking the CMNF grades. The morphological, rheological, optical, and strength properties of CMNF grades were characterized.

Morphology of the studied CMNF materials

Optical microscopy provides a rapid method for visualization of cellulosic nanomaterials (Kangas *et al*., 2014). The homogeneity, type of cellulose fibrils, and their macrostructure can quickly be assessed. Based on the images, the degree of fibrillation and the amounts of unfibrillated fibres and fibre fragments can be evaluated. Figure 18 shows optical microscopy images of the fibrillated nanomaterials used in this work. The images show a great variation in the sample appearance. The finest material observed was TCNF grade (F) not containing any fiber fragments or unfibrillated material. The VTT CNF (B) also had a fine and homogeneous film-like fibril structure. Commercial Daicel-grade (A) had a significant amount of thin, longer fibers with a heterogeneous overlook of the fibril network. The CNF (C) and LCNF (E) grades had some intact fibers, but also a significant amount of fibrillated material both as fibrils and fibril bundles. The ECMF (D) grade included a lot of microscale fibrils and also intact fibres. It had less fine material compared to the other grades and a low aspect ratio of particles. In

summary, these observations correlate to the composite properties, *i.e.* the ECMF grade together with pigments produced a rougher surface with lower strength properties (*Paper V*).

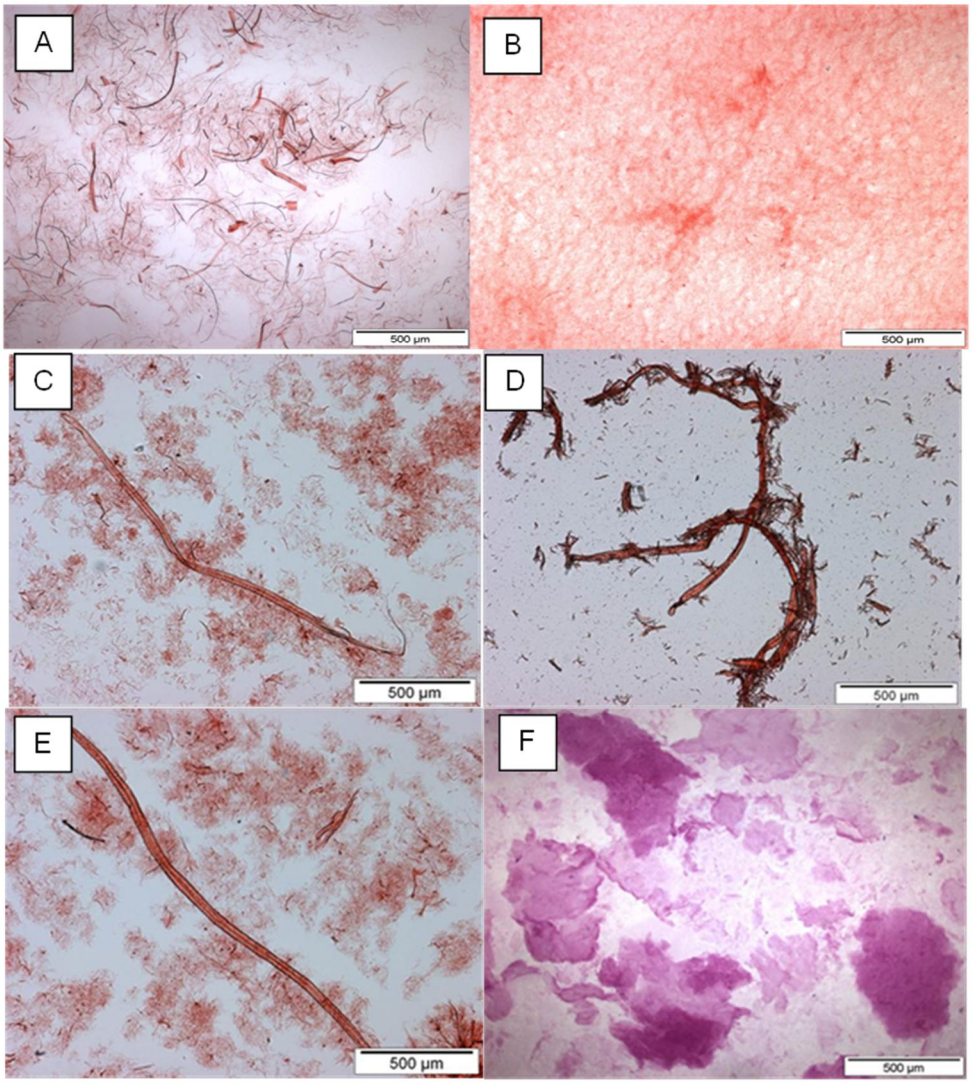

Figure 18. *Optical microscopy images of CMNF samples A) Daicel, B) VTT CNF, C) Native CNF, D) ECMF, E) LCNF, and F) TCNF*

The structural and dimensional appearance of cellulosic nanomaterials can be evaluated from the SEM images, which provide a tool for measuring the fibril thickness and for estimating the fibril length and branching degree. The images (Figure 19) showed that the studied cellulosic materials had different fibril morphologies. The ECMF grade (D) had a bulky and porous fibrillar network with

larger fiber widths. Commercial Daicel grade also had more porosity in the fibrillar network compared to the other used grades (B, C, E and F). The most homogeneous and film-like fibrillar structure was observed with TCNF grade (F). Overall, all the studied fibrillar cellulose materials had unique structures except for the samples Native CNF and LCNF that had rather similar morphologies.

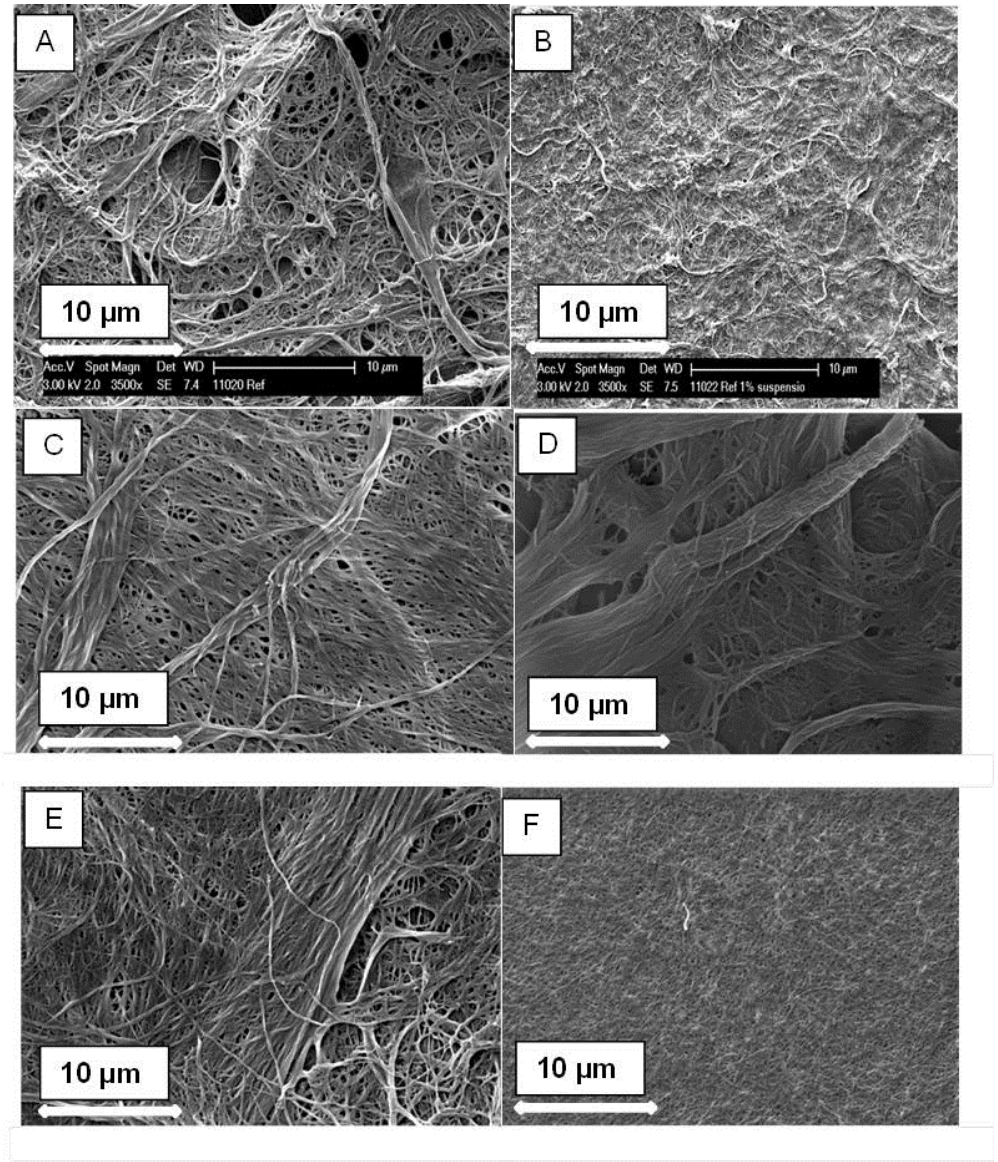

Figure 19. *Scanning electron microscope images of CMNF samples A) Daicel, B) VTT CNF, C) Native CNF, D) ECMF, E) LCNF and F) TCNF. The scale bar is 10 µm in all images.*

Rheological, optical and strength properties

Viscosity describes the internal resistance of suspension to flow. For fibrillated celluloses, the viscosity generally increases with an increasing fibrillation degree. This leads to a higher number of fibril-fibril interactions and also a higher number of smaller particles, which both increase the internal friction within the suspension. On the other hand, the aspect ratio of fibers will also decrease with a higher fibrillation degree, which can have an opposite effect on the viscosity.

In this work, the rheology of the cellulosic material suspensions was measured at 0.5% consistency using an Anton Paar viscometer device except in the case of the VTT CNF (laboratory and semi-pilot scale) samples. The rheological properties of VTT CNF laboratory and semi-pilot scale grades were measured by a Brookfield device at 1.5% consistency using a vane spindle V73 (*Paper IV*). The study of the characteristics of four samples (LCNF, Native, TCNF and ECMF) was presented in *Paper V.* The characteristics of the studied CMNF grades are presented in Table 4.

Table 4. *Characterization data of studied cellulose nanofibril materials. The data was combined from Papers IV and V.*

Character	Unit	LCNF	CNF	TCNF	ECMF
Pulp		Unbleached kraft	Bleached kraft	Tempo SW pulp	Bleached kraft
Charge	mmol/g	0.07	0.02	1	0.02
Fibrillation Method		Grinding	Grinding	Microfluidization	Enzymatic
DP	SCAN	2087	1430	286	833
Transmittance, 800 nm	%	28	26	74	4
pH	pH	8.8	6.3	7.5	5.3
Consistency	%	1.75	1.76	1.16	18.56
Conductivity	µS/cm	403	116	794	51
Residual fibers	Fibers/mg	3272	2699	341	48105
Storage Modulus	Pa	37.5	14.8	56.8	0.02
Loss Modulus	Pa	5.8	2.2	7.3	0.3
Shear viscosity, 10 1/s	Pa·s	0.98	0.43	4.39	0.002
ÅAGWR, 30 sec.	g/g	297	233	446	229
SEC	kWh/kg	15.7	16	12	0.6

TCNF had clearly the highest viscosity compared to the other grades. VTT CNF (pilot) sample had a high gel viscosity but this cannot be directly compared to the other samples due to the different measurement technique used. The high specific surface area and aspect ratio increased the apparent viscosity. The fibrillation degree for ECMF grade was clearly lower compared to the other grades, as observed in Figure 19, resulting in a low shear viscosity (Figure 20A) with a high amount of residual fibers (Figure 20B). In addition, the ECMF grade was not a gel-like structure at 0.5% consistency, and therefore thixotrophic behaviour was not observed (Figure 20A). The TCNF grade had the lowest amount of residual fibers

compared to the other studied grades (*Paper V*), as presented in Figure 20B. The high fibrillation degree based on SEM images resulted in the strongest gel structure according to both storage and loss modulus compared to the other CNMF grades (Figure 20C). A high loss and storage modulus means a higher yield stress and usually high water retention behavior. LCNF also had a significantly higher storage and loss modulus compared to the CNF grade, which was produced in a similar way from the same raw material. However, the bleaching process was only excluded in the production of the LCNF grade, resulting in a stronger gel.

The light transmittance of cellulosic nanomaterial suspensions can be influenced by many parameters such as particle size, particle shape, concentration, and color. However, the most relevant factor is the particle size. Generally, finer materials have a higher transmittance than coarser materials in the lowest wavelengths of light. The color of fibrillated cellulose suspensions is white or opaque, indicating that they contain larger nanoparticles than, for example, nanocrystal suspensions. The transmittance of the studied ECMF material was at a significantly lower level (4 %-unit) compared to the other grades, with transmittances from 26% to 74% (Figure 20B). The highest transmittance values were observed in TCNF and VTT CNF (pilot) grades, indicating that the samples have a large number of smaller particles and finer fibrillar network than the others.

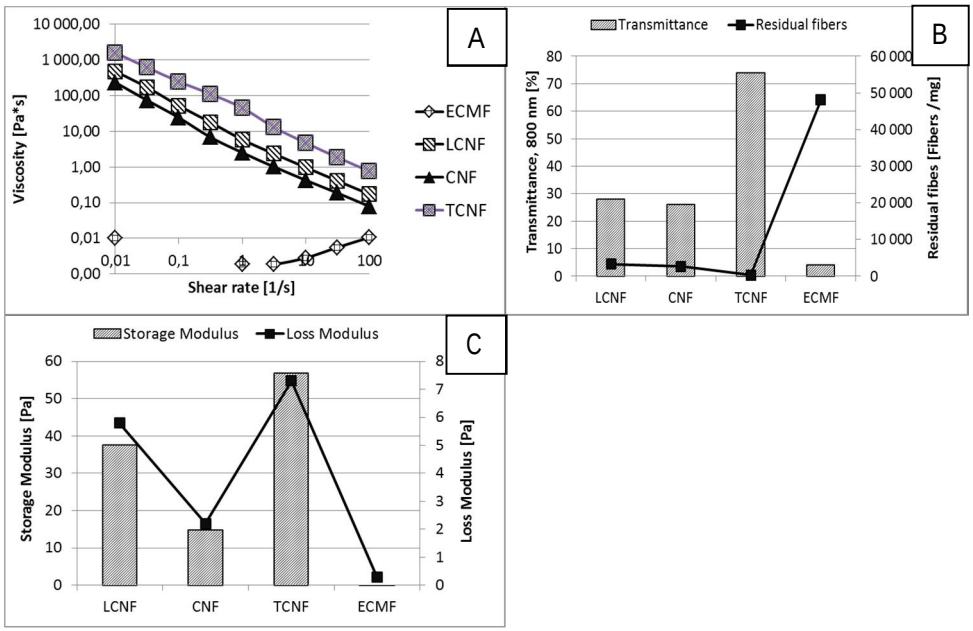

Figure 20. *A viscosity curve as a function of the shear rate (A), transmittance and residual fibers (B), and the storage and loss modulus (C) of the CNF grades.*

Water retention values (modified ÅAGWR) of fibrillated cellulose materials were studied in *Paper V*. These values simulate different water removal mechanisms and hence they correlate with the fibrillation degree and the network structure. The water retention values of the fibrillated samples showed significant differences. The lower values indicate better dewatering in the filtration process. Based on both the water retention values and the duration of the filtration during the composite manufacturing, TCNF grade had a higher capability to retain water and thus a much longer dewatering time. In addition, LCNF grade had higher retention values than CNF- and ECMF grades. However, no clear effect was observed between composites of CNF-, LCNF- and ECMF grades in the filtration times.

Effect of CNMF grade on composite properties (Paper V)

The effects of four different CMNF grades on the composite properties were studied in *Paper V*: native CNF (CNF), lignocellulosic CNF (LCNF), TEMPO-oxidised CNF (TCNF) and enzymatic processed CNF (ECMF) together with kaolin clay pigment particles and also with plasticiser in some trial points. The CMNF amount varied between 20 and 43 wt-% in composites. Accordingly, the amount of kaolin pigments varied from 43 to 80 wt-%. The amount of plasticiser was set to 15 wt-%. Each of these raw material combinations resulted in different composite properties, *i.e.* surface roughness, mechanical properties, formation, and density. These characteristics were expected to have an effect on the printed electronics applications.

The different composite surfaces were characterized using Helium ion microscopy (HIM). Significant differences were observed when the type of CNF varied, as seen in Figure 21. A higher roughness was obtained with ECMF compared to the other grades, as is easily observable in Figures 21A-C. The high resolution HIM images also reveal that the formed composites consist of individual fibrils and fibril networks that are binding the pigment particles together (Figures 21D–F). Especially, the LCNF grade may produce film-like nanostructures on the surfaces of pigments.

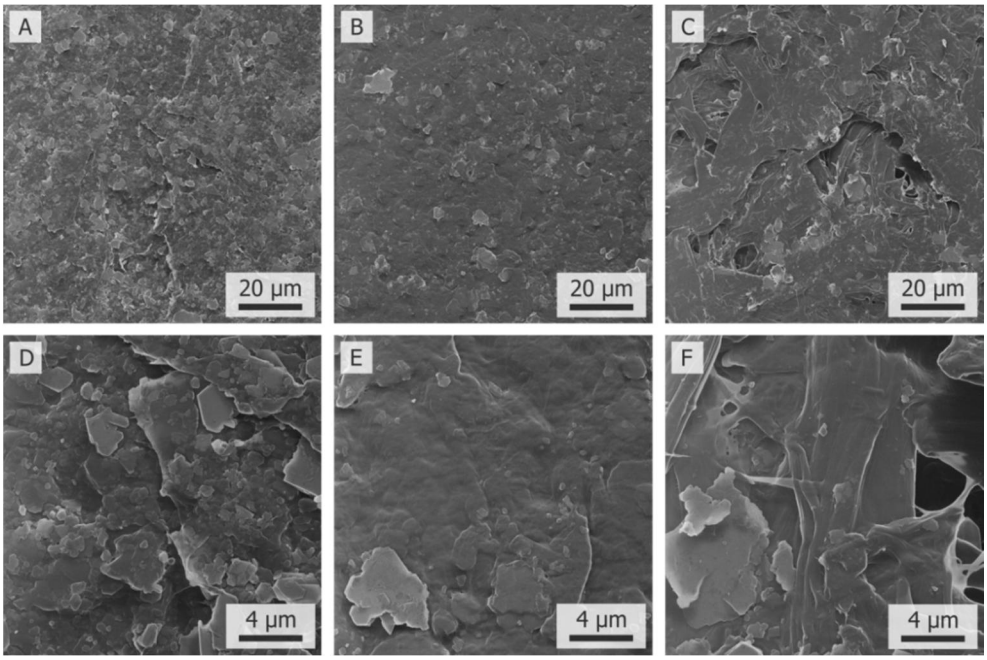

Figure 21. *Helium Ion Microscope (HIM) images of composite surface morphology. The top side of the composites was imaged, using 100 µm (A–C) and 20 µm (D–F) fields of view. In A) and D) TCNF_20, in B) and E) LCNF_20C, and in C) and F) ECMF_20 are shown.*

The higher amount of cellulose nanomaterial in the composites (~43 wt-%) had a significant effect on the shrinkage during the drying process. The drying shrinkage leads to fragile and non-elastic film structures. To avoid this, sorbitol was added at 15 wt-% to the composites. It is noteworthy that composites made without sorbitol as a plasticiser and at higher amounts of cellulosic nanomaterial were not included in this study due to their weak performance.

The density data for the composites is shown in Table 5. The lowest material densities were achieved when ECMF grade (ECMF_43) and Barrisurf (LCNF_20B) were used as raw materials. The achieved low density for the ENCF grade is due to a lower amount of fibrillated material, when compared to the other studied CNF grades. As expected, the low density achieved using the Barrisurf as a pigment was due to a higher aspect ratio of pigment particles that was followed by an increased pore volume and surface roughness in the composite. The measured air permeability was below the measurement limit for all trial points, which indicates a low porosity and good barrier properties.

Table 5. *Composite properties, including grammage, thickness, density, formation, roughness, and stain length for the produced composites, have been tabled. The strain length for the ÅA substrate* (R Bollström *et al*., 2012) *was measured to be 150 mm.*

Trial point	Grammage [g/m²]	Thickness [µm]	Density [kg/m³]	Formation Spec	Roughness Ra [µm]	Stain length [mm]
CNF_20	88.2 ± 2.2	58 ± 3	1522 ± 50	0.74	0.37 ± 0.02	138
ECMF_43	100.0 ± 7.7	75 ± 5	1332 ± 78	0.78	2.23 ± 0.55	54
ECMF_20	108.7 ± 2.5	76 ± 3	1427 ± 21	0.76	1.96 ± 0.27	-
CNF_43	112.6 ± 2.7	71 ± 1	1597 ± 28	-	0.54 ± 0.07	144
LCNF_43	102.1 ± 1.6	66 ± 1	1551 ± 19	-	0.67 ± 0.06	170
LCNF_20C	114.3 ± 2.5	76 ± 2	1512 ± 43	0.66	0.39 ± 0.04	159
TCNF_20	116.5 ± 1.5	76 ± 4	1531 ± 90	0.43	0.41 ± 0.06	138
LCNF_20B	111.6 ± 9.5	86 ± 7	1306 ± 101	0.59	0.74 ± 0.19	121

Surface smoothness is a crucial property for the composites when using them for printed electronics substrates. The lowest roughness values were measured for composites consisting of 80 wt-% Capim kaolin and 20 wt-% CNF or LCNF grade. The TCNF grade had almost the same smoothness values. On the other hand, the ECMF grade with the same pigment type and amount produced the lowest smoothness values. Therefore, the used CNF grade had a significant effect on the surface smoothness. The rough ECMF grade resulted in the lowest surface smoothness, which is logical. However, the use of a finer TCNF grade did not improve the surface smoothness compared to the CNF or LCNF grades. One explanation may be that on this particular roughness scale, the size and the shape of the pigment begins to dominate. Table 5 also shows the formation Spec-

numbers. The most even formation was obtained with TCNF, due to the low amount of residual fibers and thus a homogenous size distribution due to a high fibrillation degree and an increase of the bonding area between cellulose nanofibrils and the pigment.

A correlation between the surface smoothness and stain length can be observed if the variation in roughness scale is wide enough. The stain length depends on both surface roughness and surface porosity. Hence, a print penetration test can be used to estimate the surface porosity. Low surface porosity leads to a longer stain length in the stain test. Correspondingly, a high surface porosity leads to a shorter stain length, with a higher absorbance of the used solvent into the structure.

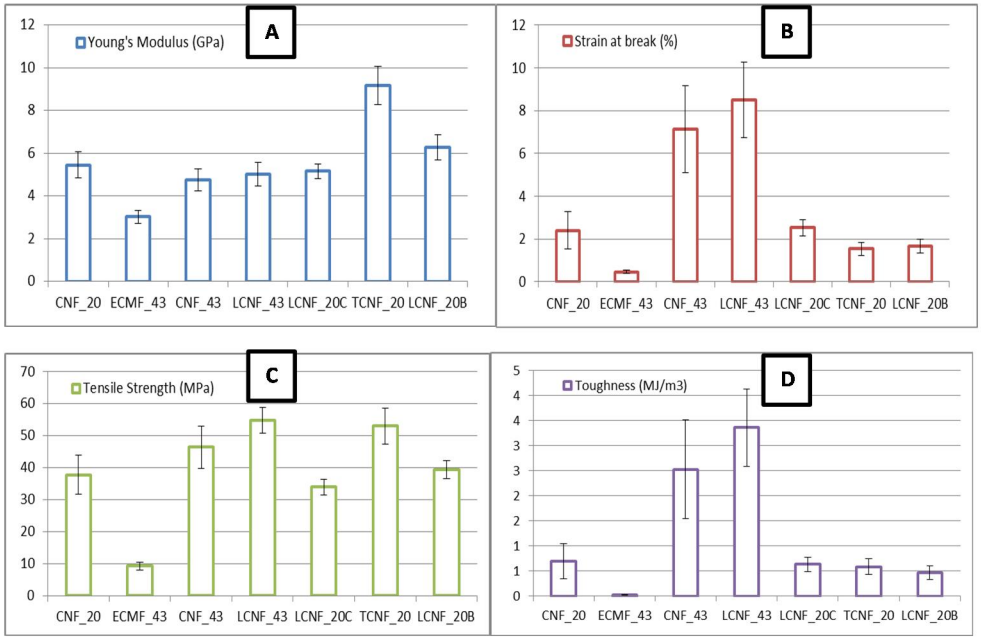

Figure 22. *Mechanical properties of the composites: A) Young's Modulus [GPa], B) Strain at break [%], C) Tensile Strength [MPa] and D) Toughness [MJ/m*

Figure 22 summarizes the measured mechanical properties of the PCMNF composites. The use of a plasticizer in the PCMNF composites clearly increased both the strain at break and the toughness for trial points CNF_43 (native grade) and LCNF_43 (LCNF grade), which are both in good agreement with literature values (Hoeng, Denneulin, Bras, *et al.*, 2016). A similar behavior was not observed for the ECMF_43, most probably due to poor ability to bind pigments together. This is due to a low fibrillation degree of ECMF fibers, which can be seen in the CNF characterization data *i.e.* a high amount of residual fibers and a lower shear viscosity. On the other hand, the use of a plasticizer and a higher amount of CNF was essential to produce adequate elasticity for the composites. Both strain at

break and toughness values of composites were insufficient for further converting processes without a plasticizer.

The use of TCNF grade produced composites with the highest Young's modulus. Additionally, the trial point with an 80 wt-% pigment loading together with the TCNF produced composites with a high tensile strength. Comparing the trial points LCNF_20C and LCNF_20B, in which the only difference was the used pigment, it can be concluded that Barrisurf produced a slightly higher tensile strength and Young's modulus compared to the Capim SP mineral. This is probably due to the high aspect ratio of Barrisurf pigment. PCMNF composites with the best mechanical properties were produced using LCNF grade together with a plasticizer (LCNF_43) that resulted in composites having a high tensile strength, strain at break, and toughness with Young's modulus at an adequate level.

4.2 The effect of manufacturing parameters on composite properties

The composites were manufactured by vacuum filtration in laboratory scale and by film casting in semi-pilot scale. The next manufacturing phases were wet pressing, drying, and calendering. Figure 23 presents schematically the differences of manufacturing technologies in laboratory and semi-pilot scale. In addition, calendering was used. The effect of calendering on the composite properties will be discussed in Section 4.2.3. In this work, the effect of manufacturing parameters on composite properties was studied and the results are presented in this section.

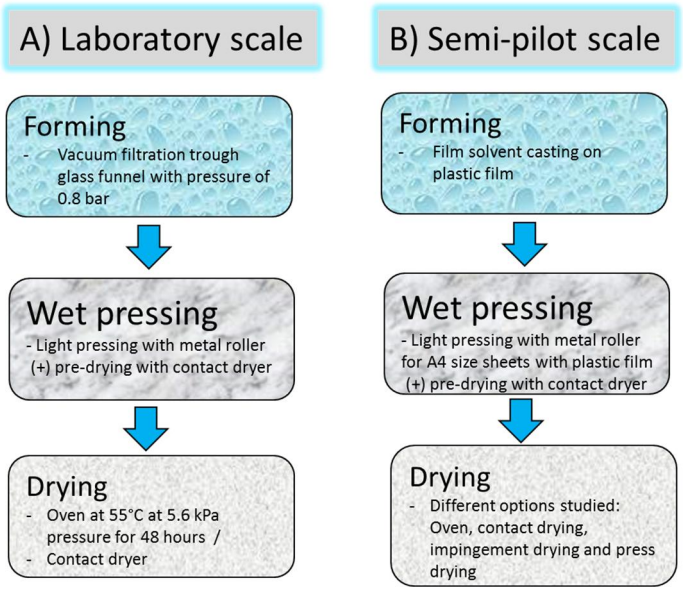

Figure 23. *Manufacturing procedure of composites in A) laboratory scale B) semi-pilot scale*

4.2.1 Forming

Vacuum filtration

Nanoporous composites were formed by vacuum filtration in laboratory scale. Forming parameters such as filter paper, vacuum level, use of polyelectrolytes, pre-drying of the composites, and the method for activating the CMNF material have a significant effect on the film properties including surface formation and smoothness. The dewatering behavior of the composites was an indicator of which composites could be suitable for large-scale mass production. Overall, a higher kaolin amount (80%) improved the dimensional stability of the composites with controllable shrinkage during drying compared to a lower amount (50%).

Pigment-CMNF (PCMNF) composites made by vacuum filtration in *Paper V* turned out to have a higher surface roughness on the bottom side than on the top side due to the effect of filtration paper, as was also observed in *Paper II*. The upper side was denser compared to the bottom side due to the higher amount of pigment particles on top. On the other hand, the bottom side included more cellulosic nanomaterial, resulting in a higher porosity (Figure 24A). The PCMNF composite was filtered from the bottom side during the forming process. Based on these observations, the upper side of the composite was selected as the surface on which the structural analysis and transistor fabrication was carried out.

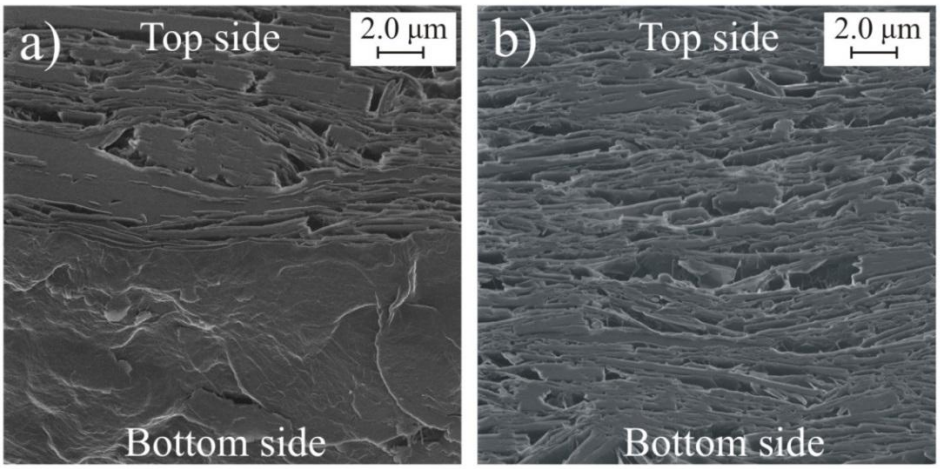

Figure 24. *Cross-sections of composite LCNF_20B measured by HIM with a 20 µm field of view at a 45˚ angle relative to the cross-section surface resolution. The smooth cross-section was prepared using a broad ion beam cutting technique. The image a) shows both the original surface (lower half of the image) and the cross-section surface (upper half of the image), whereas in b) a tortuosity of the structure*

can be detected. The average porosity of the composite was approximately 20%, based on a simple image analysis of the cross-sections.

Film casting (Paper IV)

The fabrication of low-cost pigment-cellulose nanofibril (PCMNF) composites in semi-pilot scale (VTT Coating unit environment SuTCo) was demonstrated in *Paper IV*. The composite needs to fulfil certain quality requirements in order to be classed as a suitable substrate for printed electronics applications. The main requirements consist of nanoscale porosity, surface smoothness, flexibility, and sufficient strength properties of the composite.

Several methods for upscaling the production of PCMNF substrates were tested, including vacuum-assisted hand sheet-making, foam forming, solvent casting, and spraying. The most promising way for industrial-scale manufacturing was found to be the solvent casting method. Pigment-CNF dispersion was spread in semi-pilot scale at 7% consistency on the plastic carrier material. The dispersion contained 80 wt-% of pigment (PCC, different types of kaolin) and 20 wt-% of VTT CNF. The grammage of the final wet PCMNF sheets varied from 142 to 221 g/m², and there was a similar variation in the initial solids content in the range of 20–35% after a gentle initial off-line wet pressing phase.

Controlled adhesion between the pigment-CNF dispersion and the carrier plastic film with the high consistency of the dispersion in film casting enabled excellent pigment-CNF substrate properties, as shown in Figure 25. The main advantages of the solvent casting method were prevention of shrinkage of substrate during drying, and the use of high consistency (over 7%) dispersion. Furthermore, control of toughness and flexibility of substrate by pressing, and even formation were obtained. The semi-pilot scale tests were successful and samples were further studied with different wet pressing and drying parameters. However, the film casting method still needs additional work, including parameter optimization to be used as a composite production method.

Figure 25. *A smooth layer of pigment-CNF dispersion was spread on top of the support material.*

4.2.2 Wet pressing and drying (Papers I, III, and IV)

The porosity of the film cast PCMNF substrate was successfully controlled and optimized with suitable wet pressing and drying conditions. These were also found to be crucial for obtaining smooth and flexible composite structures.

It was important to optimize the drying conditions. Quick drying of the pigment-CMF/CNF web resulted in cracks, and the dried structure was non-elastic and brittle. Slow drying at room temperature resulted in a smooth and more flexible structure. The best results were obtained by using pressing of the formed web before or during drying. The smoothest surface was obtained for the sample that was dried in the oven under a weight. The excess water can easily be pressed out of the structure, which clearly speeds up the drying process. Wet pressing also improved the flexibility of the formed structure.

When manufacturing of CMNF composite films it is critical to avoid drying shrinkage. In this study it was noticed that the drying shrinkage appeared to a larger extent when high surface area fibrils were used, i.e. finer CNF grades. In order to achieve flexibility and to decrease brittleness, the composite structure consisting of fibrils and pigment particles benefited of pressing. The best found solution to prevent shrinkage and to obtain desired structure was to use contact drying for a short time directly after the forming phase before peeling off the support filter material. The optimal final drying process was carried out by restraining the structure between glass plates pressed by a weight in an oven. Although the influence of temperature was studied in *Paper III* there is still room for parameter optimization in the different manufacturing phases.

The effect of different drying conditions on pilot-scale manufactured PCMNF sheet properties was studied in *Paper IV*. Drying at room temperature resulted in a rougher surface on PCMNF substrates. The smoothest surface was obtained after drying at 50°C in an oven with applied pressure. In earlier semi-pilot scale studies, the contact dryer was not included in the test plan. Based on drying studies published in *Paper III*, a contact dryer was chosen as the drying method in *Papers IV* and *V*.

Drying studies were published in *Paper III*. In this work, several drying methods were used and their effects on the composite properties were studied. Before drying, the solids content of composites was approximately 20–35%. In this publication, the studied composite structure contains 80 wt-% of kaolin pigments and 20 wt-% of CNF. The goal was to achieve a smooth and closed surface while maintaining drying efficiency at a high level. The studied drying methods were drying on a hot metal surface (contact drying), air impingement drying, and hot pressing.

Drying efficiency

Figure 26 shows the drying curves of the contact drying tests in two different temperatures normalized by initial moisture ratio [kg/kg]. The initial moisture ratio of the PCMNF sheets before drying was approximately 2 to 3 times higher than that of the reference board samples, in the range of 2.5–3.8 kg/kg. Assuming that all of the water was bound to the CNF with 20 w-%, this corresponds to 13–19 kg water/kg of CNF. This agrees well with water retention values measured earlier for wet CNF (Katarina Dimic-Misic, Puisto, Paltakari, Alava, & Maloney, 2013). Moreover, the grammage of the PCMNF sheets was also almost 2 times higher. Both factors increase the drying time required for complete drying of the PCMNF sheets in comparison to the board samples. This can also be seen in the drying curves of the contact drying tests shown in Figure 26 for the PCMNF composite and board samples. For example, a hot surface temperature of 80 °C resulted in a total drying time of approximately 220 s for the PCMNF sheets, whereas for the board samples it was less than 90 s.

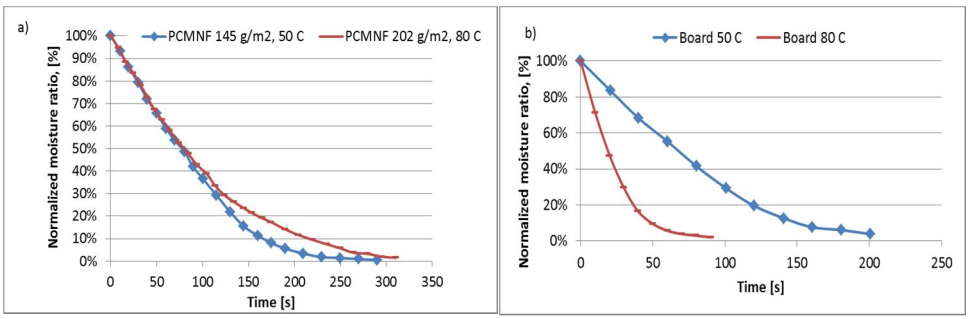

Figure 26. *Drying curves for the contact drying of (a) PCMNF composites and (b) the board at two different temperature conditions normalized by initial moisture ratio.*

All drying curves indicate two phases: first, the constant rate phase followed by the falling rate phase. For air impingement drying, the development of the moisture ratio is shown in Figure 27a for three combinations of air jet velocity and air temperature for both types of composites. The transition from the constant drying rate phase to the falling rate phase takes place at a similar moisture ratio level of 1.0 kg/kg for the PCMNF sheets (and 0.5–0.6 kg/kg for the board as a comparison), similarly to the contact drying. On the other hand, the difference in the total drying time between the PCMNF composite and the reference board was slightly greater for the impingement drying than for the contact drying. This was partly explained by the higher initial moisture content of the studied PCMNF composites. The hot press dewatering curves are shown in Figure 27b. A significant effect of pressure and temperature on dewatering time was observed. The dewatering curves can be divided into two phases. In the first phase, the dewatering rate was very high until a moisture ratio of 0.75–1.0 kg/kg was reached. In this phase, water was mainly squeezed out from the sheet under the applied pressure. In the second phase, the

dewatering rate was much lower due to slower evaporation and diffusion processes.

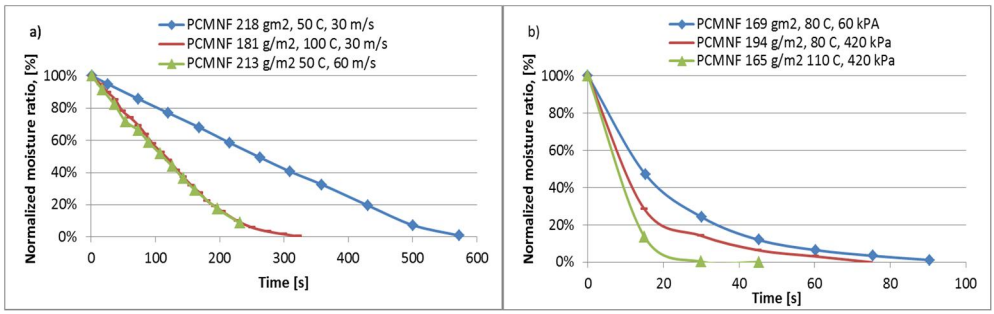

Figure 27. *Drying curves for a) the air impingement drying and b) press drying of PCMNF composites at three different drying conditions (temperature, air speed and pressure) normalized by initial moisture ratio.*

Figure 28 show that there was actually no major difference in the initial drying rates for the PCMNF composites and the reference board samples. The lowest and the highest drying rates were observed for the contact drying method for both sample types. The air impingement method resulted in intermediate values in between the two extremes above. In general, drying rates measured for the PCMNF sheets and the reference board samples were comparable with the same drying parameters. In the first drying phase, the drying rate was controlled by external drying conditions, with this rate depending less on material properties. The smooth surface of the PCMNF substrate helped in contact drying when compared to the board. On the other hand, air impingement appeared to be more effective for removing free water from the pores of the board than from the denser PCMNF structure.

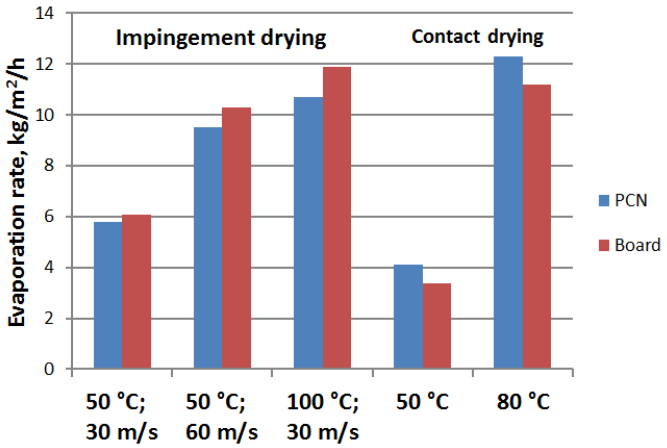

Figure 28. *Drying rates determined from the initial linear part of the drying curve for the air impingement and contact drying methods for both PCMNF composites and reference board in varied drying conditions (temperature and air speed).*

Substrate properties

The produced composites need to fulfil certain quality requirements for printed electronics applications. One main requirement is sufficient surface smoothness. In addition, adequate strength, flexibility, and stretch of the substrate are required for printing processes. The applied drying process has significant effects on these parameters. The measured properties after calendering of the PCMNF sheets are shown in Table 6. For contact and impingement drying, the sheet density before calendering decreased slightly with the drying rate. The longer drying time was followed by a greater shrinkage of the PCMNF sheet in the thickness direction.

The lowest roughness value of 0.34 μm for the bottom surface was observed for the combination of the contact and impingement drying. In this case, impingement drying was first carried out until the moisture ratio reached approximately 1.0 kg/kg. Contact drying was applied afterwards to obtain the final solids content. However, the drying parameters were not optimized. This means that even better smoothness could potentially be achieved. In *Paper II*, the surface roughness of the composites formed with a vacuum filtration in laboratory scale was measured after oven drying and calendering. The surface roughness was measured for VTT CNF as fine material and commercial Daicel grades using the same pigment type as here and the same weight contents (80 wt-% of kaolin and 20 wt-% of CMNF). The values obtained after calendering were 0.51 μm (VTT CNF fine quality) and 0.60 μm (Daicel quality). The lowest roughness values obtained here were thus clearly better than the above values. The short-range surface smoothening effect was strongly affected

by the forming and drying method, leading to relatively wide variation of the roughness values.

The properties of the PCMNF sheets after calendering could be significantly affected by the drying method (Table 6). Unfortunately, hot pressing led to partially unconformable structures with poorer surface smoothness than with the other drying methods. The best surface smoothness was obtained with a combination of impingement and contact drying. Contact drying led to an almost equally smooth surface. The required smoothness level for various applications, for example inkjet-printed conductors, screen-printed near-field communication RFID antennas and fabricated thin transistors, was achieved with both methods.

Table 6. *Comparison of different drying methods for PCMNF composite properties after calendering.*

DRYING METHOD	Impingement			Contact		Impingement and Contact	Press			
Temperature, °C	50	50	100	50	80	50 (Impingement), 80 (Contact)	80	80	110	110
Air speed, m/s	30	60	30			30				
Pressure, kPa							60	420	60	420
Thickness, µm	178	148	144	127	145	116	148	168	101	154
Density, kg/m^3	1,421	1,534	1,438	1,523	1,448	1,518	1,467	1,309	1,437	1,350
Roughness, top side, mm	0.48	0.51	–	0.71	0.41	0.45	0.63	0.86	0.82	0.60
Roughness, bottom side, mm	0.45	0.38	–	0.42	0.49	0.34	0.43	0.43	0.43	0.42
Tensile strength index, Nm/g	13.4	16.6	16.0	12.5	15.8	15.8	12.4	14.3	17.5	15.6
Elastic modulus, GPa	4.6	5.2	4.3	4.3	4.7	4.6	4.2	4.1	3.8	3.6
Breaking strain, %	1.3	1.9	1.3	0.9	1.3	1.6	1.0	1.0	1.6	1.5

As a conclusion, in laboratory-scale drying experiments it was shown that the PCMNF composite can be dried using conventional drying methods such as contact drying and air impingement drying. Despite the very high bound water content of the CNF gel, the estimated drying rates for the PCMNF substrate were comparable with the drying rates of typical board with the same external drying conditions. It was also demonstrated that before drying, the water can be effectively removed from the PCMNF sheets by hot pressing. Removal of water mechanically in the hot contact press will dramatically reduce the energy consumption required for drying of an initially highly wet PCMNF substrate.

4.2.3 Calendering

The developed composites were calendered to maximize the smoothness of the surface and to achieve dense structures for printing applications. Different calendering conditions were tested with variable pressure, temperature, and number of nips. Smooth and dense surfaces without cracking and darkening effects were obtained using one hard nip with approximately 170 °C surface temperature on the lower roll and with 20 MPa applied pressure.

The calendering removed most of the voids between the filler aggregates, resulting in a dense structure with a smooth surface having a plastic-like tactile property (Figure 29). It can be observed from SEM images that calendering significantly reduced the porosity of the surface layer. Thickness of the PCC-based composites decreased in calendering from 210 to 100 µm. Furthermore, the density increased from 560 kg/m³ to 1160 kg/m³. This indicates that CMNF material makes the structure flexible under the applied pressure and temperature. The pigment particles can move inside the structure for dense packing, leaving CMNF compressed between the particles. The calendering also significantly decreased the roughness of the composites, as presented previously in Section 4.1.1. The calendering decreased the roughness values (R_a) from the level of 3–4 µm to 0.3–0.5 µm depending on the used pigment type and their shape.

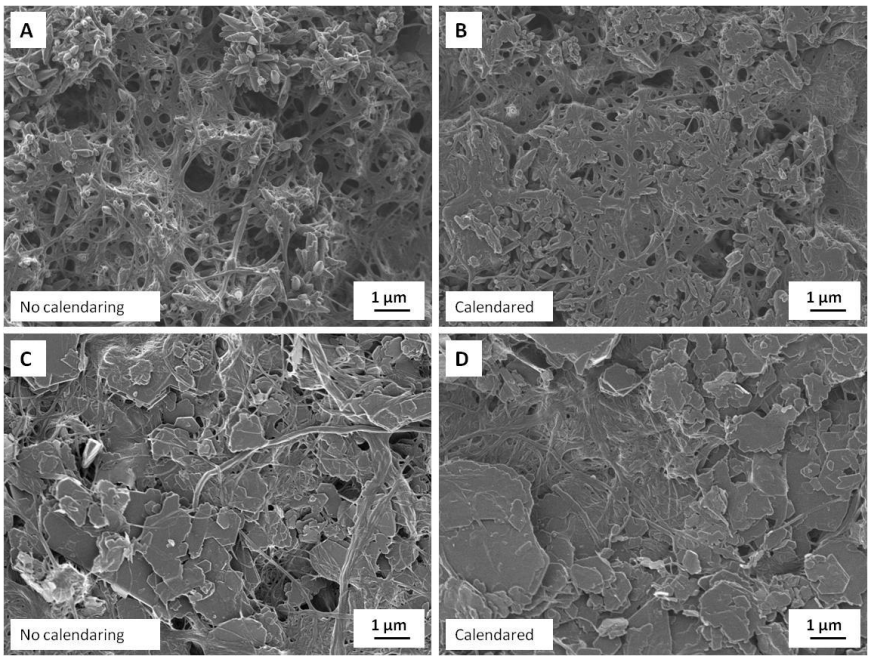

Figure 29. *SEM images of PCC Albacar (upper row) and kaolin (lower row) sheet before and after calendering (Paper I). The CMF was commercial Daicel KY-100G in this study.*

4.3 Composites for printed electronics applications

The developed pigment-cellulose micro- and nanofibril (PCMNF) composites have a nanoporous pigment-CMNF network structure that allows control of the ink absorption properties. Therefore, high quality functional printing is possible on such smooth and nanoporous surfaces without short circuit problems in the devices fabricated on the surface. The required substrate porosity and smoothness properties strongly depend on the used printing method, ink, solvent, and device design, which are affected by absorption, surface charge, and binding properties. These substrate properties can be controlled by selection of the used raw materials, including mineral pigments, cellulose micro/nanofibrils, and other additives.

Different functional devices were manufactured as proof-of-concept structures to demonstrate the usability of the developed composites for printed electronics applications. The composite suitability for printed electronics applications was demonstrated firstly by ink-jet printing with a silver-nanoparticle ink in *Papers I and II*. The conductors and patters were printed on different PCMNF types and structural effects were studied. It was also demonstrated that, in addition to the smoothness, porosity is the most relevant property for the composite performance (*Paper II*). Secondly, the fabrication of low-cost PCMNF composite in semi-pilot scale and its application as a double-functional separator substrate for printed supercapacitors was published in *Paper IV*. The supercapacitor structure was obtained simply by printing the active layers on both sides of the nanoporous separator substrate. Finally, an ion-modulated transistor was deposited on the substrate with varying pigments and CMNF constituents as the last demonstrator in *Paper V*. Unpublished demonstrators include screen-printed antennas produced using silver ink and a commercial RFID chip attached using a silver epoxy resin. This proof-of-concept works as a functional NFC RFID tag on flexible substrate.

4.3.1 Ink-jet printed conductors and patterns (Papers I and II)

The potential of PCMNF composites for printed electronics applications was studied using a silver nanoparticle ink and an ink-jet printer as a versatile technique to produce printed patterns. The conductors were printed on calendered PCC- and kaolin-based composites. Figure 30 shows an image of printed conductors that look sharp, with the ink not spread too much on the composite surface.

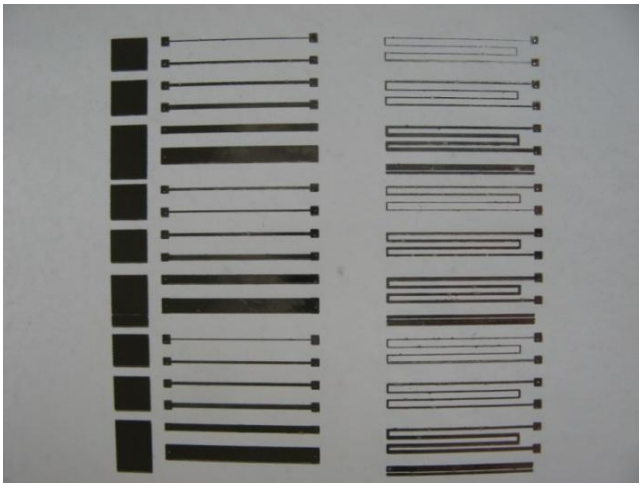

Figure 30. *Image of a pattern printed on PCC- based composite.*

As a summary, the detected silver ink penetration into the composite structure was minimal. At the same time, the porous structure enables ink solvent absorption through the composite, which is a benefit compared to plastic films. For kaolin-based composites the ink layer was thicker than for the PCC-based substrates. The reason for this was the higher porosity of the PCC-based composite surface layer. Higher porosity enables ink penetration deeper into the structure.

Conductivity of printed lines was analyzed by measuring the resistances for various line widths. The sheet resistances were between 0.03 and 1.77 Ω for all studied composites in *Paper I*. The sheet resistance systematically increased with increasing line width (Figure 31). The ink layer printed on kaolin-based composites was thicker, and therefore sheet resistances were smaller compared to the PCC-based composites, despite the higher surface roughness. The sheet resistances of conductors printed on kaolin-based composites were between 0.08 and 0.23 Ω and the corresponding values for reference film Mylar A were between 0.11 and 0.34 Ω. As a conclusion, similar conductivity of printed patterns was achieved on kaolin-based composites to that for the reference PET-film. In general, better surface smoothness does not always correlate with better conductivity. It was shown (Kattumenu *et al*., 2009) that compatibility of the ink to the substrate can also affect the conductivity. Based on the studies, the porosity of the composite surface layer had more effect on the conductivity of the printed lines than the surface smoothness.

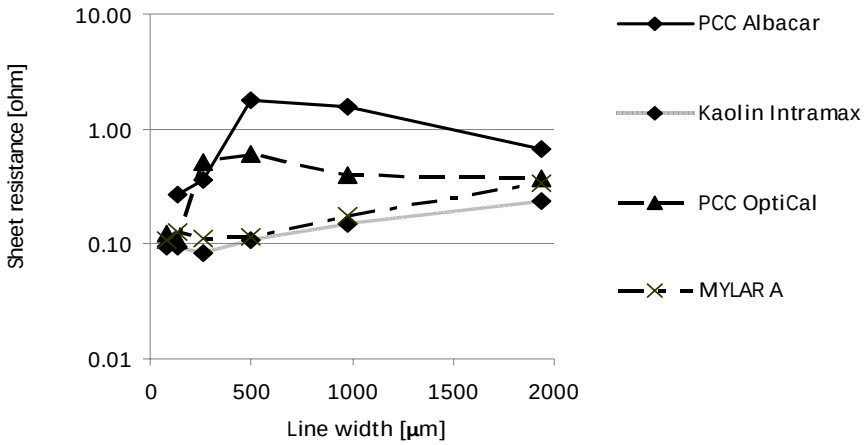

Figure 31. *Sheet resistances measured for various line widths. One silver nanoparticle ink layer was printed on PCMNF composites and reference plastic film Mylar A. The CMF was commercial Daicel KY-100G in this study.*

Printing of two conductive ink layers on the sheets reduced resistances significantly compared to the single layer due to thicker lines, as shown in Figure 32. Sheet resistances of PCC-based composites decreased significantly. It was not possible to print two ink layers on the reference plastic film Mylar A due to uncontrolled ink spreading. The plastic film does not have a porous structure, which is a challenge for printing and coating processes in which it is beneficial that the solvent is absorbed into the structure. As a summary, a nanoporous surface layer of PCMNF composite really does have a potential for certain printed electronics due to the possibility for optimized porosity and ink setting.

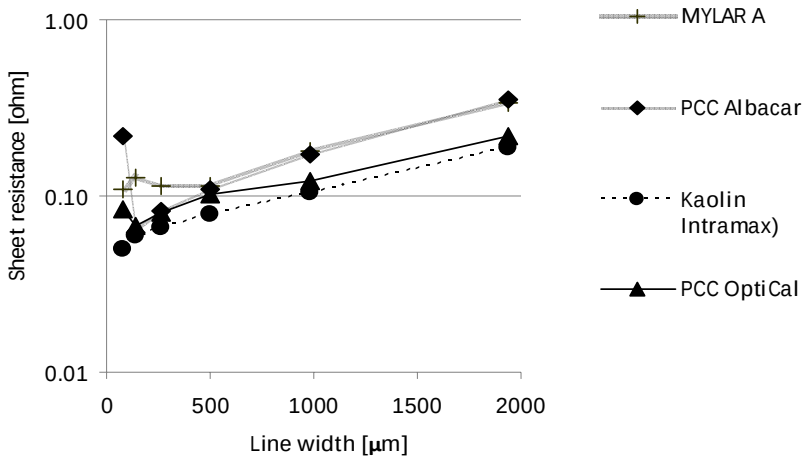

Figure 32. *Sheet resistances measured for various line widths. Two silver nanoparticle ink layers were printed on PCMNF composites and only one for Mylar A reference film due to the challenges in the printing process. The CMF was commercial Daicel KY-100G in this study.*

The hypothesis for better conductivity is the smoother surface of the PCC-based substrates, as presented earlier in Section 4.1.1, which results in a lower requirement for the amount of conductive ink. However, resistance results presented in Figure 33 showed a contradiction to this hypothesis. Despite the smoother surface of PCC-based composites, remarkably better conductivity was obtained for conductors printed on kaolin-based sheets. Furthermore, the lines printed on the PCC-based composite using a rougher CMF grade did not conduct electricity at all. Instead, for kaolin-based sheets, the conductivity of both studied CMNF grades (Daicel and VTT CNF) was at a similar level to that of the reference substrates (plastic film Mylar A and paper-grade PEL). The PCC pigment particles produced a rough, more open and porous structure on a smaller scale than the profilometer spot size measurements. These features enabled silver ink to absorb deeper into the structure more easily than the kaolin-based composites.

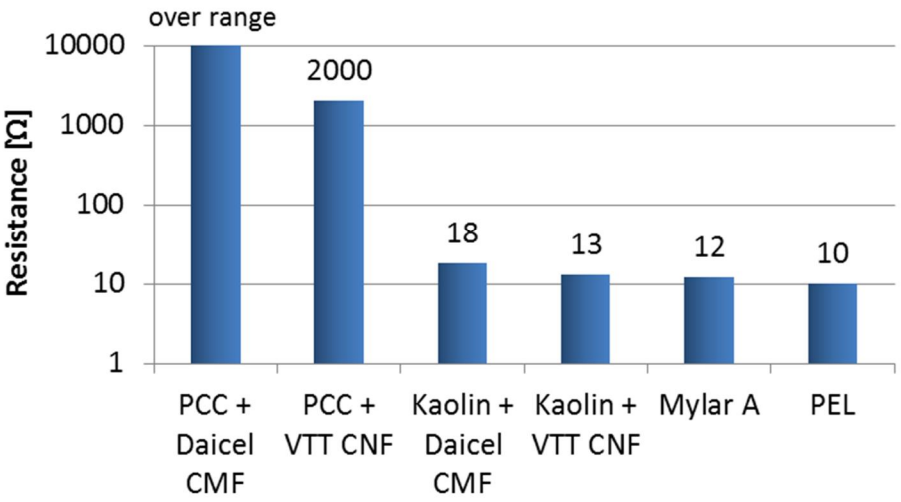

Figure 33. *Measured resistances of conductive lines published in Paper II. The resistance of PCC + Daicel composite was above the measurement range, meaning that the conductor line did not work at all. Plastic film Mylar A and Paper for printed Electronics PEL were used as references in this work. The used pigment grades were kaolin Intramax and PCC Albacar with an 80 wt-% of composites.*

The ink absorption can be experimentally validated from the surface and the printed line height data using an imaging profilometer, as presented in Figure 34. It can clearly be seen that the ink in PCC-based samples has vanished from the top of the surface. On kaolin-based composites the lines are clearly visible, with red color indicating that the line is higher than the composite surface. It is believed that a more open surface with channels into the PCC-based composite enabled the conductive ink to penetrate and absorb into the structure. Therefore, the continuous conductive path for electrons to travel was destroyed. The situation can be different if the flexo-printing method is used, due to the larger particles of flexo-grade silver ink.

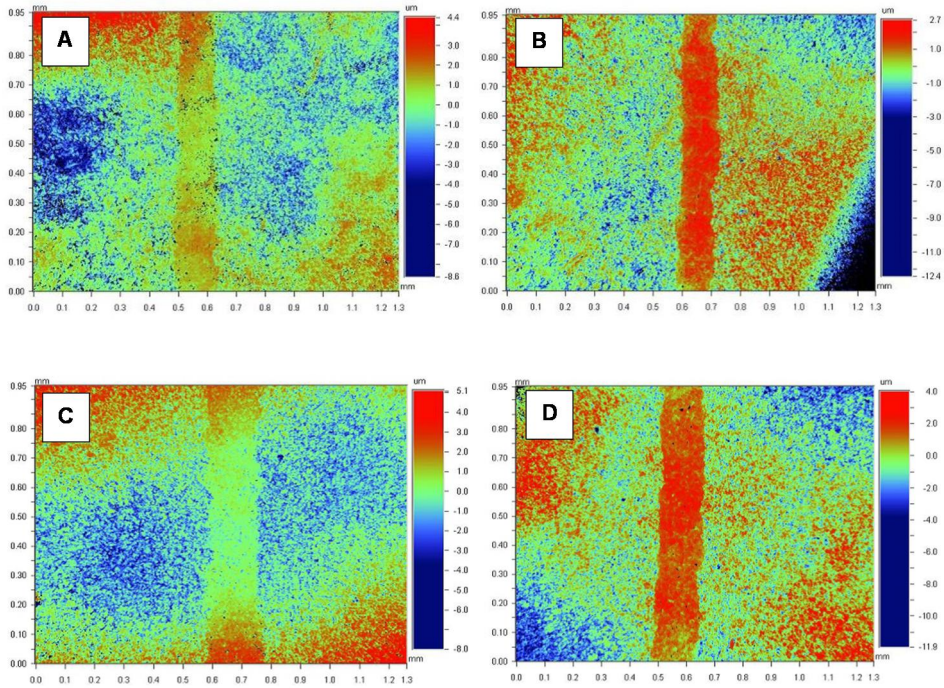

Figure 34. *Surface height maps for PCC- and kaolin-based composites measured using a Wyko profilometer. Vertical printed conductor lines are located in the middle of the images. The studied samples were A) PCC + Daicel, B) Kaolin + Daicel, C) PCC + VTT CNF and D) Kaolin + VTT CNF. The composites consisted of 80 wt-% pigment and 20 wt-% CMNF.*

As a summary, similar conductivities were achieved on kaolin-based composite substrates compared to commercial references in ink-jet printed conductors using a nanoscale silver ink. The smoothness was observed not to be the most critical property for producing conductive lines. Based on the studies, the porosity of the surface layer plays the most significant role in printed electronics applications. Successful printing requires optimization of nanoscale porosity and density of composites. These parameters can be adjusted by choosing the right raw material combinations for desired applications. An additional benefit of using PCMNF composites instead of plastics is that the relevant surface and structural properties can be adjusted with low costs.

4.3.2 Screen-printed and spray-coated supercapacitors

Figure 35 shows the demonstrated, proof-of-concept integrated structure in which the PCMNF composite was used as a separator and substrate for both screen-printed graphene electrodes and spray-coated CNT electrodes. The graphene and carbon nanotube (CNT) based inks were used as a high surface area active layer

material, and they simultaneously served as current collectors for the supercapacitor. The double functional separator-substrate with kaolin pigments and cellulose nanofibrils (CNFs) worked well as an active element in the supercapacitor. The calendered substrates were used, as it was observed that the uncalendered substrates absorbed too much ink, resulting in short-circuiting of the electrodes on the opposite sides of the substrate.

Adhesion of the graphene ink on the PCC-based composite was poor, as the layer delaminated immediately the ink was dried, and the device did not function as a supercapacitor. However, good results were achieved for both kaolin-based composites. The sheet resistance of the printed graphene layers, measured using the 4-probe method, was 10 Ω/□, and the corresponding values for the CNT layers varied between 30 and 70 Ω/□. The wide variance of the CNT layer resistance was due to difficulties in depositing layers of similar thickness with a handheld spray-coater.

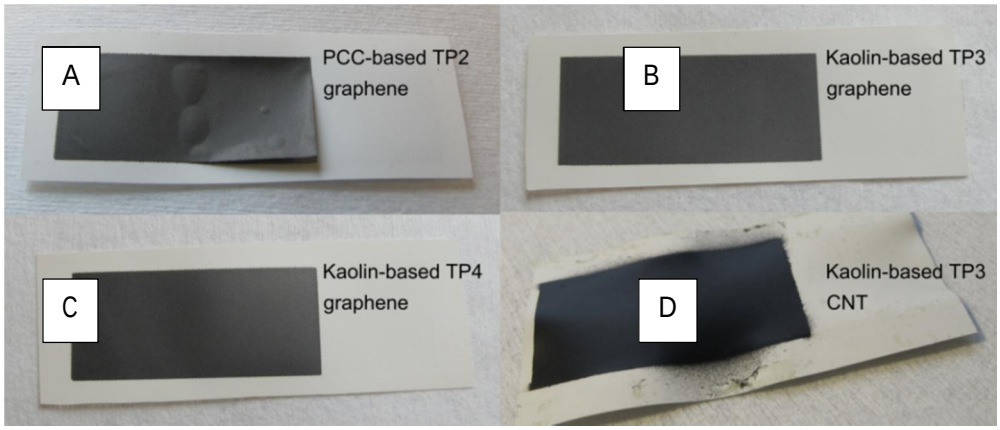

Figure 35. *Printed graphene and CNT layers on the studied composites: A) PCC + graphene, B) Kaolin1 + graphene, C) Kaolin2 + graphene and D) Kaolin + CNT. Good results were achieved for both kaolin-based substrates when graphene ink was used for printing. The adhesion of the ink to the PCC-based composite was poor, resulting in delamination of the printed electrode layer. Spray-coating of the CNT ink resulted in the sheet buckling due to absorption and spreading of the ink under the mask.*

CV curves of the produced devices are shown in Figure 36. The CNT supercapacitor had a more rectangular curve, whereas the graphene-based supercapacitor curves were less rectangular. The presence of a voltage maximum indicates the presence of Faradaic reactions. A possible source of reactive species is the graphene ink, which contains different binders and other additives designed to improve printability. The CNT ink, composed only of carbon nanotubes and xylan polymer (Lehtimäki, Tuukkanen, *et al.*, 2014), does not exhibit this behavior, but the printability is poorer than that of the graphene ink.

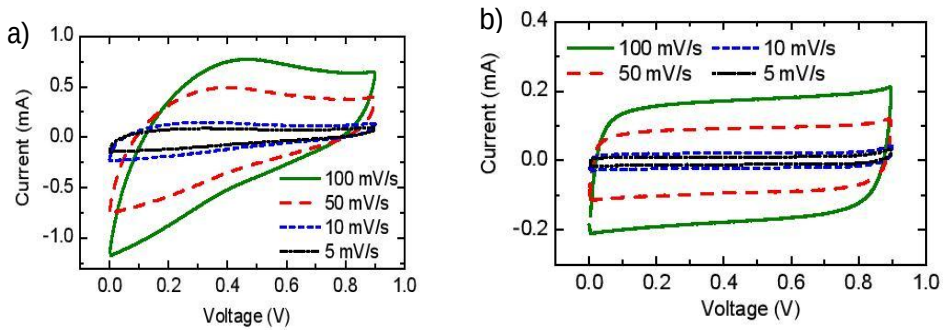

Figure 36. *CV curves of the devices with a) graphene and b) CNT electrodes.*

The quantitative properties were determined from galvanostatic measurements. An example curve is shown in Figure 37. There were no significant differences between the two types of kaolin pigment materials used in the graphene supercapacitors: the capacitances for kaolin-based composites varied between 17 and 20 mF. The specific capacitances were 4.9 and 4.2 F/g, respectively, when accounting only for the active material mass on the electrode overlap area. The difference in specific capacitances may be due to uncertainty in weighing the ink layers, as the increase in mass of the substrate due to the ink is very small, resulting in inaccuracy of the determined specific capacitance. Based on these results, kaolin-based composites worked better as supercapacitors compared to the PCC-based substrates, due to the closed surface and adequate porosity as presented in *Papers II and V.*

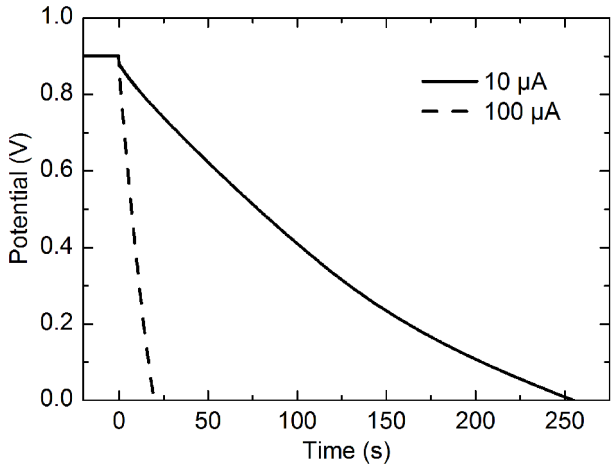

Figure 37. *An example of standard supercapacitor characterization by galvanostatic discharge curves in the case of CNT supercapacitors.*

4.3.3 Screen-printed LC-resonator and antennas

Figure 38 presents an unpublished functional NFC RFID demonstrator consisting of an antenna that was screen-printed using a silver ink on a PCMNF composite combined with a commercial RFID chip (strap) attached using a silver epoxy resin. The tags for NFC are more sophisticated versions of the information that was previously stored in bar codes. This information is readable using many smartphones, and *e.g.* in consumer goods they can be used for gathering information about products or about payment methods. The DC-resistance of the printed antenna, 33Ω (33 m Ω /sq sheet resistance), was at a similar level with PET film (30–45 Ω depending on the sintering temperature) and lower than for a copy paper. Benefits of the PCMNF composite include, beside the recyclability and renewable material base, a better temperature tolerance compared to the PET film. This enables higher sintering temperatures and opens a way to reach even lower resistance levels. Furthermore, the dimensional stability was better compared to the normal paper grade due to a high amount of inorganic pigments. In addition, the composites tolerate moisture changes better, as was presented in *Paper I.*

Figure 38. *An image of a screen-printed antenna combined with a commercial RFID ship as demonstrator of an RFID tag manufactured on PCMNF composite. The device has been hot-laminated into a plastic pocket. The content of the tag can be read with a mobile phone supporting NFC technology.*

4.3.4 Transistors

The physico-chemical characterization of the fabricated transistors on PCMNF composites and the performance of the deposited transistors were studied in *Paper V* as the last proof-of-concept device. A schematic view of the model transistor device structure is shown in Figure 39.

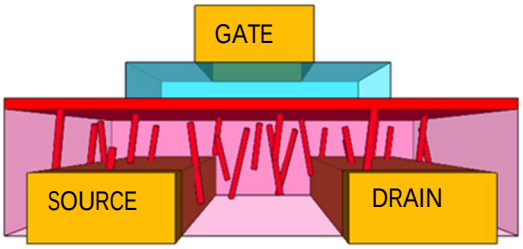

Figure 39. *A schematic view of the device structure. The transistor electrodes have been drawn in orange, the solid electrolyte in blue, the semiconductor in red, and the polymer insulator in pink.*

Figure 40 shows two examples of transfer curves of PCMNF composite and the reference ÅA paper. Table 7 summarizes the figure of merit (FOM) values that were extracted from the measured transfer curves. No clear difference in the film forming properties of the semiconductor layer can be distinguished from the appearance of the devices. Typically, during the casting of this particular semiconductor, it will show different colors depending on the semiconductor crystallinity and thickness.

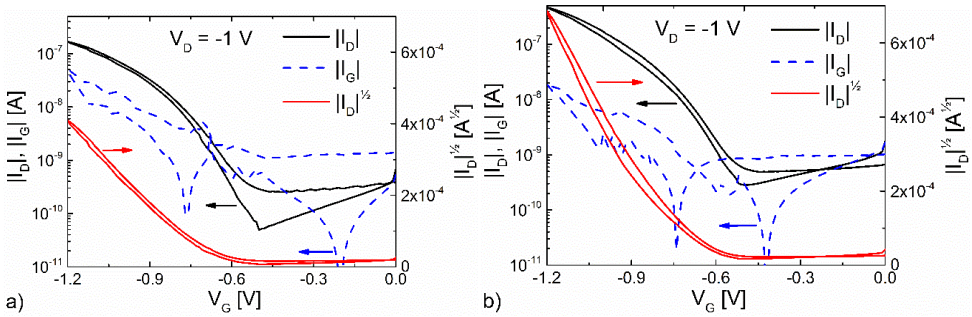

Figure 40. *Transfer curves of transistors fabricated on a) composite including kaolin (80 wt-%) and TCNF (20 wt%) and b) ÅA reference paper. The black curves represent the* I_D *in saturation mode during gate sweeps between 0 V and -1.2 V, the red curve is the square root of* I_D *and the dashed curve is the* I_G*.*

Table 7 shows that several studied trial points had similar transistor properties compared to that of the reference ÅA paper. These had slightly lower ON-currents and higher leakage currents, but are still comparable to the ÅA reference device. The PCMNF composites can thus be used as a natural fiber-based substrate for electronic devices without any significant loss of performance. The trial point, which included kaolin 80 wt-% and TEMPO CNF 20 wt-%, showed the highest ON/OFF-ratio, but it also showed the highest leakage current. This would result in increased power consumption and would not be a desirable alternative for the ÅA paper. Transistors produced on composite including ECMF (enzymatic) grade showed no transistor characteristics at all. As a summary, the used CMNF grade

had a significant effect on transistor performance processed on the studied composite films.

Table 7. *FOMs, calculated using the transfer curves of the same transistor model, fabricated on different substrates. Trial point ECMF_43 did not show transistor characteristics and therefore no FOMs could be calculated. Åbo Akademi multilayer paper was used as a reference (Roger Bollström et al., 2009). All units are in amperes except for the dimensionless ratios.*

Trial point	ON-current [E-07 A]	OFF-current [E-10 A]	ON/OFF-ratio	Leakage [E-08 A]	Leakage/ON-current
CNF_20	1.4	9.1	150	14	1.01
ECMF_43	-	-	-	-	-
CNF_43	3.0	2.1	1460	4.0	0.13
LCNF_43	2.8	2.1	1370	3.3	0.12
LCNF_20C	0.3	10	30	0.4	0.13
TCNF_20	1.7	0.5	3460	5.0	0.29
LCNF_20B	3.9	2.5	1570	3.0	0.08
ÅA	4.7	2.9	1650	2.0	0.04

The CMNF grade played a significant role in surface smoothness and porosity of composites. Such characteristics had a clear effect on the properties of transistors fabricated on these composite substrates. Furthermore, the low fibrillation degree and the particle aspect ratio were observed to decrease the performance of composites. Several of the studied PCMNF composite types had similar transistor properties compared to that of a reference paper designed for printed electronics. The PCMNF composites had slightly lower ON-currents and higher leakage currents. However, they are still comparable and these PCMNF composites can be used as a natural fiber-based substrate for transistor devices, without any significant loss of device performance.

4.4 Feasibility and techno-economical potential of composites *(Paper IV and unpublished data)*

The feasibility of novel PCMNF composites for printed electronics applications was studied using the following main assumptions: structure consists of 80 wt-% of pigment filler (*e.g.* $CaCO_3$, kaolin) and 20 wt-% of CNF. The composite was formed by vacuum filtration, dried under pressure, and then calendered. A potential composite manufacturing concept was calculated for solvent casting on top of a plastic or a metal substrate. The wet pressing and drying conditions are critical and need further development.

The following assumptions based on the experiments were made during the techno-economic analysis: The composite substrates are compatible with printing methods such as inkjet, flexo, and screen printing, and have sufficient quality for low-cost applications such as disposable personal electronics and diagnostic applications. In this unpublished analysis, the use of CNF was reported as a cellulose material, but a similar pigment-cellulose composite can also be composed using cellulose microfibrils (CMF). The price of CMF is still somewhat lower that of CNF due to its shorter cellulose processing times.

The composite consists of 80 wt-% of pigment (*e.g.* $CaCO_3$, kaolin) and 20 wt-% of CMF. The composite is formed by vacuum filtration, dried under pressure, and calendered. These assumptions result in a lower capital expenditure (Capex), with a total cost of a line producing 3 000 t/a of about 10 M€ (approximately 3 300 €/t investment cost), whereas PET film production lines typically cost 40–75 M€ and produce 10 000–20 000 t/a (approx. 3 800 €/t investment cost). Lower investment cost per ton and smaller investment size are favorable from the economic point of view. In addition, the use of cheaper raw materials will result in a lower operational expenditure (Opex), assuming approximately equal salary costs. The production cost estimate is shown in Figure 41.

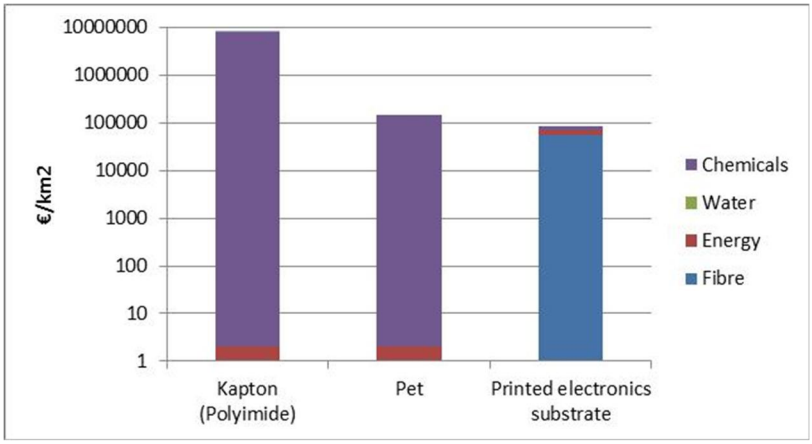

Figure 41. *Production cost estimates of printed electronics substrates. References in calculations were Kapton (polyimide) and PET films.*

New product opportunities and markets can be captured with PCMNF composites for printed electronics applications. However, it must be emphasized that this concept still requires development. The environmental performance of these products was excellent compared to the reference PET / BoPET films, as shown in Figure 42. The evaluation was made using a standardized life cycle assessment (LCA) approach, which includes fossil greenhouse gases (CO_2, CH_4 and N_2O), expressed as carbon dioxide equivalents (CO_2 eq). No water consumption data was available for the reference product.

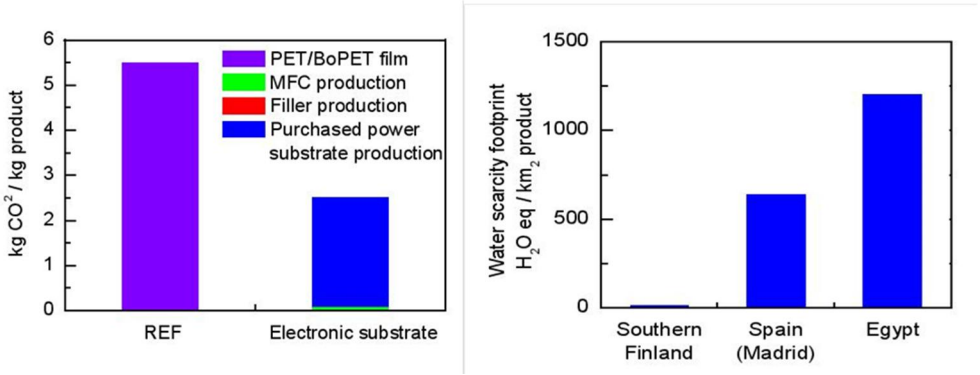

Figure 42. *Environmental performance screening for PCMNF composites: Left: Calculated cradle-to-gate carbon footprint for printed electronics substrate in comparison with PET/BoPET film reference (range 5–8 kg CO_2/kg from the literature). Right: water consumption of composite production weighted with local scarcity indices.*

5 Conclusions

The PCMNF composites manufactured and studied in this thesis work differ from traditional paper and board materials due to the high amount of inorganic pigment (up to 90%) and the characteristics of cellulose nanofibrils (CNF). PCMNF composites are sustainable, flexible, and can tolerate high sintering temperatures for printed electronics applications to replace plastic materials. An additional benefit of PCMNF composites is that the relevant surface and structural properties can be adjusted at low cost. The composite films can be manufactured by a film casting method in a semi-pilot scale. Moreover, the results of this work show that it will be possible to up-scale the production method to industrial scale in future.

The developed composites need to fulfill certain quality requirements for printed electronics applications. The used manufacturing process significantly influences these properties. The porosity of the structure was found to be a more relevant property than surface smoothness in printed electronics applications for production of conductive lines. This means that a successful printing of functional devices needs to be optimized with the nanoscale porosity of the composites. The main effort of this work was to understand the interactions between composite raw materials and manufacturing process phases and the obtained properties of composites. Moreover, these properties of composites had a great influence on the characteristics of manufactured proof-of-concept functional devices. Hence, the targeted end-use application determines the necessary substrate properties.

Based on this work, the porosity of surface layer plays the most significant role in printed electronics applications. The surface pore volume can be optimized for the used printing method and ink by the choice of pigment type, amount, and CMNF material grade. These parameters can be adjusted by using the right raw material combinations for the desired applications. Based on these results, kaolin-based composites work better as a substrate compared to PCC-based composites due to their more suitable porosity. The CMNF grade also played a significant role in surface smoothness and porosity of composites. These characteristics had a clear effect on the functional devices fabricated on the composite substrates. Furthermore, low fibrillation degree and particle aspect ratio were observed to reduce the performance of composites.

Drying experiments in laboratory scale showed that the PCMNF composite can be dried by using conventional drying methods such as contact drying and air impingement drying. Despite the very high bound water content of the CNF gel, the estimated drying rates for the PCMNF substrate were comparable with the drying rates of a typical paperboard with the same external drying conditions. It was also demonstrated that before drying, the water can be effectively removed from the PCMNF sheets by hot pressing. The removal of water mechanically in the hot

contact press dramatically reduces the energy consumption required for drying of an initially highly wet PCMNF substrate.

In order to increase the number of sustainable and economically feasible products in the printed electronics markets, the production costs need to be taken into account. In this work, it was shown that using CMNF together with inorganic pigments to produce cost-effective, feasible, and novel films can have advantages. However, more work is needed to obtain smooth and surface nano-porous composite films suitable for the wet pressing method. A roll-to-roll production process for inexpensive energy storage devices, e.g. supercapacitors, is possible using such a composite as a separator-substrate. The porous electrode layers made with environmentally friendly aqueous dispersions of carbon nanotubes (CNT) or graphene can be used. The electrodes can be coated or printed in pilot scale on both sides of the separator substrate. This will be a considerable advantage compared to the current production methods of supercapacitors.

6 Suggestions for further work

The industrial production of functional devices using paper or novel composites is still currently rather limited. The volume needs for these specialty papers are not comparable to those of traditional paper grade production, due to the currently low market demand. As a future scenario, smaller and more specialised machinery is needed with flexible and movable production units. This will allow the production of different end-use application devices with the same machinery.

Foam coating (Kenttä *et al*., 2014, Kinnunen-Raudaskoski *et al*., 2014) and foam forming (Lehmonen *et al*., 2013) are currently attracting a growing interest in paperboard industry. The use of foam allows an addition of a wide variety of alternative raw materials, such as nanoparticles, CMNF and long flexible fibers into the paperboard webs. These technologies will also lead to more versatile production methods that are required for manufacturing totally new high-value added end products. Naturally, energy efficient technologies are also of great interest and with foam-based technologies in paper making, water consumption can be reduced and less energy is needed in drying.

A possible future study could be to use a wet laid process for the next generation cost-effective mass production of separator substrate in real industrial conditions. A good candidate here is the impregnation of the PCMNF with a foam coating technique on a fiber web made from conventional cellulose pulp in a wet laid process before the forming section. The advantage of such an approach would be an increase in the strength of the PCMNF separator substrate, and a dramatic increase in production capacity due to a higher production speed and a wider web.

References

Abdul Khalil, H. P. S., Bhat, A. H., & Ireana Yusra, A. F. (2012). Green composites from sustainable cellulose nanofibrils: A review. *Carbohydrate Polymers*. https://doi.org/10.1016/j.carbpol.2011.08.078

Aitomäki, Y., & Oksman, K. (2014). Reinforcing efficiency of nanocellulose in polymers. *Reactive and Functional Polymers, 85,* 151–156. https://doi.org/10.1016/j.reactfunctpolym.2014.08.010

Allen, M. L., Aronniemi, M., Mattila, T., Alastalo, A., Ojanperä, K., Suhonen, M., & Seppä, H. (2008). Electrical sintering of nanoparticle structures. *Nanotechnology, 19*(17), 175201. https://doi.org/10.1088/0957-4484/19/17/175201

An, K. H., Kim, W. S., Park, Y. S., Choi, Y. C., Lee, S. M., Chung, D. C., ... Lee, Y. H. (2001). Supercapacitors using single-walled carbon nanotube electrodes. *Advanced Materials, 13*(7), 497–500. https://doi.org/10.1002/1521-4095(200104)13:7<497::AID-ADMA497>3.0.CO;2-H

Andersson. (2012). Contacting paper-based supercapacitors to printed electronics on paper substrates. *Nordic Pulp and Paper Research Journal, 27*(2), 476–480. https://doi.org/10.3183/NPPRJ-2012-27-02-p476-480

Asensio, M. C., Seyed-Yagoobi, J., Lehtinen, J. A., Karlsson, M. A., Timofeev, O. N., & Juppi, K. (2007). Comparison of Several Multi-Cylinder Paper Drying Simulation Models. *Drying Technology,* (787743727). https://doi.org/10.1080/07373939508916992

Aulin, C., Salazar-Alvarez, G., & Lindström, T. (2012). High strength, flexible and transparent nanofibrillated cellulose-nanoclay biohybrid films with tunable oxygen and water vapor permeability. *Nanoscale, 4*(20), 6622–8. https://doi.org/10.1039/c2nr31726e

Azarova, N. A., Owen, J. W., McLellan, C. A., Grimminger, M. A., Chapman, E. K., Anthony, J. E., & Jurchescu, O. D. (2010). Fabrication of organic thin-film transistors by spray-deposition for low-cost, large-area electronics. *Organic Electronics: Physics, Materials, Applications, 11*(12), 1960–1965. https://doi.org/10.1016/j.orgel.2010.09.008

Azeredo, H. M. C., Mattoso, L. H. C., Avena-Bustillos, R. J., Filho, G. C., Munford, M. L., Wood, D., & McHugh, T. H. (2010). Nanocellulose reinforced chitosan composite films as affected by nanofiller loading and plasticizer content. *Journal of Food Science, 75*(1), 1–7. https://doi.org/10.1111/j.1750-3841.2009.01386.x

Bai, Y. (2016). Samuel Greengard, The Internet of Things, *10,* 5604–5607.

Berggren, M., Nilsson, D., & Robinson, N. D. (2007). Organic materials for printed electronics. *Nature Materials, 6*(1), 3–5. https://doi.org/10.1038/nmat1817

Berglund, L. (2005). Cellulose-based nanocomposites. *Natural Fibers, Biopolymers, and Biocomposites,* 807–832. https://doi.org/10.1201/9780203508206.ch1

Bollström, R., Määttänen, A., Tobjörk, D., Ihalainen, P., Kaihovirta, N., Österbacka, R., ... Toivakka, M. (2009). A multilayer coated fiber-based substrate suitable for printed functionality. *Organic Electronics: Physics, Materials, Applications, 10*(5), 1020–1023. https://doi.org/10.1016/j.orgel.2009.04.014

Bollström, R., Tobjörk, D., & Dolietis, P. (2012). Roll-to-roll printed electronics on paper.

Roll-to-Roll Printed Electronics on Paper. Retrieved from http://scholar.google.com/scholar?q=Roll-to-roll printed electronics on paper&btnG=&hl=en&num=20&as_sdt=0%2C22 VN - readcube.com

Boluk, Y., Lahiji, R., Zhao, L., & McDermott, M. T. (2011). Suspension viscosities and shape parameter of cellulose nanocrystals (CNC). *Colloids and Surfaces A: Physicochemical and Engineering Aspects, 377*(1–3), 297–303. https://doi.org/10.1016/j.colsurfa.2011.01.003

Bras, J., Viet, D., Bruzzese, C., & Dufresne, A. (2011). Correlation between stiffness of sheets prepared from cellulose whiskers and nanoparticles dimensions. *Carbohydrate Polymers, 84*(1), 211–215. https://doi.org/10.1016/j.carbpol.2010.11.022

Brodin, F. W., Gregersen, Ø. W., & Syverud, K. (2014). Cellulose nanofibrils: Challenges and possibilities as a paper additive or coating material - A review. *Nordic Pulp and Paper Research Journal, 29*(1), 156–166. https://doi.org/10.3183/NPPRJ-2014-29-01-p156-166

Bundy, W. M., & Ishley, J. N. (1991). Kaolin in paper filling and coating. *Applied Clay Science, 5*(5–6), 397–420. https://doi.org/10.1016/0169-1317(91)90015-2

Chan, Y. J., Kung, C. P., & Pei, Z. (2005). Printed RFID: technology and application. In *2005 IEEE International Wkshp on Radio-Frequency Integration Technology: Integrated Circuits for Wideband Comm & Wireless Sensor Networks* (pp. 139–141). https://doi.org/10.1109/RFIT.2005.1598894

Chang, J., Ge, T., & Sanchez-Sinencio, E. (2012). Challenges of printed electronics on flexible substrates. In *Midwest Symposium on Circuits and Systems* (pp. 582–585). https://doi.org/10.1109/MWSCAS.2012.6292087

Chen, T., & Dai, L. (2013). Carbon nanomaterials for high-performance supercapacitors. *Materials Today*. https://doi.org/10.1016/j.mattod.2013.07.002

Chen, Z., Augustyn, V., Wen, J., Zhang, Y., Shen, M., Dunn, B., & Lu, Y. (2011). High-performance supercapacitors based on intertwined CNT/V2O5 nanowire nanocomposites. *Advanced Materials, 23*(6), 791–795. https://doi.org/10.1002/adma.201003658

Ching, Y. C., Rahman, A., Ching, K. Y., Sukiman, N. L., & Chuah, C. H. (2015). Preparation and Characterization of Polyvinyl Alcohol- Based Composite Reinforced with Nanocellulose and, *10*(2), 3364–3377.

Chinga-Carrasco, G., & Syverud, K. (2014). Pretreatment-dependent surface chemistry of wood nanocellulose for pH-sensitive hydrogels. *Journal of Biomaterials Applications, 29*(7491), 423–432. https://doi.org/10.1177/0885328214531511

Choi, K.-H., Yoo, J., Lee, C. K., & Lee, S.-Y. (2016). All-inkjet-printed, solid-state flexible supercapacitors on paper. *Energy Environ. Sci., 12,* 871–872. https://doi.org/10.1039/C6EE00966B

Costa, S. V., Pingel, P., Janietz, S., & Nogueira, A. F. (2016). Inverted organic solar cells using nanocellulose as substrate. *Journal of Applied Polymer Science, 133*(28). https://doi.org/10.1002/app.43679

Das, R., & Harrop, P. (2012). *Printed, Organic \& Flexible Electronics Forecasts, Players \& Opportunities 2011-2021*. *Sandler Research Market Research Reports Database*.

De Oliveira, M. H., Tejado, A., & Van De Ven, T. G. M. (2009). Effects of fillers on the wet

web strength of paper. *Nordic Pulp and Paper Research Journal, 24*(2).

Dimic-Misic, K., Gane, P. A. C., & Paltakari, J. (2013). Micro and nanofibrillated cellulose as a rheology modifier additive in CMC-containing pigment-coating formulations. *Industrial and Engineering Chemistry Research, 52*(45), 16066–16083. https://doi.org/10.1021/ie4028878

Dimic-Misic, K., Puisto, A., Paltakari, J., Alava, M., & Maloney, T. (2013). The influence of shear on the dewatering of high consistency nanofibrillated cellulose furnishes. *Cellulose, 20*(4), 1853–1864. https://doi.org/10.1007/s10570-013-9964-9

Dogome, K., Enomae, T., & Isogai, A. (2013). Method for controlling surface energies of paper substrates to create paper-based printed electronics. *Chemical Engineering and Processing: Process Intensification, 68,* 21–25. https://doi.org/10.1016/j.cep.2013.01.003

Eda, G., & Chhowalla, M. (2009). Graphene-based composite thin films for electronics. *Nano Letters, 9*(2), 814–818. https://doi.org/10.1021/n18035367

Eom, S. H., Senthilarasu, S., Uthirakumar, P., Yoon, S. C., Lim, J., Lee, C., … Lee, S. H. (2009). Polymer solar cells based on inkjet-printed PEDOT:PSS layer. *Organic Electronics: Physics, Materials, Applications, 10*(3), 536–542. https://doi.org/10.1016/j.orgel.2009.01.015

Fao. (2013). Food waste harms climate , water , land and biodiversity – new FAO report. *Food and Agriculture Organization of The United Nations*. Retrieved from od waste harms climate, water, land and biodiversity ? new FAO report

Fujisawa, S., Okita, Y., Fukuzumi, H., Saito, T., & Isogai, A. (2011). Preparation and characterization of TEMPO-oxidized cellulose nanofibril films with free carboxyl groups. *Carbohydrate Polymers, 84*(1), 579–583. https://doi.org/10.1016/j.carbpol.2010.12.029

Fukuzumi, H., Saito, T., Iwata, T., Kumamoto, Y., & Isogai, A. (2009). Transparent and high gas barrier films of cellulose nanofibers prepared by TEMPO-mediated oxidation. *Biomacromolecules, 10*(1), 162–165. https://doi.org/10.1021/bm801065u

Galagan, Y., Coenen, E. W. C., Abbel, R., Van Lammeren, T. J., Sabik, S., Barink, M., … Blom, P. W. M. (2013). Photonic sintering of inkjet printed current collecting grids for organic solar cell applications. *Organic Electronics: Physics, Materials, Applications, 14*(1), 38–46. https://doi.org/10.1016/j.orgel.2012.10.012

Gaspar, C., Passoja, S., Olkkonen, J., & Smolander, M. (2016). IR-sintering efficiency on inkjet-printed conductive structures on paper substrates. *Microelectronic Engineering, 149,* 135–140. https://doi.org/10.1016/j.mee.2015.10.006

Georgi-Maschler, T., Friedrich, B., Weyhe, R., Heegn, H., & Rutz, M. (2012). Development of a recycling process for Li-ion batteries. *Journal of Power Sources, 207,* 173–182. https://doi.org/10.1016/j.jpowsour.2012.01.152

González, I., Alcalà, M., Chinga-Carrasco, G., Vilaseca, F., Boufi, S., & Mutjé, P. (2014). From paper to nanopaper: Evolution of mechanical and physical properties. *Cellulose, 21*(4), 2599–2609. https://doi.org/10.1007/s10570-014-0341-0

Grau, G., Kitsomboonloha, R., Swisher, S. L., Kang, H., & Subramanian, V. (2014). Printed transistors on paper: Towards smart consumer product packaging. *Advanced Functional Materials, 24*(32), 5067–5074. https://doi.org/10.1002/adfm.201400129

Graupner, N., Herrmann, A. S., & Müssig, J. (2009). Natural and man-made cellulose fibre-reinforced poly(lactic acid) (PLA) composites: An overview about mechanical characteristics and application areas. *Composites Part A: Applied Science and Manufacturing, 40*(6–7), 810–821. https://doi.org/10.1016/j.compositesa.2009.04.003

Guillén, C., & Herrero, J. (2005). Comparison study of ITO thin films deposited by sputtering at room temperature onto polymer and glass substrates. In *Thin Solid Films* (Vol. 480–481, pp. 129–132). https://doi.org/10.1016/j.tsf.2004.11.040

Halper, M., & Ellenbogen, J. (2006). Supercapacitors: A brief overview. *Report No. MP 05W0000272, The ...,* (March), Report No. MP 05W0000272, 1-29. https://doi.org/Report No. MP 05W0000272

He, M., Cho, B. U., & Won, J. M. (2016). Effect of precipitated calcium carbonate - Cellulose nanofibrils composite filler on paper properties. *Carbohydrate Polymers, 136,* 820–825. https://doi.org/10.1016/j.carbpol.2015.09.069

He, X. (2015). Flexible, Printed and Thin Film Batteries 2015-2025: Technologies, Forecasts, Players. *Idtechex,* 2014–2016. Retrieved from http://www.idtechex.com/research/reports/flexible-printed-and-thin-film-batteries-2015-2025-technologies-forecasts-players-000410.asp

Henriksson, M., Berglund, L. A., Isaksson, P., Lindström, T., & Nishino, T. (2008). Cellulose nanopaper structures of high toughness. *Biomacromolecules, 9*(6), 1579–1585. https://doi.org/10.1021/bm800038n

Henriksson, M., Henriksson, G., Berglund, L. A., & Lindström, T. (2007). An environmentally friendly method for enzyme-assisted preparation of microfibrillated cellulose (MFC) nanofibers. *European Polymer Journal, 43*(8), 3434–3441. https://doi.org/10.1016/j.eurpolymj.2007.05.038

Hodgson, A. (2011). The role of paper in the future of printed electronics. In *2nd International Workshop on Collaborating over Paper and Digital Documents CoPADD London November* (Vol. 2011, pp. 3–6). Retrieved from http://www.copadd07.ethz.ch/papers/3.pdf

Hoeng, F., Denneulin, A., & Bras, J. (2016). Use of nanocellulose in printed electronics: A review. *Nanoscale, 8,* 13131–13154. https://doi.org/10.1039/C6NR03054H

Hoeng, F., Denneulin, A., Bras, J., Siqueira, G., Abdillahi, H., Bras, J., … Gregersen, Ø. (2016). Use of nanocellulose in printed electronics: a review. *Nanoscale, 8*(27), 13131–13154. https://doi.org/10.1039/C6NR03054H

Hong, G.-B., Ma, C.-M., Chen, H.-W., Chuang, K.-J., Chang, C.-T., & Su, T.-L. (2011). Energy flow analysis in pulp and paper industry. *Energy, 36*(5), 3063–3068. https://doi.org/10.1016/j.energy.2011.02.051

Honorato, C., Kumar, V., Liu, J., Koivula, H., Xu, C., & Toivakka, M. (2015). Transparent nanocellulose-pigment composite films. *Journal of Materials Science, 50*(22), 7343–7352. https://doi.org/10.1007/s10853-015-9291-7

Hsieh, M., Kim, C., Nogi, M., & Suganuma, K. (2013). Electrically conductive lines on cellulose nanopaper for flexible electrical devices. *Nanoscale, 5*(19), 9289–95. https://doi.org/10.1039/c3nr01951a

Hu, L., Choi, J. W., Yang, Y., Jeong, S., La Mantia, F., Cui, L.-F., & Cui, Y. (2009). Highly conductive paper for energy-storage devices. *Proceedings of the National Academy of Sciences of the United States of America, 106*(51), 21490–21494. https://doi.org/10.1073/pnas.0908858106

Hu, L., Wu, H., & Cui, Y. (2010). Printed energy storage devices by integration of electrodes and separators into single sheets of paper. *Applied Physics Letters, 96*(18). https://doi.org/10.1063/1.3425767

Huang, J., Zhu, H., Chen, Y., Preston, C., Rohrbach, K., Cumings, J., & Hu, L. (2013). Highly transparent and flexible nanopaper transistors. *ACS Nano, 7*(3), 2106–2113. https://doi.org/10.1021/nn304407r

Huang, Y., Liang, J., & Chen, Y. (2012). An overview of the applications of graphene-based materials in supercapacitors. *Small*. https://doi.org/10.1002/smll.201102635

Hubbe, M. a., Rojas, O. J., Lucia, L. a., & Sain, M. (2008). Cellulosic Nanocomposites: a Review. *BioResources, 3*(3), 929–980. https://doi.org/10.15376/biores.3.3.929-980

Hübler, A., Trnovec, B., Zillger, T., Ali, M., Wetzold, N., Mingebach, M., … Dyakonov, V. (2011). Printed paper photovoltaic cells. *Advanced Energy Materials, 1*(6), 1018–1022. https://doi.org/10.1002/aenm.201100394

Hyun, W. J., Secor, E. B., Rojas, G. A., Hersam, M. C., Francis, L. F., & Frisbie, C. D. (2015). All-Printed, Foldable Organic Thin-Film Transistors on Glassine Paper. *Advanced Materials, 27*(44), 7058–7064. https://doi.org/10.1002/adma.201503478

Ihalainen, P., Määttänen, A., Järnström, J., Tobjörk, D., Österbacka, R., & Peltonen, J. (2012). Influence of surface properties of coated papers on printed electronics. In *Industrial and Engineering Chemistry Research* (Vol. 51, pp. 6025–6036). https://doi.org/10.1021/ie202807v

Isogai, A., Saito, T., & Fukuzumi, H. (2011). TEMPO-oxidized cellulose nanofibers. *Nanoscale, 3*(1), 71–85. https://doi.org/10.1039/c0nr00583e

Iwamoto, S., Nakagaito, A. N., & Yano, H. (2007). Nano-fibrillation of pulp fibers for the processing of transparent nanocomposites. *Applied Physics A: Materials Science and Processing, 89*(2), 461–466. https://doi.org/10.1007/s00339-007-4175-6

Jang, S., Lee, D. J., Lee, D., & Oh, J. H. (2013). Electrical sintering characteristics of inkjet-printed conductive Ag lines on a paper substrate. In *Thin Solid Films* (Vol. 546, pp. 157–161). https://doi.org/10.1016/j.tsf.2013.05.015

Jung, S., & Kim, J. H. (2010). Sintering characteristics of TiO2 nanoparticles by microwave processing. *Korean Journal of Chemical Engineering, 27*(2), 645–650. https://doi.org/10.1007/s11814-010-0057-2

Jung, Y. H., Chang, T.-H., Zhang, H., Yao, C., Zheng, Q., Yang, V. W., … Ma, Z. (2015). High-performance green flexible electronics based on biodegradable cellulose nanofibril paper. *Nature Communications, 6*(May), 7170. https://doi.org/10.1038/ncomms8170

Kaempgen, M., Chan, C. K., Ma, J., Cui, Y., & Gruner, G. (2009). Printable thin film supercapacitors using single-walled carbon nanotubes. *Nano Letters, 9*(5), 1872–1876. https://doi.org/10.1021/nl8038579

Kajanto, I., & Kosonen, M. (2012). The potential use of micro-and nanofibrillated cellulose as a reinforcing element in paper. *J-FOR, 2*(6), 42–48.

Kamyshny, A., & Magdassi, S. (2014). Conductive nanomaterials for printed electronics. *Small*. https://doi.org/10.1002/smll.201303000

Kang, B., Lee, W. H., & Cho, K. (2013). Recent advances in organic transistor printing processes. *ACS Applied Materials and Interfaces*.

https://doi.org/10.1021/am302796z

Kang, H., Park, J., & Shin, K. (2014). Statistical analysis for the manufacturing of multi-strip patterns by roll-to-roll single slot-die systems. *Robotics and Computer-Integrated Manufacturing, 30*(4), 363–368. https://doi.org/10.1016/j.rcim.2013.12.004

Kangas, H., Lahtinen, P., Sneck, A., Saariaho, A.-M., Laitinen, O., & Hellén, E. (2014). Characterization of fibrillated celluloses. A short review and evaluation of characteristics with a combination of methods. *Nordic Pulp & Paper Research Journal, 29*(1), 129–43.

Kantola, V., Kulovesi, J., Lahti, L., Lin, R., Zavodchikova, M., & Coatanéa, E. (2009). *Printed Electronics, Now and Future. Bit Bang - Rays to the Future*.

Kattumenu, R., Rebros, M., Joyce, M., Fleming, P. D., & Neelgund, G. (2009). Effect of substrate properties on conductive traces printed with silver-based flexographic ink. *Nordic Pulp and Paper Research Journal, 24*(1), 101–106. Retrieved from http://www.scopus.com/inward/record.url?eid=2-s2.0-65149090960&partnerID=40&md5=eba1498f35893ac61855cc018ac39e5c

Kenttä, E., Kinnunen-Raudaskoski, K., Hjelt, T., "Characterization of thin pigment coating layers produced by foam coating," TAppi J. 13 (2014)

Kim, H. S., Kim, J. H., & Kim, J. (2011). A review of piezoelectric energy harvesting based on vibration. *International Journal of Precision Engineering and Manufacturing, 12*(6), 1129–1141. https://doi.org/10.1007/s12541-011-0151-3

Kim, J. H., Shim, B. S., Kim, H. S., Lee, Y. J., Min, S. K., Jang, D., ... Kim, J. (2015). Review of nanocellulose for sustainable future materials. *International Journal of Precision Engineering and Manufacturing - Green Technology*. https://doi.org/10.1007/s40684-015-0024-9

Kim, J., Yun, S., Mahadeva, S. K., Yun, K., Yang, S. Y., & Maniruzzaman, M. (2010). Paper actuators made with cellulose and hybrid materials. *Sensors, 10*(3), 1473–1485. https://doi.org/10.3390/s100301473

Kinnunen-Raudaskoski, K., Hjelt, T., Kenttä, E., Forsström, U., "Thin coatings for paper by foam coating,", Tappi J. 13 (2014)

Klemm, D., Heublein, B., Fink, H-P., and Bohn, A., (2005). "Cellulose: Fascinating biopolymer and sustainable raw material, " Angew. Chem. 44, 2-37.

Klemm, D., Kramer, F., Moritz, S., Lindstr??m, T., Ankerfors, M., Gray, D., & Dorris, A. (2011). Nanocelluloses: A new family of nature-based materials. *Angewandte Chemie - International Edition*. https://doi.org/10.1002/anie.201001273

Koga, H., Nogi, M., Komoda, N., Nge, T. T., Sugahara, T., & Suganuma, K. (2014). Uniformly connected conductive networks on cellulose nanofiber paper for transparent paper electronics. *NPG Asia Materials, 6*(3), e93. https://doi.org/10.1038/am.2014.9

Kopeček, J. (2007). Hydrogel biomaterials: A smart future? *Biomaterials, 28*(34), 5185–5192. https://doi.org/10.1016/j.biomaterials.2007.07.044

Krebs, F. C. (2009). Polymer solar cell modules prepared using roll-to-roll methods: Knife-over-edge coating, slot-die coating and screen printing. *Solar Energy Materials and Solar Cells, 93*(4), 465–475. https://doi.org/10.1016/j.solmat.2008.12.012

Kumar, V., Bollström, R., Yang, A., Chen, Q., Chen, G., Salminen, P., ... Toivakka, M. (2014).

Comparison of nano- and microfibrillated cellulose films. *Cellulose*. https://doi.org/10.1007/s10570-014-0357-5

Lahtinen, P., Torvinen, K., Kangas, H., Liukkonen, S., Sneck, A., Peresin, M. S., ... Meyer, V. (2014). Effect of fibrillated cellulosic additives on paper strength properties. In *Paper Conference and Trade Show, PaperCon 2014* (Vol. 1, pp. 362–371).

Larcher, D., & Tarascon, J.-M. (2015). Towards greener and more sustainable batteries for electrical energy storage. *Nature Chemistry, 7*(1), 19–29. https://doi.org/10.1038/nchem.2085

Layani, M., Cooperstein, I., & Magdassi, S. (2013). UV crosslinkable emulsions with silver nanoparticles for inkjet printing of conductive 3D structures. *Journal of Materials Chemistry C, 1*(19), 3244. https://doi.org/10.1039/c3tc30253a

Lee, K. Y., Aitomäki, Y., Berglund, L. A., Oksman, K., & Bismarck, A. (2014). On the use of nanocellulose as reinforcement in polymer matrix composites. *Composites Science and Technology*. https://doi.org/10.1016/j.compscitech.2014.08.032

Lee, S. Y., Mohan, D. J., Kang, I. A., Doh, G. H., Lee, S., & Han, S. O. (2009). Nanocellulose reinforced PVA composite films: Effects of acid treatment and filler loading. *Fibers and Polymers, 10*(1), 77–82. https://doi.org/10.1007/s12221-009-0077-x

Lee, Y., Choi, J.-R., Lee, K. J., Stott, N. E., & Kim, D. (2008). Large-scale synthesis of copper nanoparticles by chemically controlled reduction for applications of inkjet-printed electronics. *Nanotechnology, 19*(41), 415604. https://doi.org/10.1088/0957-4484/19/41/415604

Lehmonen, J.,..."Potential of foam-laid forming technology in paper applications," Nordic Pulp and Paper Res. J. 28 (2013) 392-298.

Lehtimäki, S., Li, M., Salomaa, J., Pörhönen, J., Kalanti, A., Tuukkanen, S., ... Lupo, D. (2014). Performance of printable supercapacitors in an RF energy harvesting circuit. *International Journal of Electrical Power and Energy Systems, 58,* 42–46. https://doi.org/10.1016/j.ijepes.2014.01.004

Lehtimäki, S., Pörhönen, J., Tuukkanen, S., Moilanen, P., Virtanen, J., & Lupo, D. (2014). Fabrication and characterization of solution-processed carbon nanotube supercapacitors. *MRS Proceedings, 1659,* mrsf13-1659-ss05-03. https://doi.org/10.1557/opl.2014.178

Lehtimäki, S., Tuukkanen, S., Pörhönen, J., Moilanen, P., Virtanen, J., Honkanen, M., & Lupo, D. (2014). Low-cost, solution processable carbon nanotube supercapacitors and their characterization. *Applied Physics A: Materials Science and Processing, 117*(3), 1329–1334. https://doi.org/10.1007/s00339-014-8547-4

Li, R. Z., Hu, A., Zhang, T., & Oakes, K. D. (2014). Direct writing on paper of foldable capacitive touch pads with silver nanowire inks. *ACS Applied Materials and Interfaces, 6*(23), 21721–21729. https://doi.org/10.1021/am506987w

Li, S., Xu, L. Da, & Zhao, S. (2015). The internet of things: a survey. *Information Systems Frontiers, 17*(2), 243–259. https://doi.org/10.1007/s10796-014-9492-7

Liimatainen, H., Ezekiel, N., Sliz, R., Ohenoja, K., Berglund, L., & Hormi, O. (2013). High-Strength Nanocellulose – Talc Hybrid Barrier Films.

Liu, J., Chinga-Carrasco, G., Cheng, F., Xu, W., Willf??r, S., Syverud, K., & Xu, C. (2016). Hemicellulose-reinforced nanocellulose hydrogels for wound healing application. *Cellulose, 23*(5), 3129–3143. https://doi.org/10.1007/s10570-016-1038-3

Macdonald, C. (2015). More filler, less fibre: Fibre-based additives and new methods of

introducing additives to the sheet were the subject of much discussion at PaperCon 2015. *Pulp and Paper Canada, 116*(5), 15–17.

Madakam, S., Ramaswamy, R., & Tripathi, S. (2015). Internet of Things (IoT): A Literature Review. *Journal of Computer and Communications, 3*(3), 164–173. https://doi.org/10.4236/jcc.2015.35021

Magdassi, S., Grouchko, M., Berezin, O., & Kamyshny, A. (2010). Triggering the sintering of silver nanoparticles at room temperature. *ACS Nano, 4*(4), 1943–1948. https://doi.org/10.1021/nn901868t

Magdassi, S., Grouchko, M., & Kamyshny, A. (2010). Copper nanoparticles for printed electronics: Routes towards achieving oxidation stability. *Materials, 3*(9), 4626–4638. https://doi.org/10.3390/ma3094626

Markstedt, K., Mantas, A., Tournier, I., Martínez Ávila, H., Hägg, D., & Gatenholm, P. (2015). 3D bioprinting human chondrocytes with nanocellulose-alginate bioink for cartilage tissue engineering applications. *Biomacromolecules, 16*(5), 1489–1496. https://doi.org/10.1021/acs.biomac.5b00188

Martin, C., & Jean, B. (2014). Nanocellulose / polymer multilayered thin films : tunable architectures towards tailored physical properties. *Nordic Pulp & Paper Research Journal, 29*(1), 19–30. https://doi.org/10.3183/NPPRJ-2014-29-01-p019-030

Mazzeo, A. D., Kalb, W. B., Chan, L., Killian, M. G., Bloch, J. F., Mazzeo, B. A., & Whitesides, G. M. (2012). Paper-based, capacitive touch pads. *Advanced Materials, 24*(21), 2850–2856. https://doi.org/10.1002/adma.201200137

Molesa, S. E. (2006). Ultra-Low-Cost Printed Electronics. *Spring,* (UCB/EECS-2006-55), 43. Retrieved from http://www.eecs.berkeley.edu/Pubs/TechRpts/2006/EECS-2006-55.html

Moon, R. J., Martini, A., Nairn, J., Simonsen, J., & Youngblood, J. (2011a). *Cellulose nanomaterials review: structure, properties and nanocomposites*. *Chem. Soc. Rev. Chem. Soc. Rev* (Vol. 40). https://doi.org/10.1039/c0cs00108b

Moon, R. J., Martini, A., Nairn, J., Simonsen, J., & Youngblood, J. (2011b). Cellulose nanomaterials review: structure, properties and nanocomposites. *Chemical Society Reviews, 40*(7), 3941–3994. https://doi.org/10.1039/C0CS00108B

Mäkelä, T., Kainlauri, M., Willberg-Keyriläinen, P., Tammelin, T., & Forsström, U. (2016). Fabrication of micropillars on nanocellulose films using a roll-to-roll nanoimprinting method. *Microelectronic Engineering, 163,* 1–6. https://doi.org/10.1016/j.mee.2016.05.023

Nair, S. S., Zhu, J., Deng, Y., & Ragauskas, A. J. (2014). High performance green barriers based on nanocellulose. *Sustainable Chemical Processes, 2*(1), 1–7. https://doi.org/10.1186/s40508-014-0023-0

Nakagaito, A. N., & Yano, H. (2004). The effect of morphological changes from pulp fiber towards nano-scale fibrillated cellulose on the mechanical properties of high-strength plant fiber based composites. *Applied Physics A: Materials Science and Processing, 78*(4), 547–552. https://doi.org/10.1007/s00339-003-2453-5

Nakagaito, A. N., & Yano, H. (2005). Novel high-strength biocomposites based on microfibrillated cellulose having nano-order-unit web-like network structure. *Applied Physics A: Materials Science and Processing, 80*(1), 155–159. https://doi.org/10.1007/s00339-003-2225-2

Nge, T. T., Nogi, M., & Suganuma, K. (2013). Electrical functionality of inkjet-printed

silver nanoparticle conductive tracks on nanostructured paper compared with those on plastic substrates. *Journal of Materials Chemistry C, 1*(34), 5235. https://doi.org/10.1039/c3tc31220h

Nisha, M., Anusha, S., Antony, A., Manoj, R., & Jayaraj, M. K. (2005). Effect of substrate temperature on the growth of ITO thin films. *Applied Surface Science, 252*(5), 1430–1435. https://doi.org/10.1016/j.apsusc.2005.02.115

Njie, D. (2012). Global Initiative on Food losses and Waste Reduction. *Food And Agriculture Organization of the United Nations*.

Nogi, M., Iwamoto, S., Nakagaito, A. N., & Yano, H. (2009). Optically Transparent Nanofiber Paper. *Advanced Materials, 21*(16), 1595–1598. https://doi.org/10.1002/adma.200803174

Peng, B., & Chan, P. K. L. (2014). Flexible organic transistors on standard printing paper and memory properties induced by floated gate electrode. *Organic Electronics: Physics, Materials, Applications, 15*(1), 203–210. https://doi.org/10.1016/j.orgel.2013.11.006

Peng, Y., Gardner, D. J., & Han, Y. (2012). Drying cellulose nanofibrils: In search of a suitable method. *Cellulose, 19*(1), 91–102. https://doi.org/10.1007/s10570-011-9630-z

Peng, Y., Gardner, D. J., Han, Y., Cai, Z., & Tshabalala, M. A. (2013). Influence of drying method on the surface energy of cellulose nanofibrils determined by inverse gas chromatography. *Journal of Colloid and Interface Science, 405,* 85–95. https://doi.org/10.1016/j.jcis.2013.05.033

Persano, L., Camposeo, A., & Pisignano, D. (2015). Active polymer nanofibers for photonics, electronics, energy generation and micromechanics. *Progress in Polymer Science, 43,* 48–95. https://doi.org/10.1016/j.progpolymsci.2014.10.001

Pettersson, F., Adekanye, D., & Österbacka, R. (2015). Stability of environmentally friendly paper electronic devices. *Physica Status Solidi (A) Applications and Materials Science, 212*(12), 2696–2701. https://doi.org/10.1002/pssa.201532876

Pettersson, F., Keskinen, J., Remonen, T., Von Hertzen, L., Jansson, E., Tappura, K., ... Österbacka, R. (2014). Printed environmentally friendly supercapacitors with ionic liquid electrolytes on paper. *Journal of Power Sources, 271,* 298–304. https://doi.org/10.1016/j.jpowsour.2014.08.020

Pettersson, F., Osterbacka, R., Koskela, J., Kilpela, A., Remonen, T., Zhang, Y., ... Peltonen, J. (2014). Ion-modulated transistors on paper using phase-separated semiconductor/insulator blends. *Mrs Communications, 4*(2), 51–55. https://doi.org/10.1557/mrc.2014.10

Pettersson, F., Remonen, T., Adekanye, D., Zhang, Y., Wilén, C. E., & Österbacka, R. (2015). Environmentally friendly transistors and circuits on paper. *ChemPhysChem, 16*(6), 1286–1294. https://doi.org/10.1002/cphc.201402701

Pierre, A., Sadeghi, M., Payne, M. M., Facchetti, A., Anthony, J. E., & Arias, A. C. (2014). All-printed flexible organic transistors enabled by surface tension-guided blade coating. *Advanced Materials, 26*(32), 5722–5727. https://doi.org/10.1002/adma.201401520

Pracella, M., Haque, M. M., Puglia, D., & Alvarez, V. (2012). Preparation and characterization of PLA nanocomposites with nanocellulose filled PVAC. In *ECCM 2012 - Composites at Venice, Proceedings of the 15th European Conference on*

Composite Materials.

Pääkko, M., Ankerfors, M., Kosonen, H., Nykänen, A., Ahola, S., Österberg, M., … Lindström, T. (2007). Enzymatic hydrolysis combined with mechanical shearing and high-pressure homogenization for nanoscale cellulose fibrils and strong gels. *Biomacromolecules, 8*(6), 1934–1941. https://doi.org/10.1021/bm061215p

Qing, Y., Sabo, R., Wu, Y., Zhu, J. Y., & Cai, Z. (2015). Self-assembled optically transparent cellulose nanofibril films: effect of nanofibril morphology and drying procedure. *Cellulose, 22*(2), 1091–1102. https://doi.org/10.1007/s10570-015-0563-9

Radousky, H. B., & Liang, H. (2012). Energy harvesting: an integrated view of materials, devices and applications. *Nanotechnology, 23*(50), 502001. https://doi.org/10.1088/0957-4484/23/50/502001

Rantanen, J., Dimic-Misic, K., Kuusisto, J., & Maloney, T. C. (2015). The effect of micro and nanofibrillated cellulose water uptake on high filler content composite paper properties and furnish dewatering. *Cellulose, 22*(6), 4003–4015. https://doi.org/10.1007/s10570-015-0777-x

Rantanen, J., & Maloney, T. C. (2013). Press dewatering and nip rewetting of paper containing nano- and microfibril cellulose. *Nordic Pulp & Paper Research Journal, 28*(4), 582–587.

Rees, A., Powell, L. C., Chinga-Carrasco, G., Gethin, D. T., Syverud, K., Hill, K. E., & Thomas, D. W. (2015). 3D Bioprinting of Carboxymethylated-Periodate Oxidized Nanocellulose Constructs for Wound Dressing Applications. *BioMed Research International, 2015*(JANUARY 2014), 1–7. https://doi.org/10.1155/2015/925757

Reuter, K., Kempa, H., Brandt, N., Bartzsch, M., & Huebler, A. C. (2007). Influence of process parameters on the electrical properties of offset printed conductive polymer layers. *Progress in Organic Coatings, 58*(4), 312–315. https://doi.org/10.1016/j.porgcoat.2007.01.004

Rida, A., Yang, L., Vyas, R., & Tentzeris, M. M. (2009). Conductive inkjet-printed antennas on flexible low-cost paper-based substrates for RFID and WSN applications. *IEEE Antennas and Propagation Magazine*. https://doi.org/10.1109/MAP.2009.5251188

Rogers, J. a. (2010). Electronics: A diverse printed future. *Nature, 468*(7321), 177–178. https://doi.org/10.1038/468177a

Rånby, B. G. (1951). The Colloidal Properties of Cellulose Micelles. *Discuss. Faraday Soc., 11*(111), 158–164.

Saito, T., Nishiyama, Y., Putaux, J. L., Vignon, M., & Isogai, A. (2006). Homogeneous suspensions of individualized microfibrils from TEMPO-catalyzed oxidation of native cellulose. *Biomacromolecules, 7*(6), 1687–1691. https://doi.org/10.1021/bm060154s

Saito, T., Okita, Y., Nge, T. T., Sugiyama, J., & Isogai, A. (2006). TEMPO-mediated oxidation of native cellulose: Microscopic analysis of fibrous fractions in the oxidized products. *Carbohydrate Polymers, 65*(4), 435–440. https://doi.org/10.1016/j.carbpol.2006.01.034

Sanchez-Romaguera, V., Wünscher, S., Turki, B. M., Abbel, R., Barbosa, S., Tate, D. J., … Yeates, S. G. (2015). Inkjet printed paper based frequency selective surfaces and skin mounted RFID tags: the interrelation between silver nanoparticle ink, paper substrate and low temperature sintering technique. *J. Mater. Chem. C, 3*(9), 2132–

2140. https://doi.org/10.1039/C4TC02693D

Sehaqui, H., Zhou, Q., Ikkala, O., & Berglund, L. A. (2011). Strong and tough cellulose nanopaper with high specific surface area and porosity. *Biomacromolecules, 12*(10), 3638–3644. https://doi.org/10.1021/bm2008907

Setti, L., Piana, C., Bonazzi, S., Ballarin, B., Frascaro, D., Fraleoni-Morgera, a, & Giuliani, S. (2004). Thermal inkjet technology for the microdeposition of biological molecules as a viable route for the realization of biosensors. *Analytical Letters, 37*(8), 1559–1570. https://doi.org/Doi 10.1081/Al-120037587

Shi, S., Xu, C., Yang, C., Li, J., Du, H., Li, B., & Kang, F. (2013). Flexible supercapacitors. *Particuology*. https://doi.org/10.1016/j.partic.2012.12.004

Shimizu, M., Saito, T., Fukuzumi, H., & Isogai, A. (2014). Hydrophobic, ductile, and transparent nanocellulose films with quaternary alkylammonium carboxylates on nanofibril surfaces. *Biomacromolecules, 15*(11), 4320–4325. https://doi.org/10.1021/bm501329v

Siro, I., & Plackett, D. (2010). Microfibrillated cellulose and new nanocomposite materials: A review. *Cellulose, 17*(3), 459–494. https://doi.org/10.1007/s10570-010-9405-y

Subramanian, R., Fordsmand, H., & Paulapuro, H. (2007). Precipitated calcium carbonate (PCC) - Cellulose composite fillers; effect of PCC particle structure on the production and properties of uncoated fine paper. *BioResources, 2*(1), 91–105.

Subramanian, V., Chang, P. C., Huang, D., Lee, J. B., Molesa, S. E., Redinger, D. R., & Volkman, S. K. (2006). All-printed RFID tags: Materials, devices and circuit implications. In *Proceedings of the IEEE International Conference on VLSI Design* (Vol. 2006, pp. 709–714). https://doi.org/10.1109/VLSID.2006.34

Subramaniyan, A. K., & Sun, C. T. (2006). Enhancing compressive strength of unidirectional polymeric composites using nanoclay. *Composites Part A: Applied Science and Manufacturing, 37*(12), 2257–2268. https://doi.org/10.1016/j.compositesa.2005.12.027

Syverud, K., & Stenius, P. (2009). Strength and barrier properties of MFC films. *Cellulose, 16*(1), 75–85. https://doi.org/10.1007/s10570-008-9244-2

Syverud, K., Xhanari, K., Chinga-Carrasco, G., Yu, Y., & Stenius, P. (2011). Films made of cellulose nanofibrils: Surface modification by adsorption of a cationic surfactant and characterization by computer-assisted electron microscopy. *Journal of Nanoparticle Research, 13*(2), 773–782. https://doi.org/10.1007/s11051-010-0077-1

Taipale, T., Österberg, M., Nykänen, A., Ruokolainen, J., & Laine, J. (2010). Effect of microfibrillated cellulose and fines on the drainage of kraft pulp suspension and paper strength. *Cellulose, 17*(5), 1005–1020. https://doi.org/10.1007/s10570-010-9431-9

Tobjörk, D. (2012). *Printed low-voltage organic transistors on plastics and paper*. *Functional Materials*. Retrieved from http://doria32-kk.lib.helsinki.fi/handle/10024/76672

Tobjörk, D., Aarnio, H., Pulkkinen, P., Bollström, R., Määttänen, A., Ihalainen, P., … Österbacka, R. (2012). IR-sintering of ink-jet printed metal-nanoparticles on paper. *Thin Solid Films, 520*(7), 2949–2955. https://doi.org/10.1016/j.tsf.2011.10.017

Tobjörk, D., & Österbacka, R. (2011). Paper electronics. *Advanced Materials*. https://doi.org/10.1002/adma.201004692

Torvinen, K., Kouko, J., Passoja, S., Keränen, J. T., & Hellén, E. (n.d.). Cellulose micro- and nanofibrils as a binding material for high filler content papers.

Trifol, J., Plackett, D., Sillard, C., Szabo, P., Bras, J., & Daugaard, A. E. (2016). Hybrid poly(lactic acid)/nanocellulose/nanoclay composites with synergistically enhanced barrier properties and improved thermomechanical resistance. *Polymer International, 65*(8), 988–995. https://doi.org/10.1002/pi.5154

Trnovec, B., Stanel, M., Hahn, U., Hübler, A. C., Kempa, H., Sangl, R., & Forster, M. (2009). Coated Paper for Printed Electronics. *Professional Papermaking, 1*(1), 48–51. https://doi.org/10.1111/j.1574-6941.2011.01201.x

Tuukkanen, S., Lehtimäki, S., Jahangir, F., Eskelinen, A. P., Lupo, D., & Franssila, S. (2014). Printable and disposable supercapacitor from nanocellulose and carbon nanotubes. In *Proceedings of the 5th Electronics System-Integration Technology Conference, ESTC 2014*. https://doi.org/10.1109/ESTC.2014.6962740

WALKER, K. (n.d.). Advances in hot pressing technology. *Tappi Journal, 73*(8), 99–101. Retrieved from http://cat.inist.fr/?aModele=afficheN&cpsidt=19268706

Wang, Q. Q., Zhu, J. Y., Gleisner, R., Kuster, T. A., Baxa, U., & McNeil, S. E. (2012). Morphological development of cellulose fibrils of a bleached eucalyptus pulp by mechanical fibrillation. *Cellulose, 19*(5), 1631–1643. https://doi.org/10.1007/s10570-012-9745-x

Wei, H., Rodriguez, K., Renneckar, S., & Vikesland, P. J. (2014). Environmental science and engineering applications of nanocellulose-based nanocomposites. *Environ. Sci.: Nano, 1*(4), 302–316. https://doi.org/10.1039/C4EN00059E

Wu, C. N., Saito, T., Fujisawa, S., Fukuzumi, H., & Isogai, A. (2012). Ultrastrong and high gas-barrier nanocellulose/clay-layered composites. *Biomacromolecules, 13*(6), 1927–1932. https://doi.org/10.1021/bm300465d

Wu, Z., Chen, Z., Du, X., Logan, J. M., Sippel, J., Nikolou, M., ... Rinzler, A. G. (2004). Transparent , Conductive Carbon Nanotube Films, *305*(August), 1273–1277.

Wünscher, S., Stumpf, S., Teichler, A., Pabst, O., Perelaer, J., Beckert, E., & Schubert, U. S. (2012). Localized atmospheric plasma sintering of inkjet printed silver nanoparticles. *Journal of Materials Chemistry,* 24569–24576. https://doi.org/10.1039/c2jm35586h

Wågberg, L., Decher, G., Norgren, M., Lindström, T., Ankerfors, M., & Axnäs, K. (2008). The buildrs of microfibrillated cellulose and cationic polyelectr-up of polyelectrolyte multilayeolytes. *Langmuir, 24*(3), 784–795. https://doi.org/10.1021/la702481v

Xie, F., Pollet, E., Halley, P. J., & Av??rous, L. (2013). Starch-based nano-biocomposites. *Progress in Polymer Science*. https://doi.org/10.1016/j.progpolymsci.2013.05.002

Xie, L., Mäntysalo, M., Cabezas, A. L., Feng, Y., Jonsson, F., & Zheng, L. R. (2012). Electrical performance and reliability evaluation of inkjet-printed Ag interconnections on paper substrates. *Materials Letters, 88,* 68–72. https://doi.org/10.1016/j.matlet.2012.08.030

Xu, T., Sathaye, J., & Kramer, K. (2013). Sustainability options in pulp and paper making: Costs of conserved energy and carbon reduction in the US. *Sustainable Cities and*

Society, 8, 56–62. https://doi.org/10.1016/j.scs.2013.01.006

Xu, X., Zhou, J., Jiang, L., Lubineau, G., Ng, T., Ooi, B. S., ... Zhu, J. Y. (2016). Highly transparent, low-haze, hybrid cellulose nanopaper as electrodes for flexible electronics. *Nanoscale, 8,* 12294–12306. https://doi.org/10.1039/C6NR02245F

Yan, C., Wang, J., Kang, W., Cui, M., Wang, X., Foo, C. Y., ... Lee, P. S. (2014). Highly stretchable piezoresistive graphene-nanocellulose nanopaper for strain sensors. *Advanced Materials, 26*(13), 2022–2027. https://doi.org/10.1002/adma.201304742

Yao, S., & Zhu, Y. (2014). Wearable multifunctional sensors using printed stretchable conductors made of silver nanowires. *Nanoscale, 6*(4), 2345. https://doi.org/10.1039/c3nr05496a

Yoo, J. J., Balakrishnan, K., Huang, J., Meunier, V., Sumpter, B. G., Srivastava, A., ... Ajayan, P. M. (2011). Ultrathin planar graphene supercapacitors. *Nano Letters, 11*(4), 1423–1427. https://doi.org/10.1021/nl200225j

Zhang, Y., Nypelö, T., Salas, C., Arboleda, J., Hoeger, I. C., & Rojas, O. J. (2013). Cellulose Nanofibrils. *Journal of Renewable Materials, 1*(3), 195–211. https://doi.org/10.7569/JRM.2013.634115

Zheng, Y., Li, S., Shi, W., & Yu, J. (2014). Spray-coated nanoscale conductive patterns based on in situ sintered silver nanoparticle inks. *Nanoscale Research Letters, 9,* 145. https://doi.org/10.1186/1556-276X-9-145

Zhou, Y., Fuentes-Hernandez, C., Khan, T. M., Liu, J.-C., Hsu, J., Shim, J. W., ... Kippelen, B. (2013). Recyclable organic solar cells on cellulose nanocrystal substrates. *Scientific Reports, 3,* 1536. https://doi.org/10.1038/srep01536

Zhu, H., Luo, W., Ciesielski, P. N., Fang, Z., Zhu, J. Y., Henriksson, G., ... Hu, L. (2016). Wood-Derived Materials for Green Electronics, Biological Devices, and Energy Applications. *Chemical Reviews*. https://doi.org/10.1021/acs.chemrev.6b00225

Zhu, H., Narakathu, B. B., Fang, Z., Tausif Aijazi, A., Joyce, M., Atashbar, M., & Hu, L. (2014). A gravure printed antenna on shape-stable transparent nanopaper. *Nanoscale, 6*(15), 9110. https://doi.org/10.1039/C4NR02036G

Zimmermann, T., Pöhler, E., & Geiger, T. (2004). Cellulose fibrils for polymer reinforcement. *Advanced Engineering Materials, 6*(9), 754–761. https://doi.org/10.1002/adem.200400097

Öhlund, T., Örtegren, J., Forsberg, S., & Nilsson, H. E. (2012). Paper surfaces for metal nanoparticle inkjet printing. *Applied Surface Science, 259,* 731–739. https://doi.org/10.1016/j.apsusc.2012.07.112

Österberg, M., Vartiainen, J., Lucenius, J., Hippi, U., Seppälä, J., Serimaa, R., & Laine, J. (2013). A fast method to produce strong NFC films as a platform for barrier and functional materials. *ACS Applied Materials and Interfaces, 5*(11), 4640–4647. https://doi.org/10.1021/am401046x

PAPER I

Smooth and flexible filler-nanocellulose composite structure for printed electronics applications

Cellulose 19, Issue 3, 821–829.

PAPER II

Filler-nanocellulose substrate for printed electronics: experiments and model approach to structure and conductivity

Cellulose 20, Issue 3, 1413–1424.

PAPER III

Drying of Pigment-Cellulose Nanofibril Substrates

Materials 7, 6893–6907.

Materials **2014**, *7*, 6893-6907; doi:10.3390/ma7106893

OPEN ACCESS

materials

ISSN 1996-1944

www.mdpi.com/journal/materials

Article

Drying of Pigment-Cellulose Nanofibril Substrates

Oleg Timofeev, Katariina Torvinen, Jenni Sievänen, Timo Kaljunen, Jarmo Kouko and Jukka A. Ketoja *

VTT Technical Research Centre of Finland, P. O. Box 1000, FI-02044 VTT, Finland;
E-Mails: oleg.timofeev@vtt.fi (O.T.); katariina.torvinen@vtt.fi (K.T.); jenni.sievanen@vtt.fi (J.S.); timo.kaljunen@vtt.fi (T.K.); jarmo.kouko@vtt.fi (J.K.)

* Author to whom correspondence should be addressed; E-Mail: jukka.ketoja@vtt.fi; Tel.: +358-40-547-6146; Fax: +358-20-722-7604.

External Editor: Carlos Pascoal Neto

Received: 30 July 2014; in revised form: 5 September 2014 / Accepted: 23 September 2014 / Published: 1 October 2014

Abstract: A new substrate containing cellulose nanofibrils and inorganic pigment particles has been developed for printed electronics applications. The studied composite structure contains 80% fillers and is mechanically stable and flexible. Before drying, the solids content can be as low as 20% due to the high water binding capacity of the cellulose nanofibrils. We have studied several drying methods and their effects on the substrate properties. The aim is to achieve a tight, smooth surface keeping the drying efficiency simultaneously at a high level. The methods studied include: (1) drying on a hot metal surface; (2) air impingement drying; and (3) hot pressing. Somewhat surprisingly, drying rates measured for the pigment-cellulose nanofibril substrates were quite similar to those for the reference board sheets. Very high dewatering rates were observed for the hot pressing at high moisture contents. The drying method had significant effects on the final substrate properties, especially on short-range surface smoothness. The best smoothness was obtained with a combination of impingement and contact drying. The mechanical properties of the sheets were also affected by the drying method and associated temperature.

Keywords: cellulose nanofibril; substrate; drying; evaporation; surface; material property

---

1. Introduction

The growth of the printed electronics market is based on new low-cost materials and products. Recently, novel bio-degradable cellulose nanocomposite substrate materials have been introduced that compete well in price and material properties against oil-based plastic substrates [1,2]. Using cellulose nanofibrils (CNF) as the strength additive in the inorganic composite structure, it is possible to surpass the properties of traditional paper substrates. It has been shown that this new pigment-cellulose nanofibril (PCN) substrate can contain up to 90% of inorganic fillers and, yet, remain mechanically stable and flexible [1,3].

The composite structure includes a large proportion (approximately 20%) of CNF, which makes dewatering after structure forming very difficult, as CNF has a high water retention capacity [4]. During the development of the substrate, the drying was done in an oven at 70–80 °C. The drying process was very slow. In this work, we look for an optimal way of removing the water. Here, one should take into account both the drying efficiency and the effect of the drying method on the final product properties.

The drying of cellulose nanofibrils has been studied earlier using different methods, such as air drying, freeze drying, spray drying and supercritical drying [5,6]. Usually, the aim has been to preserve the morphology of the cellulose nanofibrils. Air drying of CNF suspensions forms a tightly packed material [6], and this drying method is often disregarded in applications where the nanostructure is essential. However, for the PCN substrate, tight packing of nanofibrils is beneficial in forming a smooth surface. On the other hand, a tight surface layer slows down the evaporation of water from inside the bulk material and may reduce drying efficiency. Thus, it is essential to determine this efficiency and material properties for drying methods that are close to air drying.

We study several available drying methods and their combinations that are in use in paper and board technology. In these industries, water from the web after the forming section is removed in the press section and the subsequent drying section. The amount of water removed by pressing is a function of applied pressure, nip width (dwell time) and water viscosity [7]. Mechanical dewatering is a much cheaper way to remove water than drying based on evaporation. After wet pressing, the typical solids content of wet web is 45%–55%.

The commonest drying methods for paper, board and cellulose are cylinder (contact) drying and air float and air impingement drying. Usually, a low steam pressure is used in cylinder dryers, and the drying rates are not very high: 10–25 kg/m^2/h [8,9]. Air impingement dryers can operate at high air temperature (300–500 °C) and air velocity (50–100 m/s). An evaporation rate of 100 kg/m^2/h is a common level for this type of dryer [10]. Another very effective method for removing moisture and improving mechanical properties is press drying. Press drying combines elements of pressing and hot surface drying. Condebelt drying represents one type of press drying, *i.e.*, drying under pressure and totally restrained [11]. Drying rates of 100–200 kg/m^2/h are possible, depending on the process parameters [12].

This investigation was concentrated on determining the final PCN substrate properties and the drying rates for contact drying, impingement drying and press drying at moderate temperatures. Despite the large amount of bound water, these conventional drying methods turned out to be quite effective also for the PCN structure. Properties of the PCN sheets after drying and calendering were measured. We found a relatively large variation in the measured surface and mechanical properties depending on the drying method.

2. Materials and Methods

2.1. Materials

PCN substrate was prepared with a mixture of kaolin as a filler and CNF as a binder. The CNF samples were made from Finnish once-dried bleached hardwood (birch, *Betula* L.) The fibril cellulose prepared at VTT was obtained after eight passes through a Masuko Sangyo (Supermasscolloider type MKZA10-15J, Masuko Sangyo Ltd., Kawaguchi, Saitama, Japan) grinder by using a decreasing gap width and increasing operating power. The rotation speed was set at 1500 rpm. The CNF amount was 20 mass% and the initial consistency (percentage of solid, filterable material in suspension) was 3.5%.

The kaolin pigment used was Intramax 60 from Imerys. The kaolin amount was 80 mass%.

PCN sheets were cut from the webs manufactured on a VTT pilot machine, SutCo (Coatema Coating Machinery GmbH, Dormagen, Germany). The web was formed by the application of a 7% wet PCN mixture on a thin plastic PET film by the solvent casting method. The film thickness was 23 μm. In order to improve the release properties, the film was given the N-Ar plasma treatment before forming the structure. After the A4-size sheets were cut, they were lightly pressed using a metal plate and filter paper and sealed in carrier plastic bags at room temperature. The grammage of the final wet PCN sheets varied from 150 to 220 g/m^2, and there was a similar variation in the initial solids content in the range of 20%–35%. This level of solids content after vacuum filtering has been found earlier in dewatering studies of similar PCN furnishes [4].

Reference board samples were cut from the never dried web made on a Metso pilot machine with a grammage of 106 g/m^2 and initial solids content close to 50%.

2.2. Experimental Procedure and Characterization

In all drying and pressing experiments, the thin PET film used in the pilot production was kept under the wet sheets, so that drying or dewatering was always one-sided, *i.e.*, through the top side of the sheet. In order to prevent thermal degradation of the nanofibrils [5], all drying tests were performed at moderate temperatures.

The moisture ratio MR_i of the sample was determined by using the initial mass, measured before each drying step m_i, and the final one m_d, measured after keeping the sample in the oven for 2 h at an air temperature of 105 °C after the drying test was complete:

$$MR_i = \frac{m_i - m_d}{m_d} \left[\mathrm{kg/kg}\right] \quad (1)$$

After drying, the PCN sheets were conditioned under a standard climate (25 °C, 50% relative humidity) before calendering and physical testing. Hot nip calendering is a standard operation in paper making by which the surface smoothness can be increased further. The calendering was done with approximately 20 MPa pressure and 150 °C temperature.

Standard characterization methods were used, except for the surface roughness measurement and mechanical testing of the samples. The grammage of the samples was determined according to [13]. The thickness was determined according to [14], and the density was determined based on the measured values of grammage and thickness.

Surface roughness was measured using an Altisurf 500 profilometer (Cotec, Évian, France) with a sampling interval of 1 μm × 1 μm and a total measured area of 1 mm × 1 mm. The results were filtered with a Gaussian 0.25-mm sized screen. The surface roughness was defined as:

$$Ra = \frac{1}{NM}\sum_{x=0}^{N-1}\sum_{y=0}^{M-1}\left|z_{x,y}\right| \quad (2)$$

where $z_{x,y}$ was the distance of the surface point to the mean surface height. The measurement was repeated nine times for each sample.

The mechanical properties of the PCN sheets were measured with the so-called C-Impact tensile tester with a sample length of 50 mm and a width of 15 mm [15]. The elongation speed was 10 mm/s (the strain rate was 20%/s). The frequency of data recording was 2 kHz. From the measured stress-strain curve, the strength and breaking strain were determined as the values corresponding to the maximal stress. The elastic modulus was obtained as the maximal slope of the tangent to the stress-strain curve. The test was repeated five times for each trial point.

2.3. Drying Methods

Drying was investigated for three methods and their combinations that are in use in paper and board technology: contact drying, impingement drying and press drying. All of these methods are able to form a compact surface for the PCN structure.

The contact dryer is shown schematically in Figure 1a. It includes a curved metal plate, heated by electrical coins from the bottom side, and a tensioned dryer fabric. Experiments were carried out at a hot plate temperature of 50 and 80 °C and a constant fabric tension of 2 kg/cm. A commercial dryer fabric made from flat yarns and with a permeability of 1600 $m^3/m^2/h$ was used. Each paper sample with thin plastic film was weighed, positioned on top of the hot plate and covered with the fabric. The timing of the drying trial began at this point and continued until the fabric was lifted up and the sheet removed from the hot plate for the second weighing.

The air impingement dryer is shown in Figure 1b. The dryer consists of an air impingement hood, a vacuum box and the air heating system. The air impingement hood has impingement geometry matching commercial dryers, with similar open area, nozzle distances, nozzle diameter and distance to the wet material. Every wet sheet on the thin plastic film was placed on the vacuum box and moved under the impingement hood. Under the hood, the vacuum box with the sample was moving back and forth with a special driving mechanism to provide uniform drying conditions.

In hot pressing experiments, a hydraulic laboratory sheet press was used with an additional hot bottom plate (Figure 1c). Tests were carried out with two pressures: 60 and 420 kPa. A steel plate with a size of 160 × 160 mm^2 and a thickness of 25 mm was used as a bottom press plate, which was pre-heated before each test. The temperature of the plate was 80 or 110 °C.

Figure 1. The main components of the studied drying methods: (**a**) contact dryer; (**b**) air impingement dryer; (**c**) hydraulic press. PCN: pigment-cellulose nanofiber.

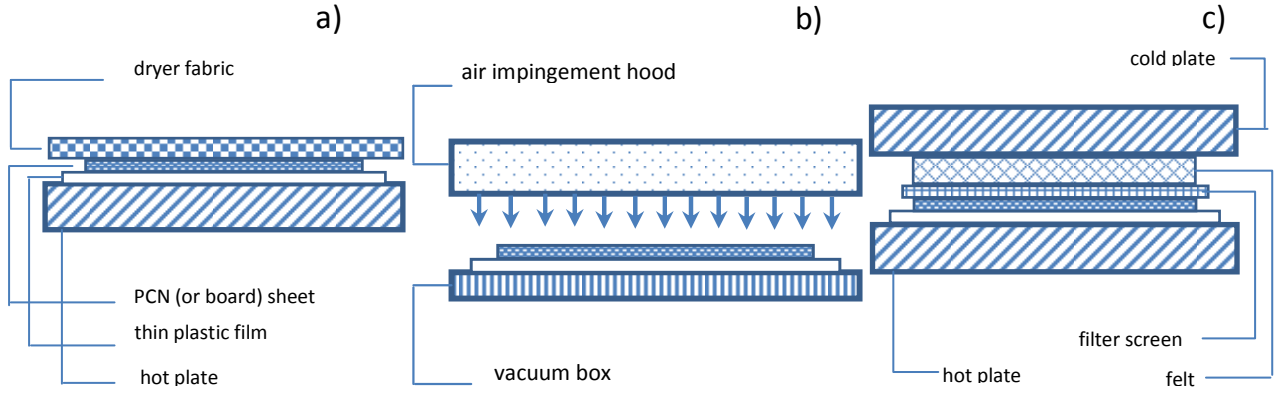

3. Drying Kinetics

The initial moisture ratio of the PCN sheets before drying is approximately 2–3-times higher than that of the board samples, in the range of 2.5–3.8 kg/kg. Assuming all of the water to be bound to the CNF with 20 mass%, this corresponds to 13–19 kg water/kg CNF. This level agrees well with the water retention values measured earlier for wet CNF [4]. Moreover, the grammage of the PCN sheets is also almost 1.5–2-times higher. Both factors increase the drying time required for complete drying of the PCN sheets in comparison with board samples. This is seen in the drying curves of the contact drying tests shown in Figure 2 for the PCN substrate and board samples. For example, at a hot surface temperature of 80 °C, the total drying time of the PCN sheets is about 220 s, and for the board samples, it is less than 90 s.

Figure 2. Drying kinetics for the contact drying of (**a**) PCN and (**b**) board sheets at two different temperatures: 50 °C (blue) and 80 °C (red).

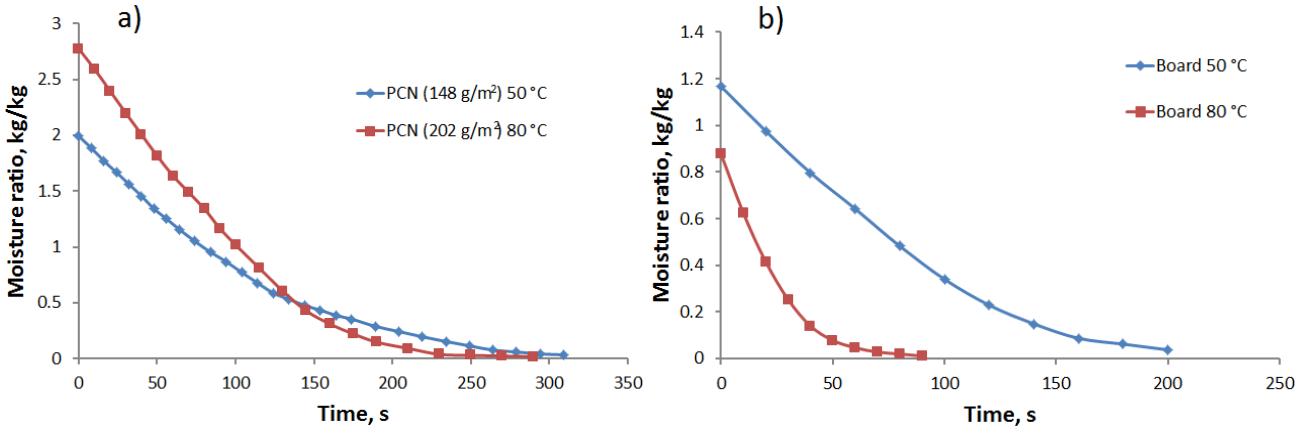

All drying curves in Figure 2 indicate two phases: the constant rate phase and the falling rate phase. In the constant rate phase, moisture removal is dominated by the surface evaporation rate from the wet sheets containing significant amounts of free water [16,17]. In the falling rate phase, the drying rate decays with time, as residual moisture requires more time to be removed from the interior of the sheet. The moisture content at which the constant rate phase ends is for the PCN sheets close to 1.0 kg/kg,

corresponding to 5.0 kg water/kg CNF, if we assume all water to be bound to CNF. This can be compared to the transition to the falling rate phase in the range of 0.5–0.6 kg/kg for the board sheets, which is a typical maximal bound water content in mechanical wood fibers [16,17]. In other words, the bound water content in CNF can be an order of magnitude larger than in the board when the transition between different drying phases takes place. This huge difference would mean that internal moisture transport would limit the drying rate at much higher cellulose water content for the PCN substrates than it does for the board. In fact, the cellulose structures of the two types of samples are quite different. In the PCN sheets, CNF gel agglomerates during drying to micro-membranes/networks that bind filler particles together [1], as shown in Figure 3. The forming agglomerates within inter-particle pores can begin to limit the moisture transport at a relatively early drying stage. On the other hand, even dry membranes contain nano-scale pores that allow effective vapor diffusion. Therefore, the total drying time is reasonable compared to the board where the slow diffusion [18,19] in the fiber walls is the main cause for the decaying drying rate at low moisture ratios.

Figure 3. High resolution SEM images of the PCN sheet before calendering. The cellulose micro-"membranes" seen at a lower resolution between the kaolin pigment particles (**a**) are actually porous fibrillar networks in the nanoscale (**b**).

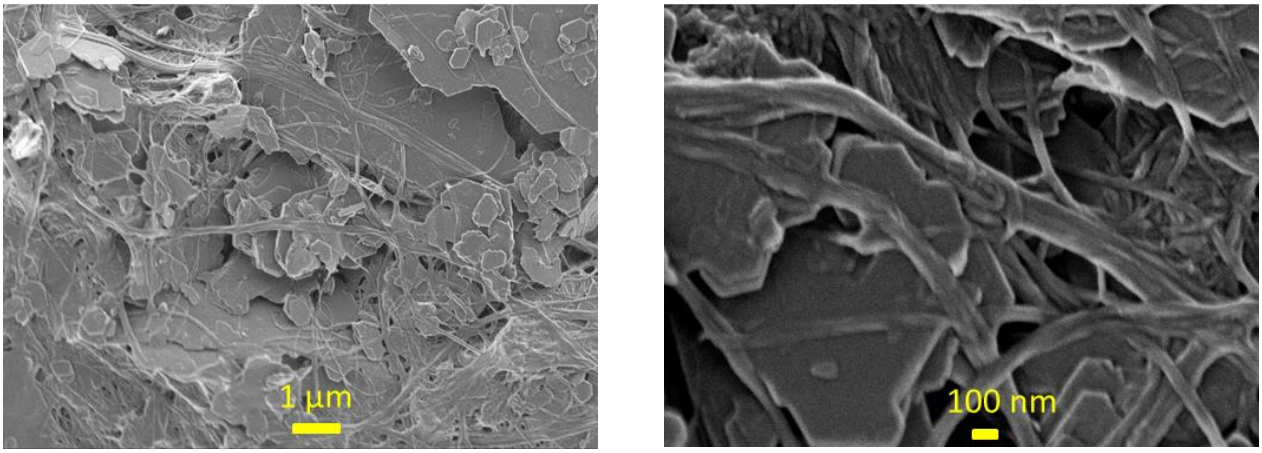

(**a**) (**b**)

The above reasoning can be justified by comparing the diffusion constants in various parts of the structure. The vapor diffusion constant in the pore space of normal board is of the order of 5×10^{-7} m^2/s [19]. This can be compared with the moisture diffusion constant in the fiber wall. This constant has a maximum level of 2×10^{-10} m^2/s for fully water-saturated fiber wall, and the diffusion constant decays exponentially with the increasing solids content as inter-fiber pores close up [18,19]. The exponentially decaying diffusion rate explains the strong falling-rate phase observed in Figure 2b for the board. On the other hand, the decay is not as strong for the PCN structure, because of the significant vapor diffusion in the remaining nano-scale pores of the CNF networks. Experimental studies [20] have shown that this diffusion is not significantly slower than the one observed in normal wood fiber networks.

For air impingement drying, the development of the moisture ratio is shown in Figure 4 for three combinations of air jet velocity and air temperature for both types of samples. The transition from the constant drying rate phase to the falling rate phase takes place at similar moisture ratio levels (1.0 kg/kg for the PCN sheets and 0.5–0.6 kg/kg for the board), as in the case with contact drying. On the other

hand, the difference in the total drying time between the PCN sheets and the board is slightly larger in this case than for the contact drying. This is partly explained by the high initial moisture content of the studied PCN sheets; see Figure 4a.

Figure 4. Drying curves for the air impingement drying for (**a**) PCN sheets and (**b**) the board at three different air speed and temperature conditions.

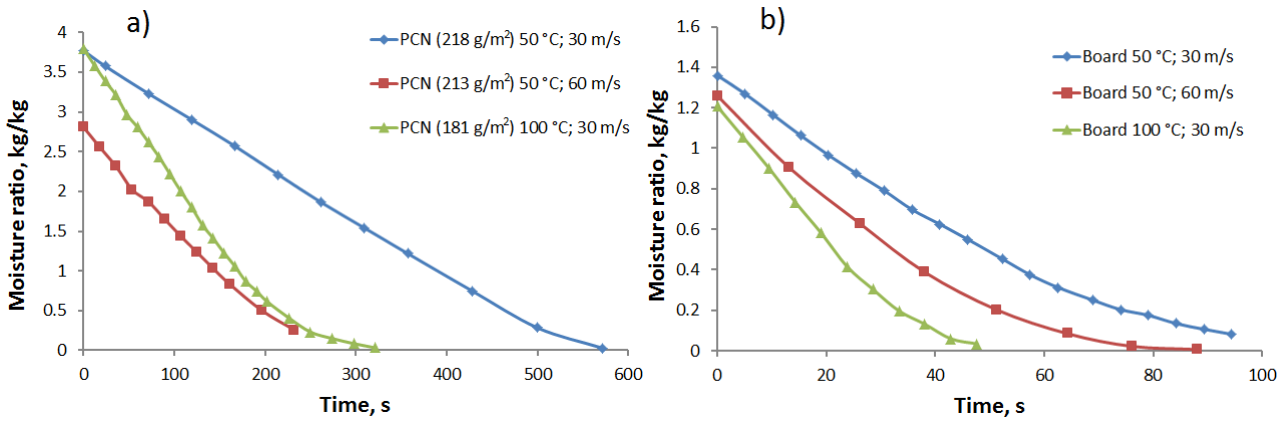

Figure 5 shows that there is actually no major difference in the initial drying rates for the two types of samples. The lowest and highest drying rates are observed for the contact drying method for both types of samples. The air impingement method leads to intermediate values in between the above two extremes. In general, drying rates measured for the PCN sheets and board samples are quite comparable at the same drying parameters. In the first drying phase, the drying rate is controlled by external drying conditions, and this rate depends less on material properties. The smooth surface of the PCN substrate helps in contact drying as compared to the board. On the other hand, air impingement appears to be more effective in removing free water from the pores of the board than from the denser PCN structure. The latter distinction is enhanced in the falling drying rate phases of Figure 4, where air speed affects the drying more for the PCN structure than what is observed for the board. Due to the high permeability of the board, air is able to penetrate into the board more easily than through the CNF gel of the PCN sheets.

Figure 5. Drying rates determined from the initial linear part of the drying curve for the air impingement and contact drying methods for both PCN sheets and board in varied drying conditions (temperature and air speed).

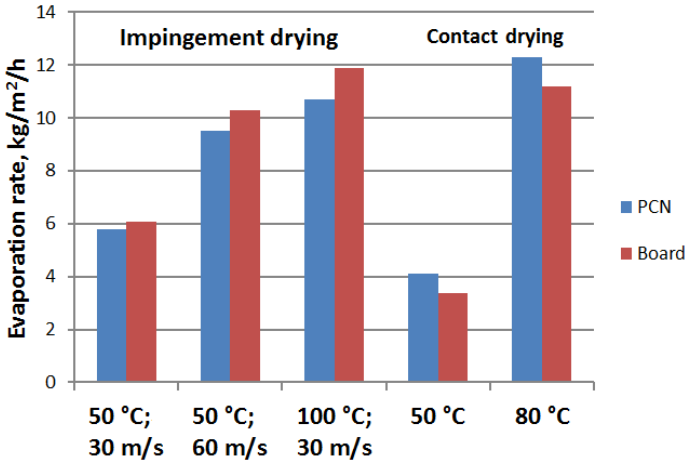

The hot press dewatering curves are shown in Figure 6. The effect of pressure and temperature on dewatering time is clearly seen. Dewatering curves can be divided into two phases. In the first phase, the dewatering rate is very high until a moisture ratio of 0.75–1.0 kg/kg is reached. In this phase, water is mainly squeezed out from the sheet under the applied pressure. In the second phase, the dewatering rate is much lower due to slower evaporation and diffusion processes.

Figure 6. Moisture ratio *vs.* time for PCN sheets in hot press dewatering for varied pressure and temperature.

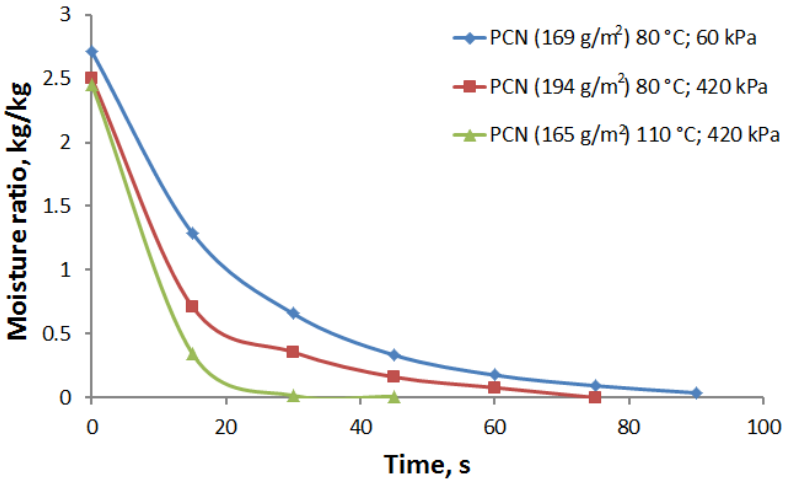

At a hot plate temperature of 80 °C, an increase in pressure from 60 to 420 kPa reduces the first-phase dewatering time to almost one half, *i.e.*, from 30 to 15 s when coming down from the initial moisture ratio to 0.75 kg/kg. Moreover, the dewatering rate can be increased further using a higher temperature due to the lower viscosity and surface tension of the water [7,21]. For example, if the temperature is increased from 20 to 90 °C, viscosity is reduced by a factor of three from 1.0 to 0.3 cP. The surface tension is also reduced, but not as much as the viscosity. The effect of these reductions is seen in Figure 6 at a plate temperature of 110 °C. If the moisture content of a PCN sheet is reduced from 2.5 kg/kg down to 1.0 kg/kg by hot pressing, the amount of water that needs to be evaporated during the second phase is reduced by 60%. This results in a dramatic reduction in energy consumption for drying.

In the second phase of the drying process, for moisture contents below 0.75–1.0 kg/kg, the drying can be significantly accelerated by a temperature increase from 80 to 110 °C. In this region, mere mechanical pressing does not help to remove water any longer. Residual moisture is removed more effectively by evaporation. Increasing the temperature of the moist sheet results in an exponential increase of the vapor pressure. In Figure 6, the temperature increase from 80 to 110 °C (at constant pressure 420 kPa) reduced the second-phase drying time by more than a factor of two. Figure 7 shows a comparison of the press dewatering rate and evaporation rates for the contact drying method. At hot pressing, the dewatering rate has an initial maximum value of 60 kg/m^2/h, which comes down almost linearly with decreasing moisture content. The evaporation rate in the contact drying is approximately 12 kg/m^2/h for moisture ratios higher than 0.75 kg/kg. Below a moisture ratio of 0.5 kg/kg, the evaporation rates for both drying methods develop in almost the same manner and also follow the drying rates measured for the board. Thus, the main advantage of the press drying is to remove a major part of the moisture as a liquid without evaporation and to correspondingly reduce the drying time and energy consumption for drying.

Moreover, mechanical pressing improves the contact heat transfer between the hot plate and the PCN substrate, which leads to faster evaporation in the beginning of the second-phase drying, as compared to contact drying (see Figure 7).

Figure 7. Comparison of the press dewatering rate (pressure 60 kPa, temperature 80 °C) with the evaporation rate in the normal contact drying (equal temperature) for the PCN sheets. The corresponding result for the contact drying of board is shown by the dots.

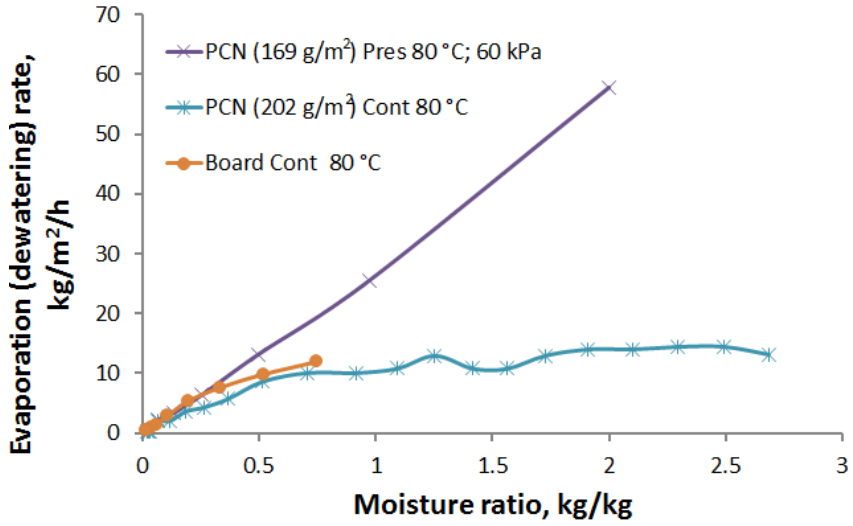

4. Effect of Drying on PCN Sheet Properties

The PCN substrate should meet certain quality requirements in order to be applied as a base for printed electronics. The main requirements concern the surface smoothness. The roughness level 0.3–0.4 μm (see Equation (2)) is sufficient for inkjet-printed conductors, screen-printed near-field communication RFID (radio-frequency identification) antennas and spin-coated thin transistors [22]. In addition, sufficient strength, flexibility and breaking strain of the substrate are required. We found significant effects from the drying process on these factors. The measured properties after calendering of the PCN sheets are shown in Table 1.

For contact and impingement drying, the sheet density before calendering decreased slightly with the drying rate, as shown in Figure 8. The longer drying time seems to lead to the greater shrinkage of the PCN sheet in the thickness direction.

The pressure in the hard nip calendering process is typically 40–80 MPa, *i.e.*, significantly higher than the pressure we used in the laboratory hot press. The calendering operation did not reduce the slight density variations of the samples observed before calendering. Moreover, there was no correlation between the densities before and after calendering for the varied drying methods. For example, press drying gave the highest density before calendering and the lowest density after calendering. This suggests that different drying methods led to deviations in the microscopic composite structure and, therefore, to different overall deformations during calendering.

Table 1. Measured properties of the PCN substrates after calendering.

Drying method	**Impingement**			**Contact**		**Impingement and contact**	**Press**			
Temperature (°C)	50	50	100	50	80	50 (Impingement), 80 (Contact)	80	80	110	110
Air speed (m/s)	30	60	30	–		30	–			
Pressure (kPa)				–			60	420	60	420
Thickness (µm)	178	148	144	127	145	116	148	168	101	154
Density (kg/m^3)	1,421	1,534	1,438	1,523	1,448	1,518	1,467	1,309	1,437	1,350
Roughness, top side (mm)	0.48	0.51	−	0.71	0.41	0.45	0.63	0.86	0.82	0.60
Roughness, bottom side (mm)	0.45	0.38	−	0.42	0.49	0.34	0.43	0.43	0.43	0.42
Tensile strength index (Nm/g)	13.4	16.6	16.0	12.5	15.8	15.8	12.4	14.3	17.5	15.6
Elastic modulus (GPa)	4.6	5.2	4.3	4.3	4.7	4.6	4.2	4.1	3.8	3.6
Breaking strain (%)	1.3	1.9	1.3	0.9	1.3	1.6	1.0	1.0	1.6	1.5

Figure 8. Sheet density before calendering is slightly affected by evaporation rate for contact and impingement drying.

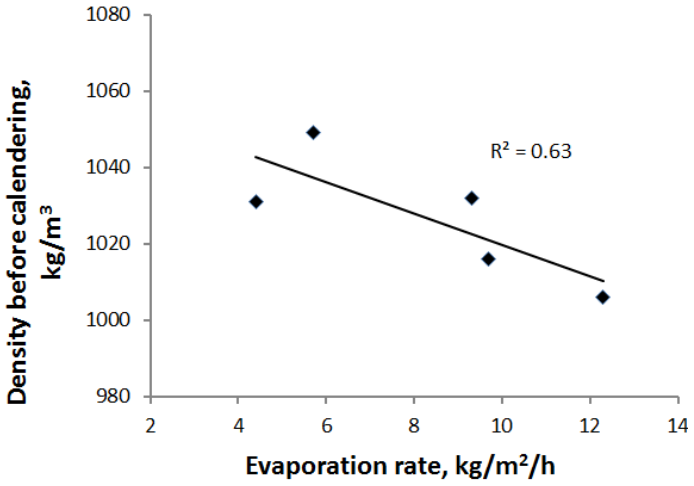

Quite surprisingly, press drying with a higher pressure level of 420 kPa led to a lower density after calendering than the lower pressure 60 kPa; see Table 1. The high pressure during press dewatering may prevent horizontal particle movement later during calendering, thus leading to reduced final density. On the other hand, the mechanical properties were dominated by pressing temperature rather than by final density. Higher tensile strength and breaking strain were observed with the higher pressing temperature of 110 °C, even though the elastic modulus was somewhat smaller in this case than at the lower pressing temperature of 80 °C.

There was a clear correlation between strength and breaking strain for all trial points, as shown in Figure 9. However, no such correlation was found between tensile strength and elastic modulus. The elastic modulus appeared to be affected by drying temperature, as indicated in Figure 10. At a high temperature, non-crystalline parts of the cellulose nanofibrils soften, and simultaneously, the drying stresses increase. These two factors may lead to significant structural deformations and permanent changes in mechanical behavior [17,23]. The way drying shrinkage is prevented may have an additional effect on the elastic modulus. Drying was most restricted for the press drying that also led to the smallest moduli. However, as mentioned earlier, temperature seemed to play a role for this method, as well.

Figure 9. Correlation between strength and breaking strain for the calendered sheets obtained with the various drying methods.

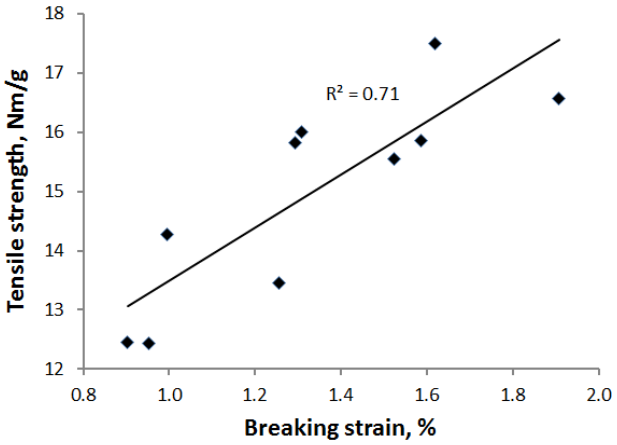

Figure 10. Elastic modulus of the calendered PCN sheets *vs.* drying temperature for all drying methods. For the combination of impingement and contact drying, the average temperature 65 °C (see Table 1) was used when plotting the figure.

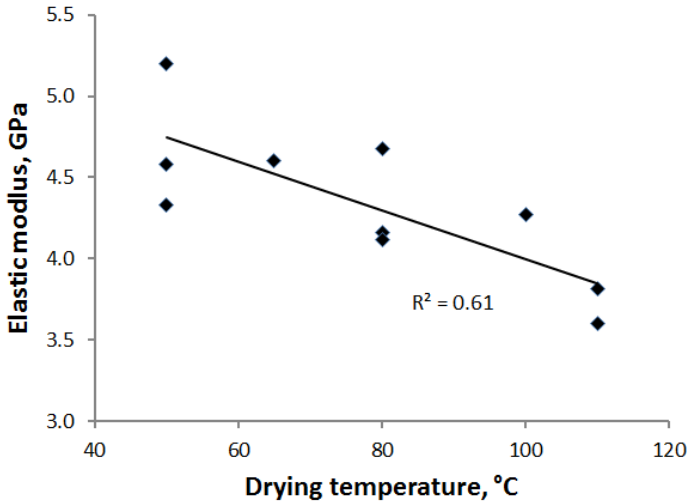

The smoothness of the bottom surface against the plastic sheet was generally higher than that of the top surface. The only exception to this rule was found for the higher temperature (80 °C) contact drying, for which the top "open" surface was slightly smoother than the bottom surface after calendering. Before calendering, the order was normal also for this trial point. The difference in the roughness of the two surfaces was particularly marked for all press drying points, further suggesting that this drying method "freezes" the structure, causing it to be less moldable in calendering. Moreover, even for the smoother bottom surface for the press drying, the roughness was greater than the best results for the other drying methods.

The lowest roughness value of 0.34 μm for the bottom surface was observed for the combination of the contact and impingement drying. In this case, impingement drying was first carried out until the moisture ratio became roughly 1.0 kg/kg, after which contact drying was applied to obtain the final solids content. However, the drying parameters were not optimized, so that even better smoothness could be possible. Earlier, in [2], the surface roughness of the substrates formed with a different laboratory-scale process was measured after oven drying and calendering. The surface roughness was measured for both "fine" and "coarse" cellulose nanofibril grades using the same pigment type as here. The values obtained after calendering were 0.51 μm (fine quality) and 0.60 μm (coarse quality). The lowest roughness values obtained here are thus clearly better than the above values.

In [2], the small-scale roughness and porosity were also simulated on a particle level by looking at the packed structure formed by the skeleton of pigment particles. Such simulations led to a roughness value of 0.67 μm for the profilometer spot size of 1 μm used in the roughness measurements (the same as in the present study). The predicted value of 0.67 μm for pure kaolin packing is reasonably close to the overall experimental range, 0.34–0.60 μm, for the kaolin-cellulose nanofibril composite. However, this comparison makes it clear that cellulose nanofibrils make the surface smoother in the scale of the profilometer spot size. This scale is similar to the length of the nanofibrils. For slightly larger scales, the variation in roughness is quite mild, even for pure pigment surfaces, as shown in Figure 11 of [2]. The short-range surface smoothening effect is strongly affected by the drying method, leading to the

above relatively large variation of the roughness values. The drying rate probably affects the size and density of the nanofibril clusters responsible for smoothing out the pigment surfaces and their edges.

5. Conclusions

In laboratory-scale experiments, it was shown that the PCN substrate can be dried using conventional drying methods, such as contact drying and air impingement drying methods. Despite the very large bound water content of the CNF gel, the estimated drying rates for the PCN substrate are comparable with the drying rates of typical board with the same external drying conditions. The CNF agglomerates seem to affect the moisture transport in an early drying stage, but for the low moisture ratios, nano-scale pores in the CNF membranes/networks speed up vapor diffusion, as compared to the moisture diffusion in the fiber walls within the board.

It was also demonstrated that, before drying, the water can be effectively removed from the PCN sheets by hot pressing. Removal of water mechanically in the hot press will dramatically reduce the energy consumption required for drying of an initially very wet PCN substrate.

The final properties of the PCN sheets after calendering could be significantly affected by the drying method. Unfortunately, hot pressing led to somewhat unconformable structures with poorer surface smoothness than with the other drying methods. The best smoothness of all of the drying methods was obtained with a combination of impingement and contact drying. Mere contact drying led to an almost equally smooth surface. The required smoothness level [22] for various applications, like inkjet-printed conductors, screen-printed near-field communication RFID antennas and spin-coated thin transistors, was achieved with both methods. By fine tuning the forming and drying processes (e.g., temperature, air speed), the substrate properties could be probably further optimized. In this development, one should take into account that the drying method and temperature affect the mechanical properties of the PCN sheets, in addition to the surface properties.

Author Contributions

Oleg Timofeev carried out the drying tests. Katariina Torvinen and Jenni Sievänen produced the PCN materials and prepared the SutCo pilot webs together with Timo Kaljunen. Jarmo Kouko was responsible for the mechanical testing. Jukka Ketoja contributed to the analysis and interpretation of the results.

Conflicts of Interest

The authors declare no conflict of interest.

References

1. Torvinen, K.; Sievänen, J.; Hjelt, T.; Hellén, E. Smooth and flexible filler-nanocellulose composite structure for printed electronics applications. *Cellulose* **2012**, *19*, 821–829.
2. Penttilä, A.; Sievänen, J.; Torvinen, K.; Ojanperä, K.; Ketoja, J.A. Filler-nanocellulose substrate for printed electronics: Experiments and model approach to structure and conductivity. *Cellulose* **2013**, *20*, 1413–1424.

3. Rantanen, J.; Lahtinen, P.; Maloney, T. Property space for fibre, microfibrillar cellulose and precipitated $CaCO_3$ composite sheets. *Int. Pap. IPW* **2013**, *5*, 46–51.
4. Dimic-Misic, K.; Puisto, A.; Paltakari, J.; Alava, M.; Maloney, T. The influence of shear on the dewatering of high consistency nanofibrillated cellulose furnishes. *Cellulose* **2013**, *20*, 1853–1864.
5. Peng, Y.; Gardner, D.J.; Han, Y. Drying cellulose nanofibrils: In search of a suitable method. *Cellulose* **2012**, *19*, 91–102.
6. Peng, Y.; Gardner, D.J.; Han, Y.; Kiziltas, A.; Cai, Z.; Tshabalala, M.A. Influence of drying method on the material properties of nanocellulose I: Thermostability and crystallinity. *Cellulose* **2013**, *20*, 2379–2392.
7. Walker, K. Advances in hot pressing technology. *Tappi J.* **1990**, *73*, 99–101.
8. Timofeev, O.; Belski, A.; Mujumdar, A. Effect of dryer fabric pressure on multi-cylinder drying of paper. In *Drying of Solids*; Mujumdar, A.S., Ed.; Science Publishers, Inc: Enfield, NH, USA, 1999; pp. 221–237.
9. Asensio, C.; Seyed-Yagoobi, J.; Lehtinen, J.; Karlsson, M.; Timofeev, O.; Juppi, K. Comparison of several multi-cylinder paper drying simulation models. *Dry. Technol.* **1995**, *13*, 945–958.
10. Kiiskinen, H.; Juppi, K.; Timofeev, O.; Karlsson, M.; Edelmann, K. Impingement drying of multi-ply linerboard. *Pulp Pap. Can.* **1999**, *100*, T8–T10.
11. Lehtinen, J. Condebelt drying of paper and paperboard for optimizing quality and production for many grades. *Dry. Technol.* **1995**, *13*, 2049–2068.
12. Timofeev, O.; Ilomäki, J.; Kuusela, J. Effect of process parameters on paper temperature in Condebelt drying. In Proceedings of the 14th International Drying Symposium (IDS 2004), Sao Paulo, Brazil, 22–25 August 2004; pp. 1327–1334.
13. *Paper and Board—Determination of Grammage*; ISO 536:1995; International Organization for Standardization: Geneva, Switzerland, 1995.
14. *Determination of Thickness and Bulk Density or Apparent Sheet Density*; ISO 534:1998; International Organization for Standardization: Geneva, Switzerland, 1998.
15. Lipponen, P.; Kouko, J.; Leppänen, T.; Hämäläinen, J. Elasto-plastic approach for paper cockling phenomenon: On the importance of moisture gradient. *Int. J. Solids Struct.* **2008**, *45*, 3596–3609.
16. Weise, U.; Maloney, T.; Paulapuro, H. Quantification of water in different states of interaction with wood pulp fibres. *Cellulose* **1996**, *3*, 189–202.
17. Niskanen, K. *Paper Physics*, 2nd ed.; Finnish Paper Engineers' Association/Paperi ja Puu Oy: Helsinki, Finland, 2008.
18. Topgaard, D.; Söderman, O. Diffusion of water absorbed in cellulose fibers studied with 1H-NMR. *Langmuir* **2001**, *17*, 2694–2702.
19. Gupta, H.; Chatterjee, S.G. Parallel diffusion of moisture in paper. Part 1: Steady-state conditions. *Ind. Eng. Chem. Res.* **2003**, *42*, 6582–6592.
20. Huang, B.; Hill, R.; van de Ven, T. Nanopaper: Thin films prepared from polymeric nanotubes. *Macromol. Mater. Eng.* **2012**, *297*, 821–830.
21. Paulapuro, H. *Papermaking Part 1, Stock Preparation and Wet End*, 2nd ed.; Finnish Paper Engineers' Association/Paperi ja Puu Oy: Helsinki, Finland, 2008.

22. Torvinen, K.; Sievänen, J.; Hassinen, T.; Mattila, T.; Hellén, E. Flexible pigment-nanocellulose substrate for printed electronics with good thermal tolerance. In Proceedings of the 1st International Symposium on Nanoparticles/Nanomaterials and Applications, Caparica-Almada, Portugal, 20–22 January 2014.
23. Paavilainen, S., McWhirter, J.L.; Róg, T.; Järvinen, J.; Vattulainen, I.; Ketoja, J.A. Mechanical properties of cellulose nanofibrils determined through atomistic molecular dynamics simulations. *Nordic Pulp Pap. Res. J.* **2012**, *27*, 282–286.

PAPER IV

Pigment-cellulose nanofibril composite and its application as a separator-substrate in printed supercapacitors

Electronic Materials Letters 11, 1040–1047.

PAPER V

Nanoporous kaolin – cellulose nanofibril composites for printed electronics

Flexible and Printed Electronics, Volume 2, Number 2,
Focus on Paper Electronics, 11 p.

Series title and number

VTT Science 162

Title	**Flexible pigment-cellulose nanofibril composites for printed electronics applications**
Author(s)	Katariina Torvinen
Abstract	The aim of this work was to expand the possibilities of novel use of cellulose micro- and nanofibrils (CMNF) for bio-based composites. The new approach in this work was to combine inorganic pigments and CMNF in a relatively wide range of component combinations for the generation of –pigment-cellulose micro- and nanofibril (PCMNF) composites. The amount of CMNF in these studies varied between 20 and 50 wt-% in the studied composites. The main focus of the work was on clarifying the relationship between the raw materials used and the composite structural properties of the final product, such as smoothness and porosity. The influence of manufacturing process steps on the composite properties was studied experimentally in both laboratory and semi-pilot scale. The composites were manufactured by vacuum filtration in laboratory scale and by film casting in semi-pilot scale, in both cases followed by wet pressing, drying, and calendering. Based on feasibility studies including techno-economic and life-cycle assessment, new product opportunities and markets can be captured with PCMNF composites for printed electronics applications. There is nowadays a growing need for the production of flexible, cost-effective, and environmentally friendly substrates for printed electronics applications. CMNF as a raw material has attracted significant interest in this field. In this work, different functional devices were manufactured as proof-of-concept structures to demonstrate the usability of the developed composites for printed electronics applications. The studied proof-of-concepts were: 1) ink-jet printing with a silver-nanoparticle ink, 2) double-functional separator substrate for printed supercapacitors, 3) an ion-modulated transistor deposited on the substrate, and 4) screen printed antennas using silver ink and a commercial radio frequency identification (RFID) chip attached using a silver epoxy resin as a functional near field communication RFID tag on the substrate. The developed PCMNF composites have a nanoporous pigment-CMNF network structure that allows controlled ink absorption properties. The required substrate porosity and smoothness strongly depend on the used printing method, ink, solvent, and device design. The PCMNF composites offer a sustainable substrate for printed electronics applications to be used at high temperatures that only very special plastic films can currently withstand.
ISBN, ISSN, URN	ISBN 978-951-38-8571-7 (Soft back ed.) ISBN 978-951-38-8570-0 (URL: http://www.vttresearch.com/impact/publications) ISSN-L 2242-119X ISSN 2242-119X (Print) ISSN 2242-1203 (Online) http://urn.fi/URN:ISBN:978-951-38-8570-0
Date	October 2017
Language	English, Finnish abstract
Pages	91 p. + app. 67 p.
Name of the project	
Commissioned by	
Keywords	cellulose nanofibrils, cellulose microfibrils, nanocellulose, composite films, printed electronics, mineral pigment, casting method, substrate
Publisher	VTT Technical Research Centre of Finland Ltd P.O. Box 1000, FI-02044 VTT, Finland, Tel. 020 722 111

Julkaisun sarja ja numero

VTT Science 162

Nimeke	**Joustavat pigmentti-nanoselluloosakomposiitit painetun elektroniikan sovelluksiin**
Tekijä(t)	Katariina Torvinen
Tiivistelmä	Joustavien, kustannustehokkaiden ja ympäristöystävällisten alustojen tuottamiseen on painetun elektroniikan sovelluksissa kasvava tarve. Nanoselluloosa on raaka-aineena herättänyt merkittävää kiinnostusta tällä alalla. Tämän työn tavoitteena oli laajentaa mikro- ja nanoselluloosafibrillien käytettävyyttä kalvomaisissa komposiittirakenteissa, joita voidaan hyödyntää uusissa painetun elektroniikan lopputuotesovelluksissa. Tutkimuksessa yhdistettiin epäorgaanisia pigmenttejä ja nanoselluloosaa uudentyyppisen materiaalipohjan valmistamiseksi. Käytetyn nanoselluloosan osuus kokonaispainosta vaihteli tutkituissa komposiittirakenteissa välillä 20 - 50 %. Työn pääpaino oli selvittää käytettyjen raaka-aineiden ja lopputuotteen komposiittisten rakenteellisten ominaisuuksien, kuten sileyden ja huokoisuuden, välisiä vuorovaikutuksia. Valmistusprosessivaiheiden vaikutusta komposiittien ominaisuuksiin tutkittiin kokeellisesti sekä laboratoriossa alipaineistetulla suodatuksella että pilot-ympäristössä filmivalumenetelmällä. Molempia tuotantomenetelmiä seurasivat märkäpuristus, kuivatus ja jälkikäsittelynä kalanterointi. Työssä valmistettiin erilaisiafunktionaalisia komponentteja, joilla testattiin kehitettyjen kalvomaisten materiaalien käytettävyyttä lopputuotesovelluksissa. Tutkittuja konsepteja olivat 1) mustesuihkutulostettu johdin, 2) superkondensaattori, joka toimii sekä erotuskalvona että painoalustana, 3) filmille prosessoitu transistori ja 4) painettu antenni, jossa käytettiin hopeamustetta ja kaupallista radiotaajuustunnistusta (RFID) komposiittiin kiinnitettynä. Sovellusten vaatima alustan sileys ja huokoisuus riippuivat voimakkaasti käytetystä painomenetelmästä, musteesta, liuottimesta ja prosessin suunnittelusta. Uudet työssä kehitetyt komposiitit tarjoavat kestävän kehityksen mukaisen, korkeita lämpötiloja kestävän materiaaliratkaisun painetun elektroniikan sovelluksiin.
ISBN, ISSN, URN	ISBN 978-951-38-8571-7 (nid.) ISBN 978-951-38-8570-0 (URL: http://www.vtt.fi/julkaisut) ISSN-L 2242-119X ISSN 2242-119X (Painettu) ISSN 2242-1203 (Verkkojulkaisu) http://urn.fi/URN:ISBN:978-951-38-8570-0
Julkaisuaika	Lokakuu 2017
Kieli	Englanti, suomenkielinen tiivistelmä
Sivumäärä	91 s. + liitt. 67 s.
Projektin nimi	
Rahoittajat	
Avainsanat	nanosellu, pigmentti, komposiitti, alusta, painettu elektroniikka
Julkaisija	Teknologian tutkimuskeskus VTT Oy PL 1000, 02044 VTT, puh. 020 722 111

Flexible pigment-cellulose nanofibril composites for printed electronics applications

Katariina Torvinen

There is nowadays a growing need for the production of flexible, cost-effective, and environmentally friendly substrates for printed electronics applications. Cellulose micro-and nanofibrils (CMNF) as a raw material has attracted significant interest in this field. The aim of this work was to expand the possibilities of novel use of cellulose micro- and nanofibrils (CMNF) for bio-based composites. The new approach in this work was to combine inorganic pigments and CMNF in a relatively wide range of component combinations for the generation of pigment - cellulose micro- and nanofibril composites. The main focus of the work was on clarifying the relationship between the raw materials used and the composite structural properties of the final product, such as smoothness and porosity. The composites were manufactured by vacuum filtration in laboratory scale and by film casting in semi-pilot scale, in both cases followed by wet pressing, drying, and calendering.
In this work, different functional devices were manufactured as proof-of-concept structures to demonstrate the usability of the developed composites for printed electronics applications. The developed PCMNF composites have a nanoporous pigment-CMNF network structure that allows controlled ink absorption properties. The required substrate porosity and smoothness strongly depend on the used printing method, ink, solvent, and device design. The PCMNF composites offer a sustainable substrate for printed electronics applications to be used at high temperatures that only very special plastic films can currently withstand.

ISBN 978-951-38-8571-7 (Soft back ed.)
ISBN 978-951-38-8570-0 (URL: http://www.vttresearch.com/impact/publications)
ISSN-L 2242-119X
ISSN 2242-119X (Print)
ISSN 2242-1203 (Online)
http://urn.fi/URN:ISBN:978-951-38-8570-0